To the Graduate Council:

I am submitting herewith a thesis written by John Joseph Arnish entitled " Bayesian Estimation of Dose-Rate Effectiveness Factors." I have examined the final copy of this thesis for form and content and recommend that it be accepted in partial fulfillment of the requirements for the degree of Master of Science with a major in Nuclear Engineering.

Peter G. Groer, Major Professor

We have read this thesis
and recommend its acceptance:

Laurence J. Miller

R. J. Michael Jr.

Accepted for the Council:

Associate Vice Chancellor
and Dean of The Graduate School

BAYESIAN ESTIMATION OF DOSE-RATE EFFECTIVENESS FACTORS

A Thesis

Presented for the

Master of Science

Degree

The University of Tenessee Knoxville

John Joseph Arnish

August 1994

DEDICATION

This thesis is dedicated in loving memory to my mother

Mrs. Gertrude Arnish

ACKNOWLEDGEMENTS

I would like to thank Dr. Peter Groer for his wisdom, guidance and patience during the past two years, without his extensive help this thesis would not be possible. My thanks also goes to Dr. Fry for supplying the low dose-rate irradiation data that was used in this thesis as well as serving on my graduate committee. I would also like to thank Dr. Laurence Miller for serving on my graduate committee and helping me with my studies during my stay at U.T. I am also grateful to the National Radiobiology Archives for supplying me with the control and high dose-rate data.

All of my endeavors would not have been possible without the help of my wonderful family: my parents Frank and Gertrude Arnish, my brother Steve Arnish, my sister-in-law Susan Arnish, and my two nieces Sarah and Victoria Arnish for always giving me love and support.

This work was supported, in whole or in part by a DOE cooperative agreement DE-FC05-920R22056. This support does not constitute an endorsement by DOE of the views expressed herein.

ABSTRACT

A Bayesian statistical method was developed to estimate the parameters for the following survival model characterized by the probability density $f(t,d)=\alpha\lambda^{\alpha}t^{\alpha-1}e^{\rho\beta d}e^{-(\lambda t)^{\alpha}e^{\rho\beta d}}$ Computer programs were developed in "Mathematica" (10) to calculate the posterior densities for the model parameters α, β, λ, and ρ. The data used in the analyses came from BALB/c female mice exposed to ^{137}Cs gamma radiation (5,6). The doses ranged from 0 to 2 Gy with dose rates from 0.083 Gy/day to 0.4 Gy/min (5,6). The data were generated at the Biology division of Oak Ridge National Lab (ORNL) and supplied by ORNL and the National Radiobiology Archives. The parameter ρ describes the effect of dose-rate on the induction of cancer in mice. The derived posterior density for ρ describes the remaining uncertainty about the parameter after updating. This thesis describes the first direct estimation of a dose-rate effectiveness factor (DREF) using the techniques of Bayesian parameter estimation and gives the first quantitative description of the uncertainty of this factor in terms of a probability density.

TABLE OF CONTENTS

LIST OF FIGURES

CHAPTER 1

INTRODUCTION

Cancer risk estimates after prolonged exposure to ionizing radiations (external and internal) are necessary to make rational decisions about radiation protection standards. One way to quantify the extent to which low LET radiation may increase or decrease carcinogenic potency at low dose rates is with Dose-Rate Effectiveness Factors (DREFs) (1). Past analyses of experimental carcinogenesis studies show a decrease in effectiveness with decreasing dose-rates for acute exposures to low LET radiations (2). Suitable human data that would permit estimation of DREFs are scarce. It is for this reason that extrapolation from animals to man must be made. The idea is to estimate the decrease or increase in carcinogenic potency using experimental mouse data and scale the results using estimates for cancer risks after acute exposure from the Japanese A-bomb survivor data. The analyses of the experimental studies and the A-bomb survivor study are treated as "data" and combined in a "hyper-model". This basic idea has been applied to Pu risk estimation in humans (3,4).

This thesis will develop a methodology to estimate DREFs using Bayesian techniques. Chapter 2 details the non-parametric analyses of the experimental carcinogenesis data. The non-parametric estimation will in part be used for model identification. Chapter 3 outlines Bayes' Theorem and likelihood construction. The

Likelihood is an important part in parameter estimation, because the likelihood contains all of the information from the experimental data. Chapter 4 explains the numerical techniques used to estimate the model parameters including the DREF.

1.1 CLASSICAL ESTIMATION OF THE DREF

A linear-quadratic dose response relationship is used in the classical estimation of the dose-rate effectiveness factor (2). If R is a measure of the endpoint of interest the linear-quadratic model is given by:

$$R=\alpha D+\beta D^2 \qquad (1.1)$$

where α and β are the parameters (2). After the fitting of linear and linear-quadratic models to the experimental carcinogenesis data, the ratio of the coefficients of D for the two fits yield the classical estimate of the dose-rate effectiveness factor (2). Typical ranges for DREF values are from 2-10 depending upon the endpoints of interest that were studied (2).

1.2 EXPERIMENTAL MOUSE DATA

The data that were analyzed in this thesis were obtained by exposing BALB/c females. The endpoints of interest considered were: lung tumors (lung carcinomas and lung adenomas), breast cancer, and all causes of death. There were three groups of mice:

the control group, the high dose-rate group, and the low dose-rate group. The control group was sham irradiated at approximately 10 weeks of age (5). The high dose-rate BALB/c females were irradiated at approximately 10 weeks of age at 0.40 Gy/min using a 2000-Ci ^{137}Cs source (5). Exposures were made at 45 cm from the source with the mice enclosed in plastic tubes (6). The low dose-rate mice were also irradiated at approximately 10 weeks of age at 0.083 Gy/day (6). The irradiation was done using a 10-Ci ^{137}Cs source at a distance of 10 feet (6). During the irradiation, the animals were housed in plastic cages with 8 mice per cage (6). Table 1.1 gives a summary of the data set used in the analyses.

Table 1.1 Summary of BALB/c females

# of mice	Dose (Gy)	Dose-Rate
833	0	———
834	0.5	0.40 Gy/min
1259	0.5	0.083 Gy/day
1269	1.0	0.083 Gy/day
809	2.0	0.40 Gy/min
1301	2.0	0.083 Gy/day

The data on the control and the high dose-rate mice were obtained from the National Radiobiology Archives. The data set contained the dates of birth, irradiation, and death. These are not the original dates, however the time lapse between them is correct. Causes of death and incidental findings were also given for each mouse. The failure times (endpoints of interest and censoring) for the control group were obtained by subtracting the date of death from the date of birth. The times to failure for high dose-rate group are defined as the date of death minus the date of irradiation.

The data for the mice exposed to low dose-rate radiation mice were obtained from the Biology Division at Oak Ridge National Laboratory (ORNL). The date of irradiation was assumed to be 73 days after the date of birth. The low dose-rate data set included the life length of the mouse, a code indicating the type of tumors each mouse had and whether the tumors were fatal. Failure times were calculated to be the amount of time the mouse lived in days minus 73 days.

1.3 BAYESIAN TECHNIQUES

This thesis utilizes techniques from Bayesian reliability analysis and applies them to the analysis of carcinogenesis data. Probability plotting methods such as hazard plotting (7) and total time on test plotting (8) have been used for many years in reliability analysis. Based on these non-parametric techniques, probability models are constructed. The model parameters are then estimated using numerical techniques. The end results are the marginal posterior densities for all the parameters including the DREF.

CHAPTER 2

NON-PARAMETRIC ESTIMATION

The preliminary data analysis is accomplished by doing non-parametric estimation of the time dependence and dose dependence of the hazard rates for the endpoints of interest. As the name implies, no parameters are used in this initial exploratory analysis. Two separate techniques are employed, the first technique plots an estimate of the cumulative hazard versus time (7), while the second procedure plots a scaled total time on test versus fraction of the endpoints of interest observed (8). The second probability plotting method is used to verify the results of the first.

2.1 NELSON'S ESTIMATE (HAZARD PLOTTING)

Nelson (7) developed a method for estimating the cumulative hazard. The cumulative hazard is defined as:

$$H(t,d)=\int_0^t h(\tau,d)\,d\tau \qquad (2.1)$$

where h(t,d) is the hazard rate. The hazard rate when multiplied by a small increment Δt yields :

$$h(t,d)\Delta t = P(t<T<t+\Delta t \mid t>T,d) \qquad (2.2)$$

where P is the probability for the endpoint of interest, T is the random time to death for the specific endpoint of interest and d is the radiation dose.

Assuming independence of the times of death, Nelson estimates H(t,d) in the following manner,

$$\hat{H}(t,d)_j = \sum_{i=1}^{j} \frac{1}{RR_i} \qquad (2.3)$$

where RR_i is the reverse rank of the ith time to death for the j^{th} cause of death with the times to death arranged in ascending order. Table 2-1 gives an example of the ordering of the times to death, for unexposed BALB/c females using lung tumors as the specified endpoint. The third column gives the indicator for lung tumors. A zero indicates that the mouse did not have either lung carcinoma or lung adenoma while the presence of a one indicates the diagnosis of the tumors. The standard deviation for the Nelson estimate is calculated in a similar manner, let $\sigma(t,d)$ be the standard deviation then

$$\sigma(t,d)_j = \left(\sum_{i=1}^{j} \frac{1}{(RR_i)^2} \right)^{1/2} \qquad (2.4)$$

Table 2.1 Summary of unexposed BALB/c females with lung tumors

Time (days)	Reverse Rank	Indicator
109	833	0
109	832	0
113	831	0
118	830	0
142	829	0
157	828	0
164	827	0
⋮	⋮	⋮
1183	2	0
1204	1	0

The Nelson estimate as well as plus (minus) one standard deviation is plotted versus time. Figure 2-1 gives the Nelson estimator for the cumulative hazard versus time for unexposed BALB/c females with lung tumors.

The plot of the cumulative hazard versus time clearly shows the time dependence of the hazard rate. As time increases the slope of the estimated cumulative hazard also increases. Since the cumulative hazard does not increase linearly with time, but rather as some power of time greater than one the hazard rates must increase with time. Figure 2-2 shows general relationships among the hazard rate and the estimated cumulative hazard.

In addition to providing information about the time dependence of the hazard cancer rates, a plot of the estimated cumulative hazard also provides information on the dose dependence of the hazard rate as well. The estimated cumulative hazard is plotted separately for each dose-rate and dose group. If the estimated cumulative hazard increases as the dose increases for constant time then we clearly have a dose dependence in the hazard rate. Figure 2-3 shows the effect of dose on the estimated cumulative hazard. Notice that the estimated cumulative hazard is greater for the 2 Gy dose group than the 0.5 Gy and the unexposed group .

The results from this non-parametric analysis are of great importance to the parametric analyses. Parameters that describe the dose and the dose-rate effect are included in the statistical model. The addition of these two parameters

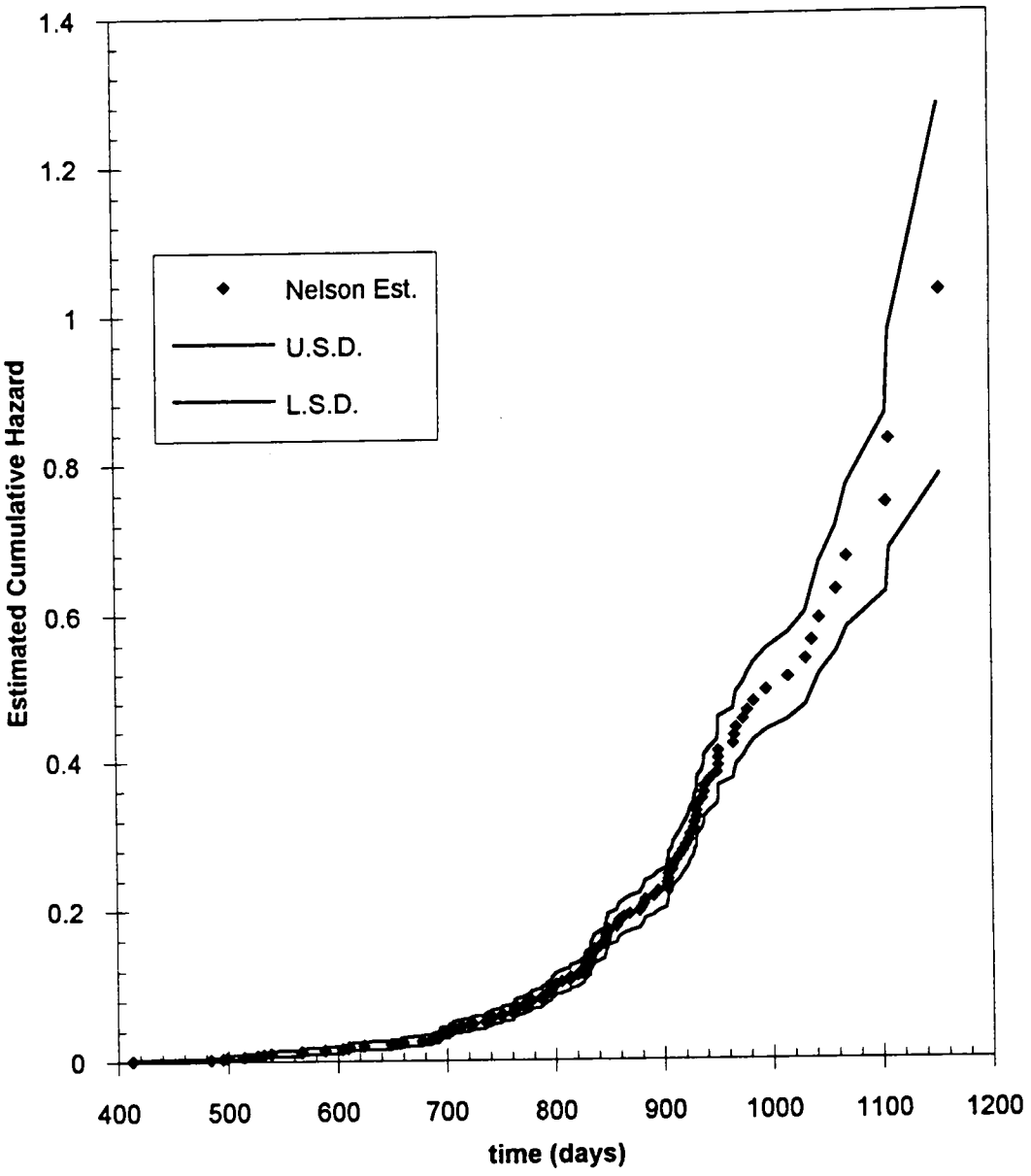

Figure 2.1 Estimated cumulative hazard versus time for unexposed BALB/c females with lung tumors

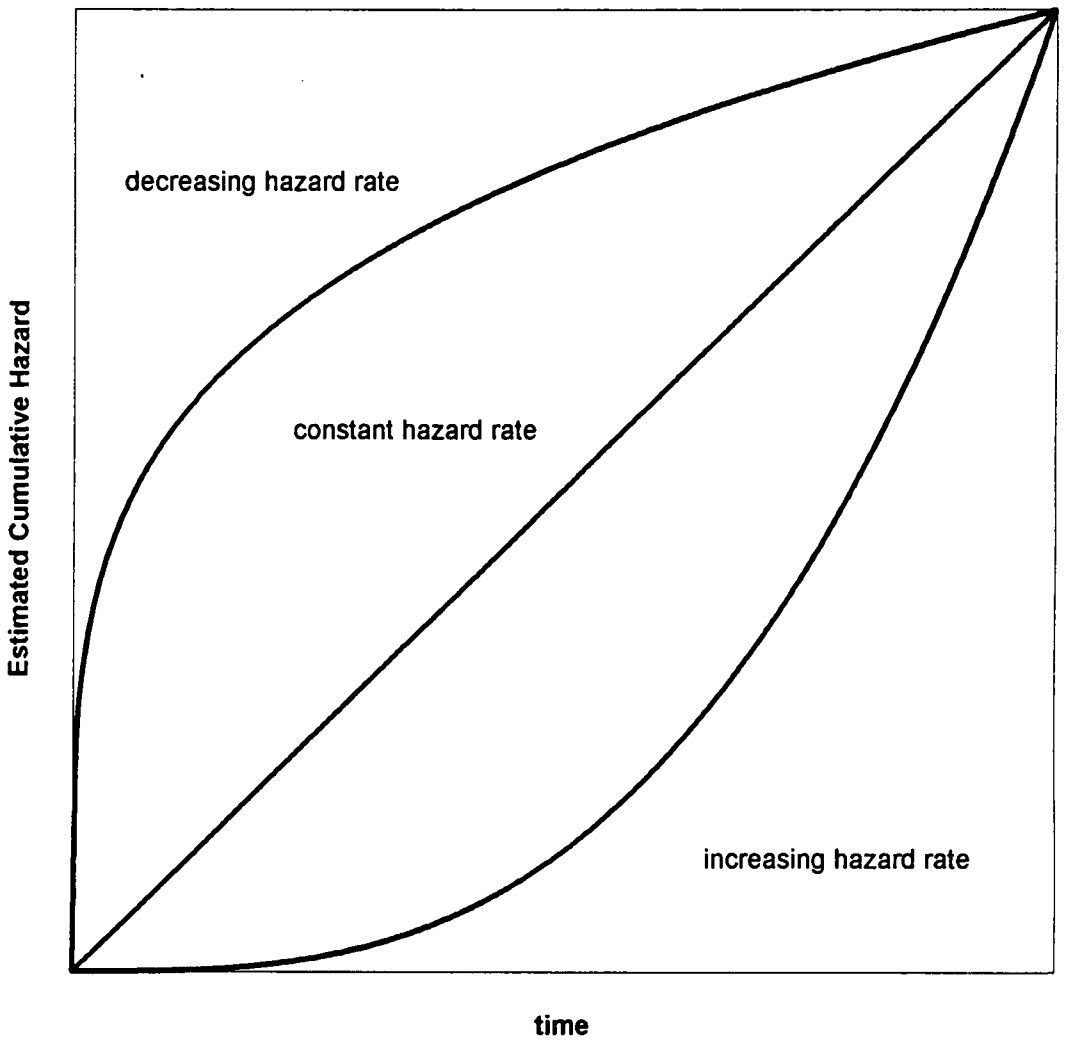

Figure 2.2 General relationships between the cumulative hazard and the hazard rates

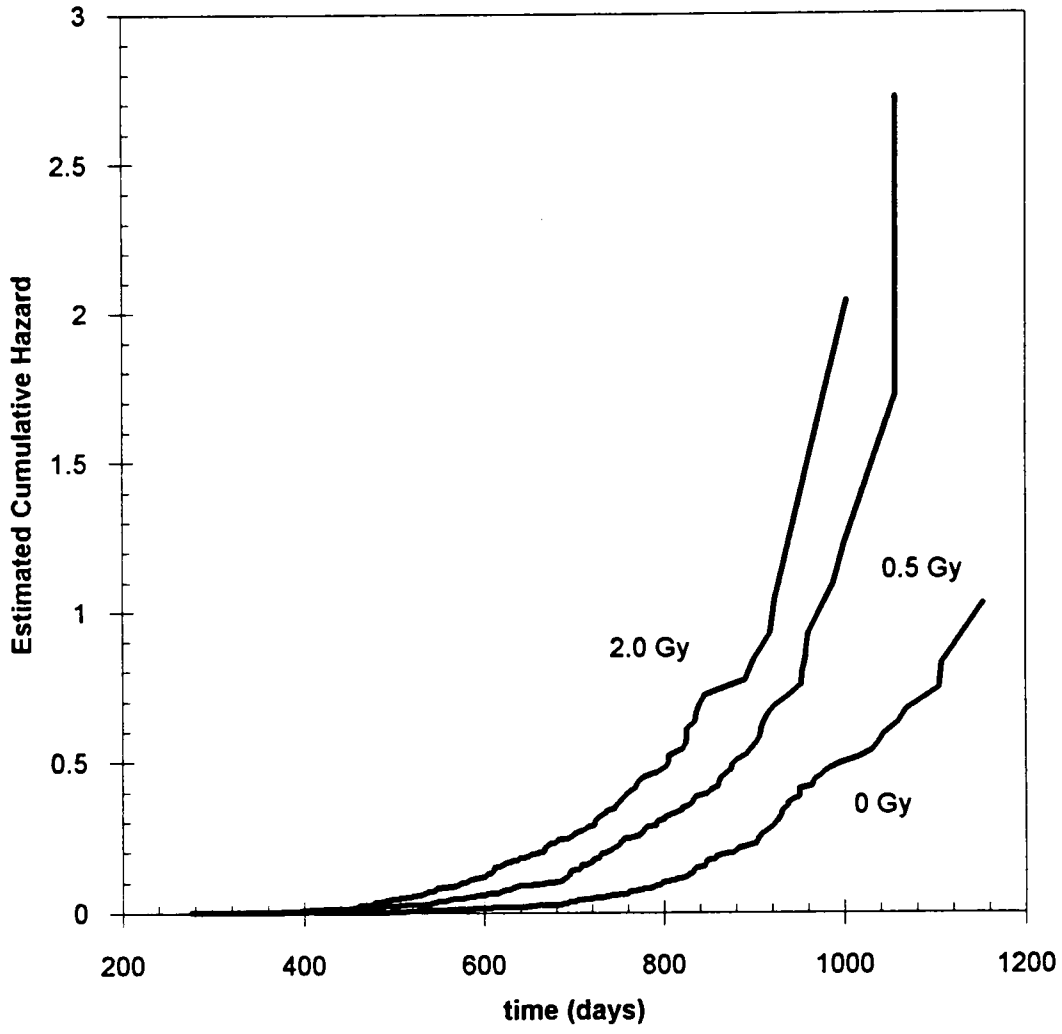

Figure 2.3 Estimated cumulative hazard for Unexposed, 0.5 Gy, and 2.0 Gy BALB/c females with lung tumors

allows better modeling of the data besides yielding the DREF.

2.2 TOTAL TIME ON TEST

A second method used to estimate the time dependence of the hazard rate is done by plotting a scaled total time on test versus the fraction of the endpoints of interest observed. The total time on test procedure as well as the Nelson procedure make the assumptions that the random times to the observation of interest are independent from the censoring times. Just as for the plots of the estimated cumulative hazard, a total time on test plot is done for each dose-rate and dose group.

The scaled total time on test transform is given by the equation:

$$TTT_{scaled_i} = \frac{TTT_i}{TTTT} \qquad (2.5)$$

where TTT_i is the total time on test up to time t_i. TTTT is the sum of all the times up to the last failure caused by the specific endpoint of interest. This may be called the "total" total time on test. "Total" total time on test is equivalent to total person years or total reactor years in other contexts. The analysis is made by looking at the shape of the graph. If the graph is convex the hazard rate is increasing, while if the graph is concave the hazard rate is decreasing. A special case of the total time on test exists if the hazard rate is constant with time, if this occurs then the total time on test plot is linear along the

45° line (8). Figure 2-4 gives an example of a total time on test plot for all three cases.

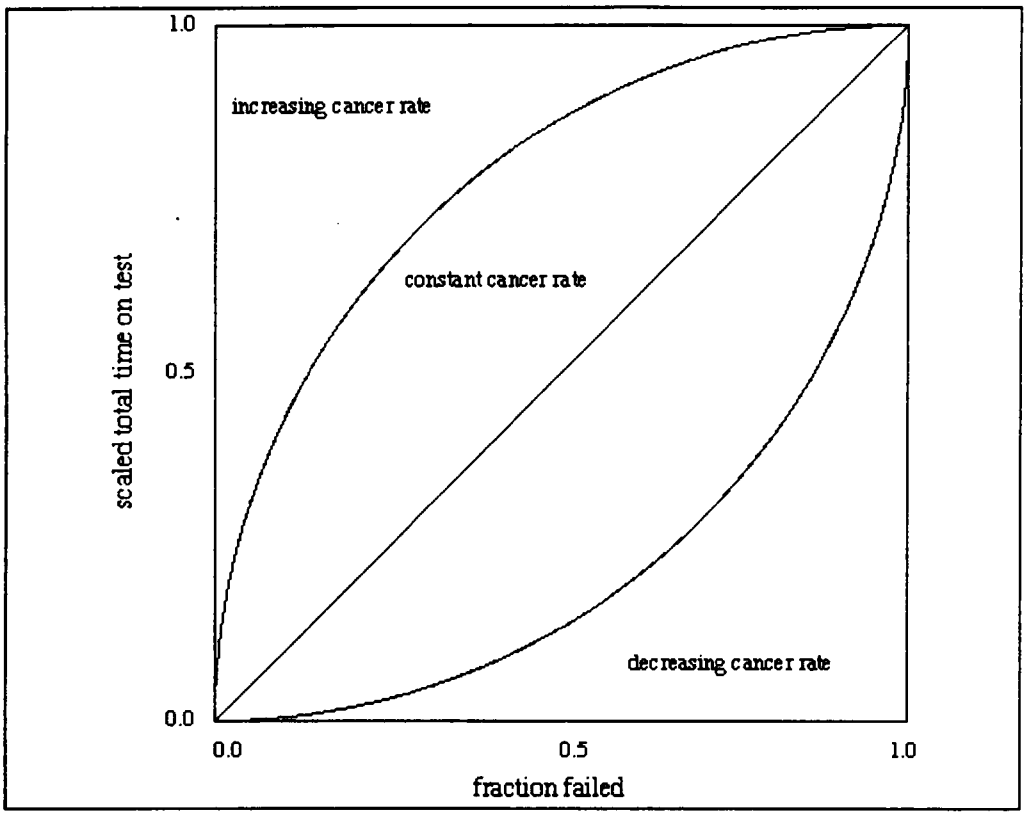

Figure 2-4 Scaled total time on test versus fraction failed for increasing, decreasing, and constant hazard rates

The total time on test transformation is begun by ordering the times to death in ascending order and ranking them in ascending order. The cancer of interest is once again indicated by a one, while other tumors not of interest receive an indicator of zero. The "total" total time on test is the sum of all of the times to death up to and including the last time of death for the endpoint of interest. The total time on test up to time t_i is given by the following expression:

$$TTT_i = \sum_{j=1}^{i} t_j + (n-i)t_i \qquad (2.6)$$

where n is the total number of mice up to the last mouse to die with the specified endpoint of interest. The scaled total time on test can now be given by:

$$TTT_{scaled_i} = \frac{\sum_{j=1}^{i} t_j + (n-i)t_i}{TTTT} \qquad (2.7)$$

The scaled total time on test is plotted versus the fraction of lung tumors or as stated earlier, the fraction failed. Figure 2-5 shows the scaled total time on test versus fraction failed for unexposed BALB/c females with lung tumors. The 45° line represents a constant lung cancer rate. Notice that the total time on test plot is convex in t which indicates an increasing lung cancer rate.

2.3 SUMMARY

This chapter detailed two non-parametric methods to estimate the time and dose dependence of the cumulative hazard. The Nelson plot shows an estimate of the cumulative hazard versus time. This method indicated that the lung and breast cancer rates were not only time dependent, but were also dependent on the dose received. In order to verify the results of the Nelson procedure, scaled total time on test plots were done for each dose-rate and dose group. The total time on test plots confirmed the time dependence established by the Nelson estimator. The convex curve indicates that the lung

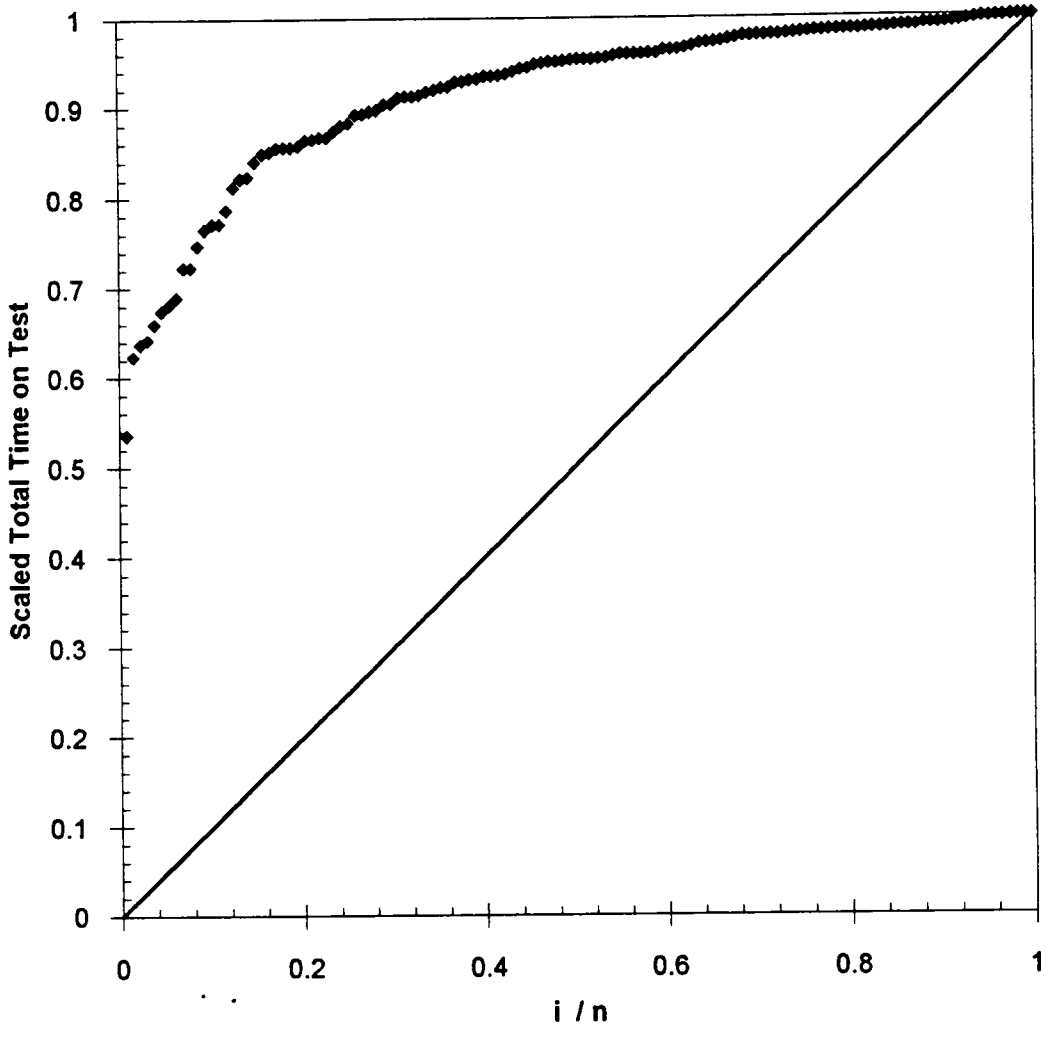

Figure 2.5 Scaled total time on test versus fraction failed for unexposed BALB/c females with lung tumors

cancer rate is increasing in time. The remainder of the non-parametric estimates for lung tumors, breast cancer, and all causes of death may be found in appendix 2.

CHAPTER 3

BAYES' THEOREM AND THE LIKELIHOOD

The non-parametric estimates of the cumulative hazard indicated that the hazard rates for the endpoints of interest are increasing in time. In addition, the plots of the estimated cumulative showed that as dose increases the estimated cumulative hazard increases for constant time. The goal is to choose a probability model whose hazard rate increases with time and dose. This may be accomplished by using a model with an increasing hazard rate multiplied by a relative risk term describing the dose and dose-rate dependence. The parameters are estimated using Bayesian techniques. Bayesian procedures yield posterior distributions for all the parameters. These distributions describe the remaining uncertainty for each parameter used in the model. The posterior distribution for the parameter describing the DREF may be obtained using this procedure. Point estimates for the parameters are obtained by using for example the mode or the mean of the posterior distribution for the parameters. The posterior modes are inserted into the model's cumulative hazard. This gives a comparison between the model (parametric) estimate and the non-parametric estimate.

3.1 BAYES' THEOREM

The Bayesian parameter estimation procedure is based on Bayes' theorem, given by:

$$p(\underline{\theta}|D)=\frac{p(D|\underline{\theta})p(\underline{\theta})}{\int_{\underline{\theta}} p(D|\underline{\theta})\,p(\underline{\theta})\,d\underline{\theta}} \qquad (3.1)$$

The theorem states that the posterior probability distribution of the parameter $\underline{\theta}$ given the data is the probability of the data given the parameter times the prior probability density of the parameter, divided by the marginal distribution of the data. Note that $\underline{\theta}$ which represents the parameter may be a vector quantity $(\theta_1 , \theta_2 , \theta_3 , \ldots , \theta_n)$. The term $p(D|\underline{\theta})$ is referred to as the likelihood and $p(\underline{\theta})$ is known as the prior density. The likelihood may be considered as a function of the parameters $\underline{\theta}$. To emphasize this aspect the likelihood will be simply written as $\mathcal{L}(\underline{\theta})$. The prior density codifies the prior knowledge about the parameter of interest. If not much is known about the parameter *a priori* then a uniform prior may be used to express this lack of knowledge. The marginal distribution of the data in the denominator of Bayes's theorem is the normalization constant, and scales the area of $p(\underline{\theta}|D)$ to one. Since the normalization constant is independent of the parameters, it may be dropped from the expression without affecting the shape of the posterior distribution.

The posterior density gives the uncertainty about the parameters after updating with the likelihood. When additional data become available, the posterior density is

updated again. Figure 3-1 illustrates the approach., D_1 in the figure is the original data set and D_2 is the new data set. The term $p_1(\underline{\theta} \mid D)$ is the posterior density after updating with $p(D_1 \mid \underline{\theta})$. The new posterior density $p_2(\underline{\theta} \mid D_2)$ is obtained after

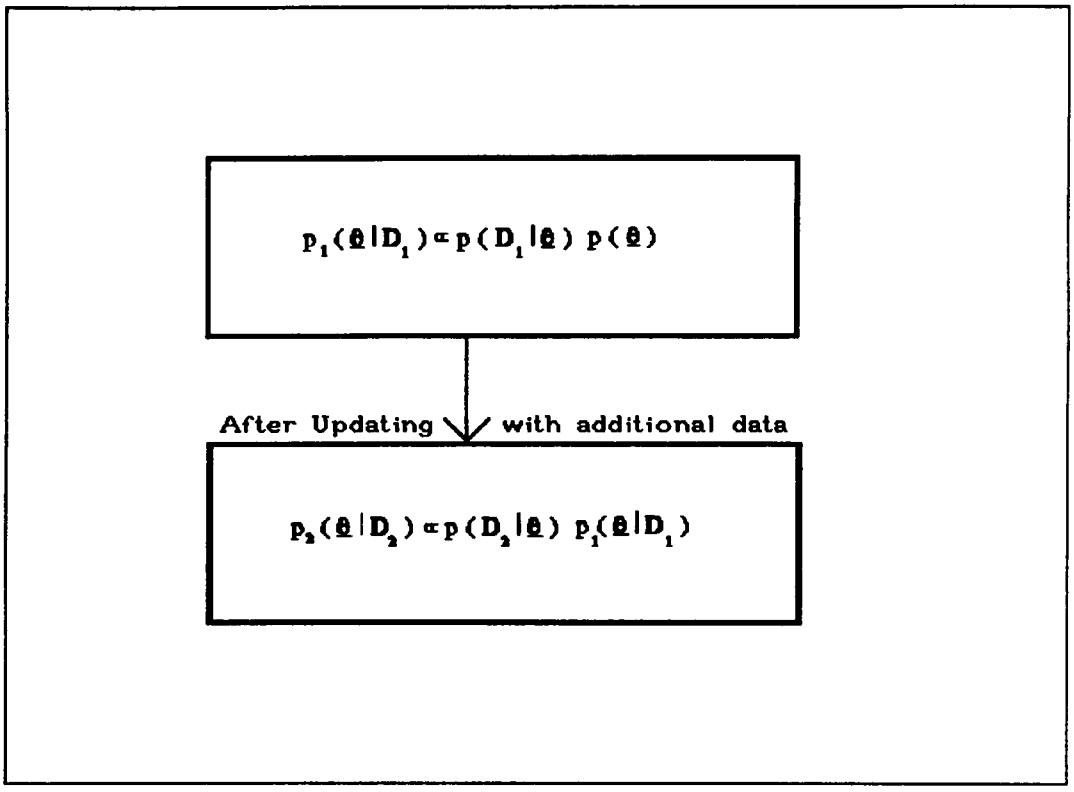

Figure 3.1 Updating the posterior density with additional data

the second update. The updating procedure can be continued each time new data becomes available. As the posterior distributions are updated the resulting distributions become more and more peaked. This indicates that the uncertainty about the parameters is decreasing.

3.2.1 MODELING THE BACKGROUND RATE

A Weibull hazard rate was chosen as a reasonable model for the background or zero dose group based on the results obtained from the non-parametric estimation of hazard rate. The hazard rate for the Weibull is given by equation (3.2).

$$h(t)=\alpha\lambda^{\alpha}t^{\alpha-1} \qquad (3.2)$$

The parameter α is the shape parameter for the Weibull distribution. This parameter determines the time dependence of the hazard rate. The parameter λ is the scale parameter for the Weibull. Notice that when α is equal to one, the hazard rate is constant and equal to λ. If α is less than one then the hazard rate is decreasing indicating failures are more prevalent at the beginning of the lifetime then at the end. When α is greater than one, the hazard rates are increasing in time. Since the non-parametric estimates show the existence of an increasing hazard rate, the parametric point estimate (the posterior mode) of α is expected to be greater than one.

The hazard rate and survival functions are linked in the following manner:

$$S(t)=e^{-H(t)} \qquad (3.3)$$

where H(t) is the cumulative hazard as defined in equation (2 .1). The survival function for the Weibull model becomes:

$$S(t)=e^{-(\lambda t)^{\alpha}} \qquad (3.4)$$

The density function for the time to the endpoint of interest for an unexposed

mouse may be written as:

$$f(t|\alpha,\lambda)=\alpha\lambda^{\alpha}t^{\alpha-1}e^{-(\lambda t)^{\alpha}} \qquad (3.5)$$

A mouse without the specified endpoint contributes a survival function term to the likelihood. The random times to censoring and to the endpoint of interest are assumed to be independent. This allows all of the density and survival function terms to be multiplied together to obtain the likelihood for the unexposed BALB/c females:

$$\mathcal{L}_0(\alpha,\lambda)\propto\alpha^{m_0}\lambda^{\alpha m_0}\left(\prod_{i=1}^{m_0}t_i^{\alpha-1}\right)e^{-\lambda^{\alpha}\sum_{i=1}^{M_0}t_i^{\alpha}} \qquad (3.6)$$

where $\mathcal{L}_0(\alpha, \lambda)$ is the contribution to the final likelihood for the unexposed BALB/c females, m_0 is the number mice that have the specified endpoint of interest in the unexposed group, and M_0 is the total number of mice in the unexposed group.

3.2.2 MODELING THE HIGH AND LOW DOSE-RATE EFFECT

The final likelihood used in the parametric analysis contains not only contributions from unexposed mice but also from mice irradiated at high and low dose-rates. The non-parametric estimates of the cumulative hazard indicated the hazard rate was dose dependent as well as time dependent. The cumulative hazard for the unexposed mice is multiplied by a term that includes a dose parameter, to model the low dose-rate cumulative hazard.

The hazard rate for the low dose-rate is

$$h_L(t,d)=h(t)e^{\beta_L d} \qquad (3.7)$$

where h(t) is the hazard rate for the unexposed mice, d is the dose in Gy and β_L is the dose parameter for the mice irradiated at the low dose rate. Notice that if β_L is positive then as dose increases the hazard rate will increase. Also notice if the dose is zero then the hazard rate for the unexposed mice is recovered. The restriction on β_L *a priori* is $0 \le \beta_L < \infty$. Combining equations (3.2) and (3.7) yields the hazard rate for a mouse irradiated at the low dose-rate.

$$h_L(t,d)=\alpha\lambda^{\alpha}t^{\alpha-1}e^{\beta_L d} \qquad (3.8)$$

Since the relative risk term is not a function of time, then the estimated cumulative hazard is simply the cumulative hazard for the unexposed mice multiplied by the relative risk term $e^{\beta_L d}$. Hence the contribution to the likelihood for a low dose-rate mouse with one of the specified endpoints may be written as:

$$f_L(t,d|\alpha,\lambda)=\alpha\lambda^{\alpha}t^{\alpha-1}e^{\beta_L d}e^{-(\lambda t)^{\alpha}e^{\beta_L d}} \qquad (3.9)$$

By assuming independent observations, the likelihood for the entire set of data for the low dose-rate irradiation set is given by equation 3.10, where m_L are the total number of mice having the desired endpoint in the low dose-rate group, q_i are the number of mice having

$$\mathcal{L}(\alpha,\beta,\lambda)_L \propto \alpha^{m_L}\lambda^{m_L\alpha}\left(\prod_{i=1}^{m_L}t_i^{\alpha-1}\right)e^{\beta_L\sum_{i=1}^{k_L}q_i d_i}e^{-\lambda^{\alpha}\left(\sum_{i=1}^{k_L}\sum_{i=1}^{s_L}t_i^{\alpha}e^{\beta_L d_i}\right)} \qquad (3.10)$$

the desired endpoint in the i^{th} dose group, k_L is the total number of dose groups in the low dose-rate data set and s_L is the number of low dose-rate mice in the l^{th} dose group.

The high dose-rate hazard rates are modeled using the same method as above. In this case β_L can be replaced by β_H indicating the dose parameter for the high dose-rate irradiated mice. The likelihood for the high dose-rate mice is written as:

$$\mathcal{L}(\alpha,\beta,\lambda)_L \propto \alpha^{m_H}\lambda^{m_H\alpha}\left(\prod_{i=1}^{m_L} t_i^{\alpha-1}\right) e^{\beta_H\sum_{i=1}^{k_H} q_i d_i} e^{-\lambda^{\alpha}\left(\sum_{h=1}^{k_H}\sum_{i=1}^{s_H} t_i^{\alpha} e^{\beta_H d_h}\right)} \qquad (3.11)$$

where m_H is the total number of mice having the desired endpoint of interest in the high dose-rate group, q_i is the number of mice having the specified endpoint in the i^{th} high dose-rate dose group, s_H is the number of mice in the l^{th} high dose-rate dose group and k_H is the number of high dose- rate dose groups

3.2.3 THE DOSE-RATE EFFECTIVENESS FACTOR ρ

The total likelihood combines the likelihoods of the unexposed mice, the low dose-rate mice and the high dose-rate mice. Because independence of all the random times of death is assumed the total likelihood is obtained by multiplying all of the "partial" likelihoods together. Before this is done another parameter is introduced that will take into account the dose-rate effect for a particular endpoint of interest. This final parameter is designated as ρ and called the DREF. The parameter is arrived at in the following way.

The dose effect on the estimated cumulative hazard was modeled only by the relative risk term $e^{\beta d}$. Since there are two dose-rates, there are consequently two different β's, β_L for the low dose-rate and β_H for the high dose-rate. The parameter ρ is defined by equation 3.12.

$$\rho = \frac{\beta_H}{\beta_L} \qquad (3.12)$$

Consequently β_H is

$$\beta_H = \rho \beta_L \qquad (3.13)$$

Subsequently the subscripts H and L are dropped for brevity. This yields:

$$\beta_L = \beta \qquad (3.14)$$

$$\beta_H = \rho \beta \qquad (3.15)$$

Equations 3.14 and 3.15 may be inserted into equations 3.10 and 3.11 yielding equations 3.16 and 3.17.

$$\mathcal{L}(\alpha,\beta,\lambda)_L \propto \alpha^{m_L} \lambda^{m_L \alpha} \left(\prod_{i=1}^{m_L} t_i^{\alpha-1} \right) e^{\beta \sum_{i=1}^{k_L} q_i d_i} e^{-\lambda^{\alpha} \left(\sum_{i=1}^{k_L} \sum_{i=1}^{s_L} t_i^{\alpha} e^{\beta d_i} \right)} \qquad (3.16)$$

$$\mathcal{L}(\alpha,\beta,\lambda)_H \propto \alpha^{m_H} \lambda^{m_H \alpha} \left(\prod_{i=1}^{m_L} t_i^{\alpha-1} \right) e^{\rho \beta \sum_{i=1}^{k_H} q_i d_i} e^{-\lambda^{\alpha} \left(\sum_{h=1}^{k_H} \sum_{i=1}^{s_H} t_i^{\alpha} e^{\rho \beta d_h} \right)} \qquad (3.17)$$

From the definition of ρ follows $0 \leq \rho < \infty$ since $0 \leq \beta_H, \beta_L < \infty$.

Notice that if ρ is less than one then low dose-rate radiation is more effective at causing the desired endpoint, and if ρ is greater than one then the high dose-rate is more effective than the low dose-rate for the same dose

3.2.4 THE JOINT POSTERIOR DENSITY FOR α, β, λ, AND ρ

The total likelihood is obtained by multiplying the "unexposed", the "low dose-rate", and the "high dose-rate" likelihoods together. The total likelihood is multiplied by the prior probability densities for the parameters α, β, λ, and ρ to obtain a quantity proportional to the joint posterior density. Since not much is known about these parameters *a priori* uniform or constant prior densities are assumed for α, β, and ρ. For the parameter λ, the prior density is given below.

$$p(\lambda) \propto \frac{1}{\lambda} \qquad (3.18)$$

For a sharply peaked likelihood, the density can be considered uniform over the range where the likelihood peaks.

Bayes' theorem can now be applied to give the joint posterior density for the parameters α, β, λ, and ρ:

$$p(\alpha,\beta,\rho,\lambda\,|\underline{t},\underline{d}) \propto \alpha^{n}\lambda^{n\alpha-1}\left(\prod_{i=1}^{n} t_i^{\alpha-1}\right) e^{\rho\beta\sum_{i=1}^{k_H} q_i d_i}\, e^{\beta\sum_{i=1}^{k_L} q_i d_i}\, e^{-\lambda^{\alpha}\left(\sum_{i=1}^{M_0} t_i^{\alpha}+\sum_{i=1}^{k_L}\sum_{i=1}^{s_L} t_i^{\alpha} e^{\beta d_l}+\sum_{h=1}^{k_H}\sum_{i=1}^{s_H} t_i^{\alpha} e^{\rho\beta d_h}\right)} \quad (3.19)$$

where n, q_i , M_0 , k_L , k_H , s_L, and s_H all have the same meaning as before.

3.3 SUMMARY

This chapter detailed the construction of the likelihood that is used in Bayes' theorem to obtain posterior densities for the parameters after updating with the available data. A relative risk Weibull model was chosen to model the data. The hazard plots given in chapter 2 and appendix 2 appear to show a minimum latent period before a particular cancer is detected. This minimum latency time or guarantee period is not included in the probability model. Since the random times to the endpoint of interest were assumed to be independent, the densities and survival functions are multiplied together to obtain a likelihood for the entire data set. The likelihood is then multiplied by the prior densities for each parameter. Uniform or constant priors were chosen for α, β, and ρ while a prior density of $1/\lambda$ was chosen for the parameter λ . A dose and a dose-rate parameter is contained in the relative risk term of the likelihood. These parameters describe the dose dependence and dose-rate effect for each of the desired endpoints of interest in BALB/c females.

CHAPTER 4

PARAMETRIC ESTIMATION

The joint posterior density for α, β, λ, and ρ was given by equation 3.19. In order to find the marginal posterior densities for the individual parameters, it is necessary to integrate out the remaining parameters. Analytical integration is only possible over the parameter λ. The other integrals need to be approximated by numerical methods. A Gauss-Legendre (9) routine is used for the approximation of the integrals. Using this procedure, marginal posterior densities may be obtained for each parameter.

4.1 GAUSS-LEGENDRE QUADRATURE

As stated above the Gauss-Legendre routine may be used to approximate an integral. The approximation involves evaluating the function at specified values and multiplying by the appropriate weights. The terms are added together to get the numerical approximation to the definite integral. Equation 4.1 gives the expression for a one-dimensional n point Gauss-Legendre routine .

$$\int_a^b f(x)dx \approx \sum_{i=1}^{n} f(x_i)w_i \qquad (4.1)$$

In this equation f is the function, x_i is the i^{th} abscissa, and w_i is the corresponding weight.

A multi-dimensional routine is developed in a similar manner. The parametric analysis will use this multi-dimensional routine. Equation 4.2 gives the approximation for a multi-dimensional integral.

$$\int_a^b \int_a^b \cdots \int_a^b f(x_1, x_2, \ldots, x_n) \approx \sum_{i=1}^{n} \sum_{j=1}^{n} \cdots \sum_{k=1}^{n} f(x_i, x_j, \ldots, x_k) w_i w_j \ldots w_k \qquad (4.2)$$

Notice that as the number of dimensions increase, the number of function evaluations increases dramatically.

$$\textit{Function Evaluations} = n^k \qquad (4.3)$$

where n is the number of weight-abscissa pairs and k is the number of dimensions. A thirty point quadrature for a three dimensional integral needs 27,000 function evaluations. The calculations of the marginal posterior densities are done using "Mathematica" (10) on a Sun Spark 10 workstation. Each approximation is verified by running a second Gauss-Legendre procedure using a different number of weights and abscissas. A comparison of the two independent methods is made, and the results must agree with each other before the approximation is accepted.

4.2 THE MARGINAL POSTERIOR DENSITY FOR λ

The marginal posterior density for the scale parameter λ is obtained by integrating out the parameters α, β, and ρ. Since there are no analytical expressions for these integrals, numerical approximations must be used.

The marginal posterior density for λ is given by equation 4.4

$$p(\lambda|t,d) \propto \int_0^\infty \int_0^\infty \int_0^\infty p(\alpha,\beta,\rho,\lambda|t,d)\,d\alpha\,d\beta\,d\rho \qquad (4.4)$$

This expression may be approximated by a Gauss-Legendre routine given by equation 4.5.

$$p(\lambda|t,d) \propto \sum_{i=1}^{n}\sum_{j=1}^{n}\sum_{k=1}^{n} p(\alpha_i,\beta_j,\rho_k,\lambda|t,d)\,w_i w_j' w_k'' \qquad (4.5)$$

where w_i is the i^{th} weight, w'_j is the j^{th} weight, w''_k is the k^{th} weight, α_i is the i^{th} abscissa, β_j is the j^{th} abscissa, and ρ_k is the k^{th} abscissa. The numerical approximation is first done using twenty five weight-abscissa pairs for each dimension. This result is verified by reducing the number of weight-abscissa pairs to twenty. The weights are generated using "Mathematica" (see appendix 1). The limits of integration for the three dimensional routine are chosen by studying the behavior (or shape) of the marginal posterior densities for α, β, and ρ. The limits of integration for each parameter are different due to the fact that the shapes of the marginal posterior densities are different for each parameter. The methods for obtaining the marginal posterior densities for α, β, and ρ are given in section 4.4. Figure 4.1 give the marginal posterior density for the parameter λ with lung

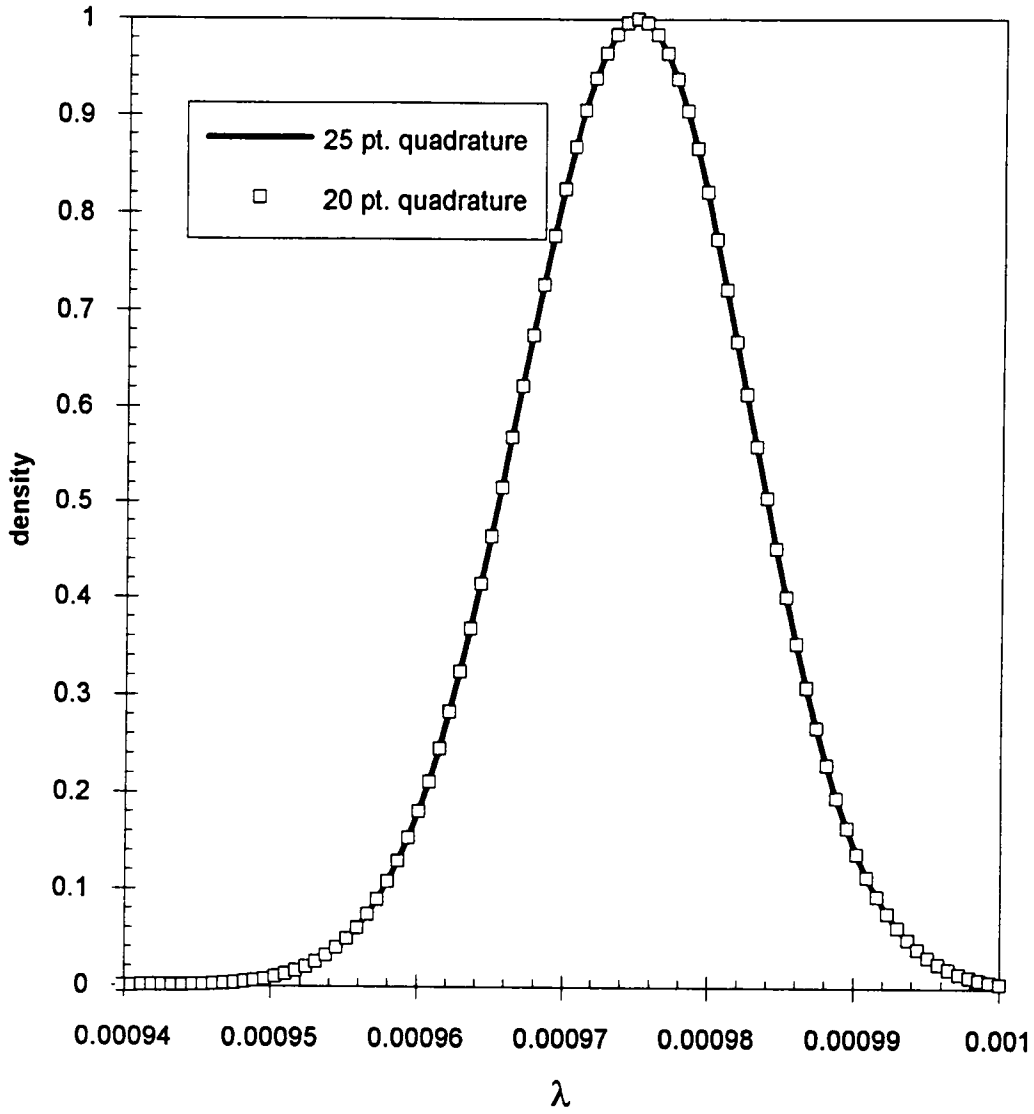

Figure 4.1 Marginal posterior density for λ for BALB/c females with lung tumors

tumors as the endpoint of interest. Notice that the twenty point Gauss-Legendre approximation yields visually the same results as the 25 point routine. The marginal posterior densities for λ for breast cancer and all causes of death are given in appendix 3 .

4.3 JOINT DENSITY FOR α, β, AND, ρ

Since the domain of λ ranges from zero to ∞, the limits of integration must cover the same domain. The joint posterior density for α, β, and ρ is obtained by analytically integrating equation 3.19 over the parameter λ . Equation 4.7 gives the joint posterior density for α, β, and ρ.

$$p(\alpha,\beta,\rho\,|\underline{t},\underline{d}) \propto \int_0^{\infty} p(\alpha,\beta,\rho,\lambda\,|\underline{t},\underline{d})\,d\lambda \qquad (4.6)$$

$$p(\alpha,\beta,\rho\,|\underline{t},\underline{d}) \propto \frac{\Gamma(n)\,\alpha^{n-1}\left(\prod_{i=1}^{n} t_i^{\alpha-1}\right) e^{\rho\beta\sum_{h=1}^{k_H} q_h d_h}\; e^{\beta\sum_{l=1}^{k_L} q_l d_l}}{\left(\sum_{i=1}^{M_0} t_i^{\alpha} + \sum_{l=1}^{k_L}\sum_{i=1}^{s_L} t_i^{\alpha} e^{\beta d_l} + \sum_{h=1}^{k_H}\sum_{i=1}^{s_H} t_i^{\alpha} e^{\rho\beta d_h}\right)^n} \qquad (4.7)$$

4.4 MARGINAL POSTERIOR DENSITIES FOR α, β, AND ρ

The marginal posterior densities for the parameters α, β, and ρ are obtained in a three step procedure. In the first step the bounds of the marginal densities are chosen. The upper (lower) bounds of the marginal posterior densities is defined as the point at which the mass to the left (right) of the lower (upper) bound can be considered negligible. The second step utilizes these bounds to determine upper and lower limits of integration. Once the upper and lower limits of integration are determined the "final" marginal posterior densities for the parameters are obtained. The final step verifies the result of step two.

All parameters have domains from zero to ∞. The limits of integration must include the domains of the parameters. A transformation is made to change the limits of integration from zero to ∞, to zero to one. The transformation is given by equations 4.8 and 4.9.

$$\alpha' = -\ln \alpha \qquad \beta' = -\ln \beta \qquad \rho' = -\ln \rho \tag{4.8}$$

where

$$d\alpha' = -\frac{1}{\alpha} d\alpha \qquad d\beta' = -\frac{1}{\beta} d\beta \qquad d\rho' = -\frac{1}{\rho} d\rho \tag{4.9}$$

Step one involves determining the limits of integration that are used when evaluating the "final" marginal posterior densities. The transformation for the two parameters that are to be integrated out are inserted into equation 4.7 . A thirty point Gauss-Legendre routine is then applied to the transformed equation while varying the

untransformed parameter of interest. This procedure yields a "preliminary" posterior density for the parameter of interest. This procedure is done again for the remaining two parameters yielding "preliminary" marginal posterior densities for each parameter.

Step two involves obtaining the final marginal posterior density for each parameter. The upper and lower bounds for each "preliminary" marginal posterior density are observed. These bounds become the new limits of integration for the corresponding parameter. For example: if the majority of the mass of the "preliminary" marginal posterior density for α was between 5.2 and 6.2, then the limits of integration for α would be from 5.0 to 6.4. This method allows equation 4.7 to be used directly in the Gauss-Legendre approximation. Also, since more Gauss points are located where the density peaks, the Gauss-Legendre procedure is more accurate. The weight-abscissa pairs are once again evaluated using "Mathematica". The final marginal posterior densities are evaluated by numerically integrating two of the parameters using the new limits of integration while varying the last parameter over a range of values.

The third and final step in obtaining the marginal density for each parameter is verifying the results of the thirty point routine. A twenty five point Gauss-Legendre method using the same limits of integration is applied to the untransformed joint density. Plots of the two independent methods are overlaid on the same graph yielding results that are within a line-width of one another .

The marginal posterior density for α may now be obtained by equation 4.10

$$p(\alpha \mid t,d) \propto \sum_{i=1}^{n} \sum_{j=1}^{n} p(\alpha, \beta_i, \rho_j \mid t,d) w_i w_j' \qquad (4.10)$$

where w_i and w'_j are the i^{th} and j^{th} weight, β_i and ρ_j are the i^{th} and j^{th} abscissa, and n is the number of weight-abscissa pairs. The weight-abscissa pairs are generated by "Mathematica" with the limits of integration coming from the preliminary marginal densities of β and ρ. Thirty quadrature points are used to obtain the marginal posterior density for α. This result is then verified by using the same limits of integration but reducing the number of Gauss points to twenty five. Figure 4.2 gives the marginal posterior density for α using lung tumors as the endpoint of interest. Notice that α is clearly greater than one. This indicates that the hazard rate for BALB/c females using lung tumors as the desired endpoint of interest is increasing with time. This corresponds with the non-parametric estimates that were obtained in chapter 2.

The marginal posterior density for β is obtained in a similar manner. The limits of integration used in obtaining the "final" marginal posterior density come from observing the bounds of the preliminary posterior densities for α and ρ. The marginal posterior density for β is obtained by using equation 4.11. Figure 4.3 gives the marginal

$$p(\beta \mid t,d) \propto \sum_{i=1}^{n} \sum_{j=1}^{n} p(\alpha_i, \beta, \rho_j \mid t,d) w_i w_j \qquad (4.11)$$

posterior density for the parameter β. Notice that β is clearly greater than zero indicating that as dose increases the lung tumor rate increases in dose for constant time.

The parameter that is of most interest for this investigation is ρ. This parameter gives an estimate of the DREF. As stated previously in chapter three, if ρ is greater than

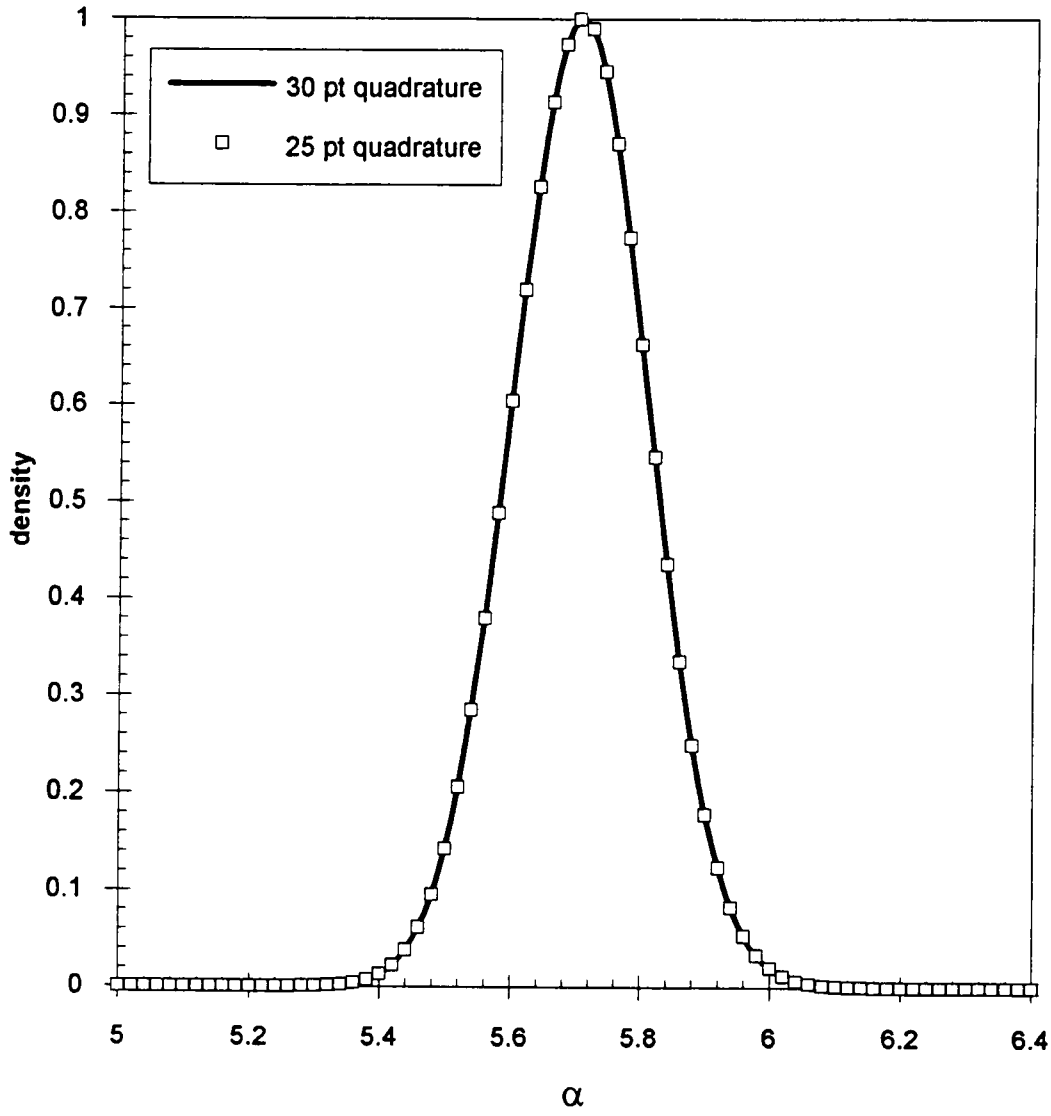

Figure 4.2 Marginal posterior density for α for Balb/c females with lung tumors

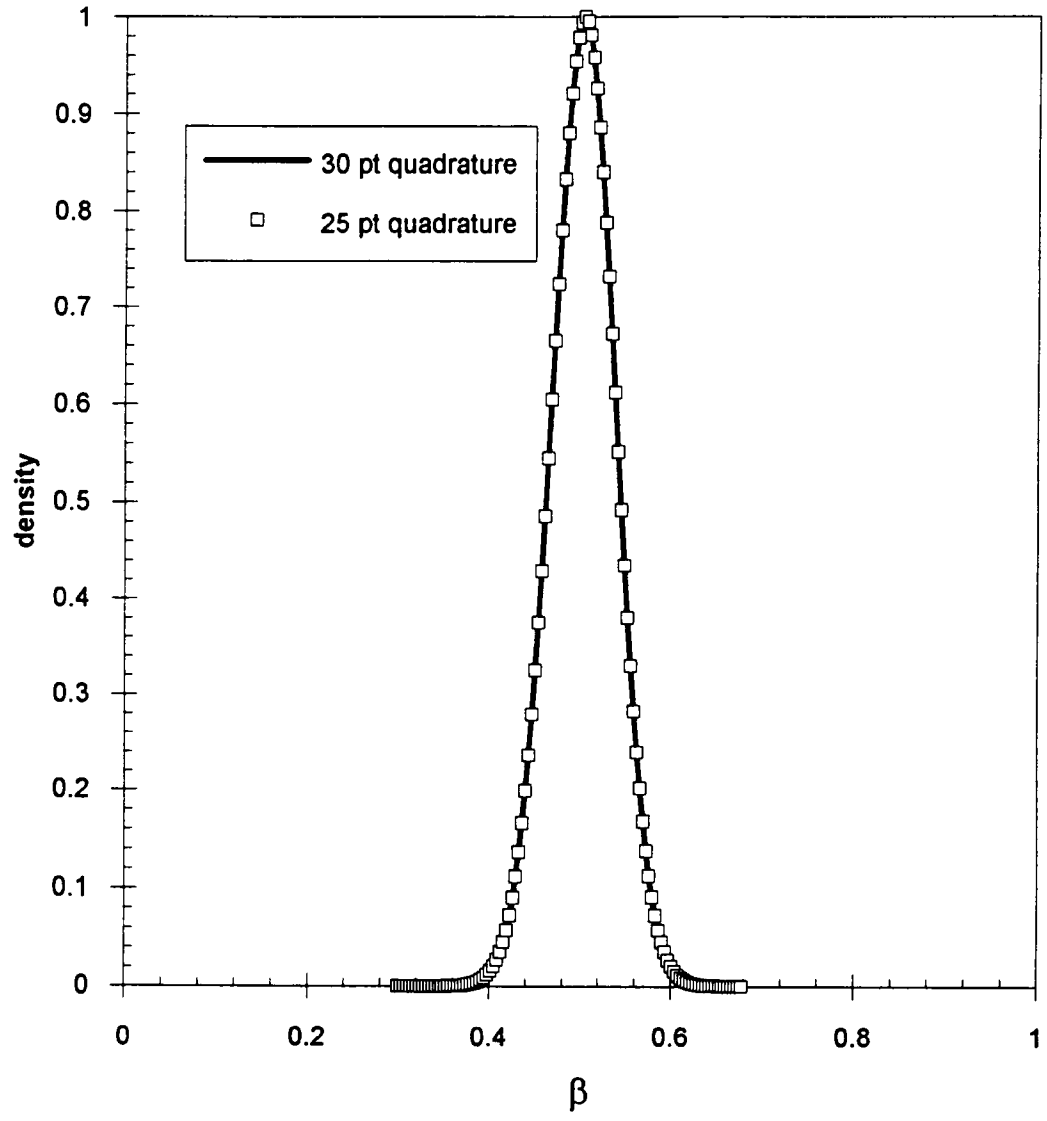

Figure 4.3 Marginal posterior density for β for BALB/c females with lung tumors

one then a dose delivered at a high dose-rate is more effective at causing the endpoint of interest than the dose delivered at a low dose-rate. Consequently if ρ is less than one, low dose-rate irradiation is more effective at causing the desired endpoint of interest.

The estimation of the parameter ρ is done in the same manner as α and β. The limits of integration are again obtained by observing the bounds of the preliminary posterior densities for α and β. A thirty point Gauss-Legendre routine is used to approximate the integrals for α and β and a twenty five point routine is used to verify the results of the first. Equation 4.12 gives the expression for the marginal posterior density for the parameter ρ.

$$p(\rho \mid \underline{t}, \underline{d}) \propto \sum_{i=1}^{n} \sum_{j=1}^{n} p(\alpha_i, \beta_j, \rho \mid \underline{t}, \underline{d}) w_i w_j \qquad (4.12)$$

Figure 4.4 shows the marginal posterior density for the dose-rate parameter ρ using Balb/c females with lung tumors. Notice that ρ is clearly less than one, indicating that the low dose-rate radiation exposure is more effective at causing lung tumors. Two other posterior densities for ρ are given in figures 4.5 and 4.6. Figure 4.5 gives the marginal posterior density for ρ with breast cancer as the endpoint of interest. Notice that the posterior density for ρ shifts from less than one for lung tumors to greater than one for breast cancer. Figure 4.6 gives the marginal posterior density for ρ for all causes of death. This distribution gives the overall dose-rate effect for the Balb/c female mice. Notice the marginal posterior density for ρ is clearly greater than one indicating that the high dose-rate radiation exposures are more effective at causing death than the low dose-rate radiation.

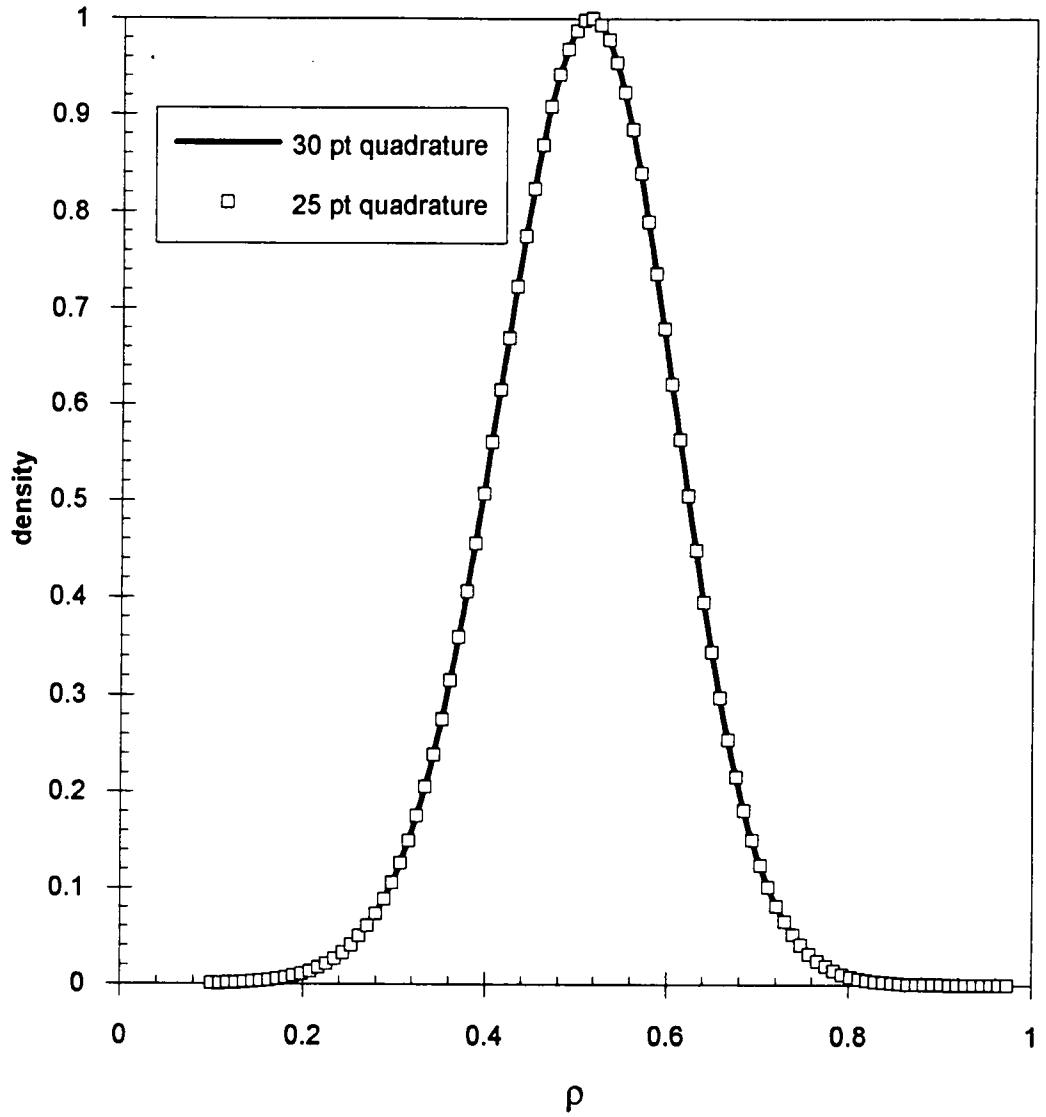

Figure 4.4 Marginal posterior density for ρ for Balb/c females with lung tumors

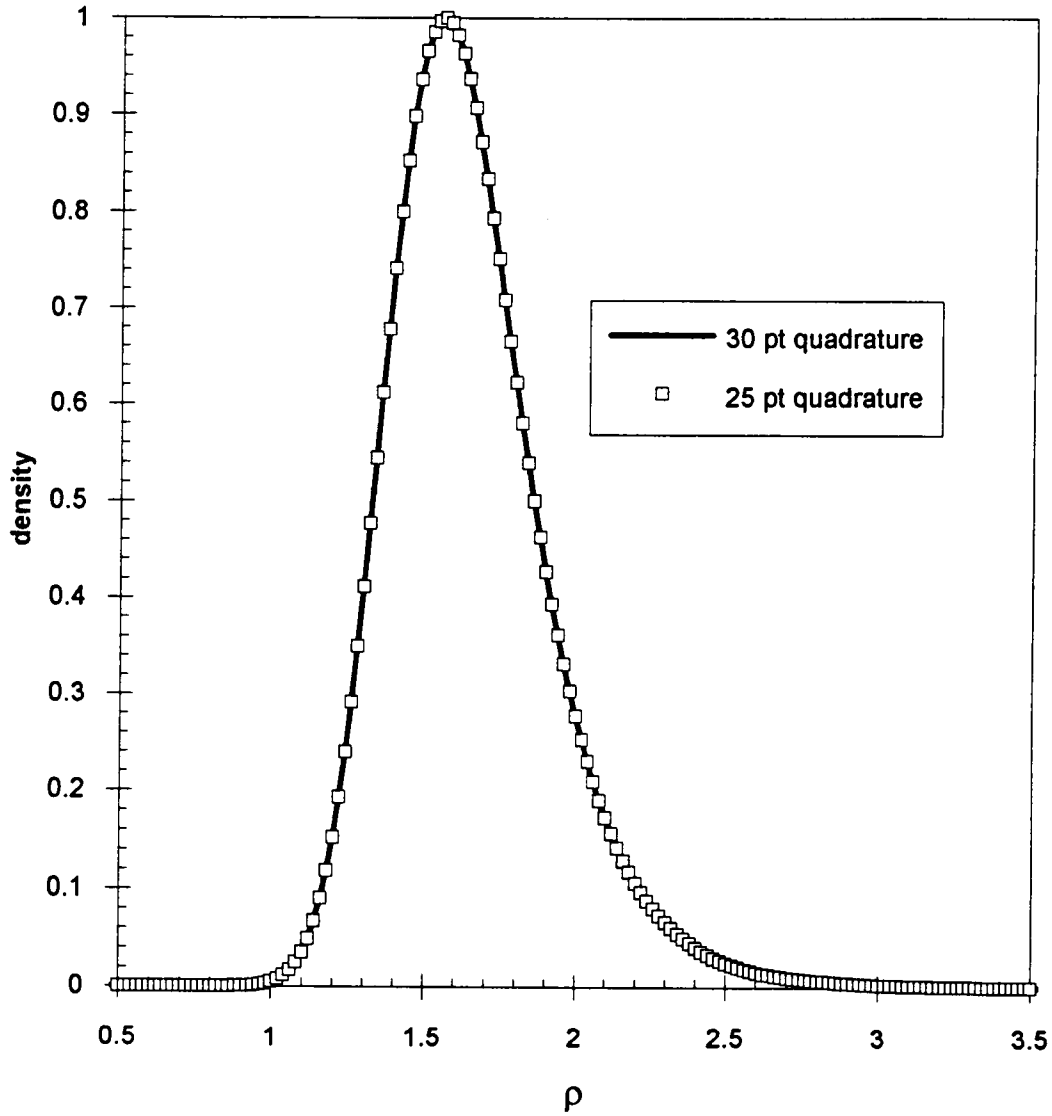

Figure 4.5 Marginal posterior density for ρ for BALB/c females with breast cancer

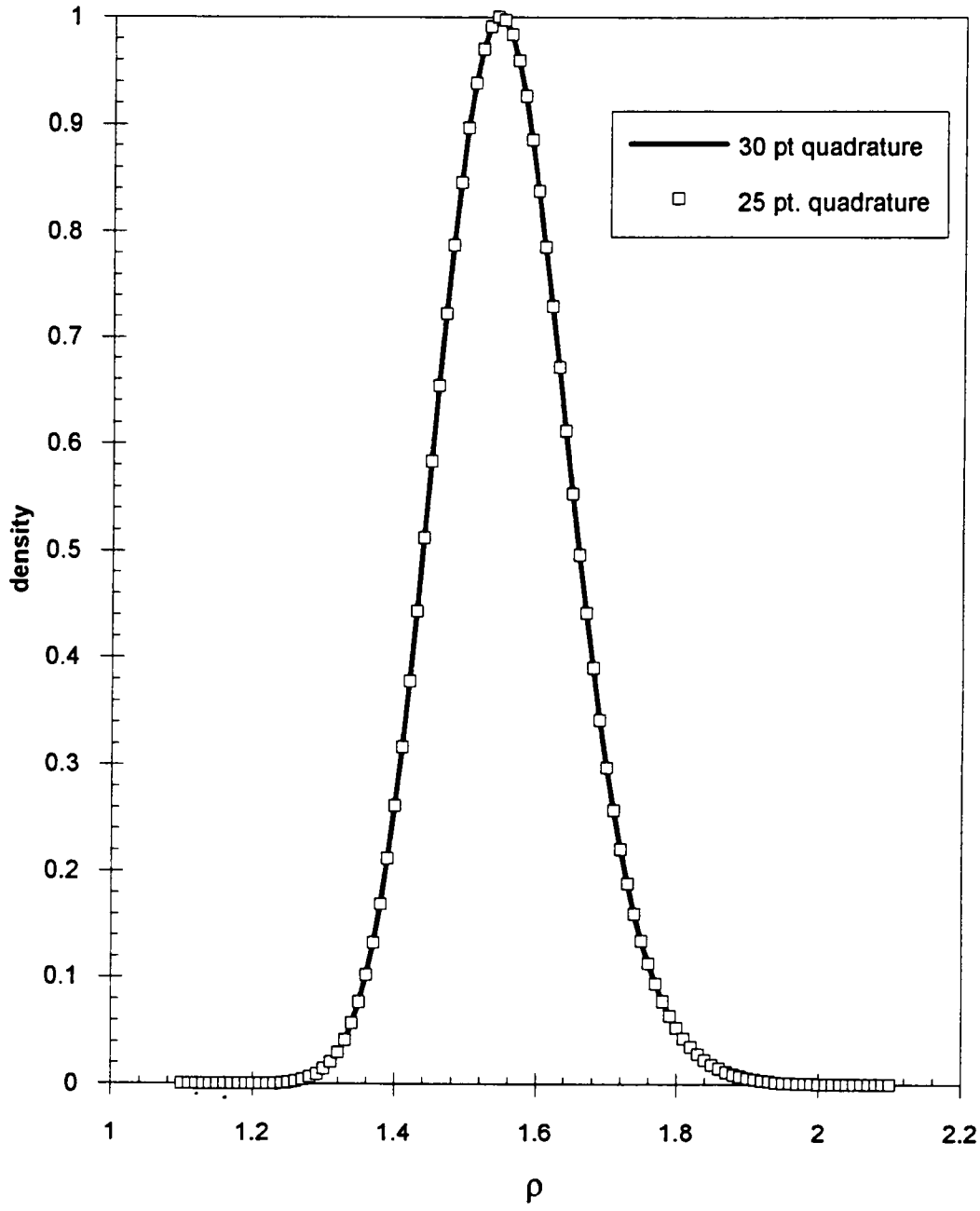

Figure 4.6 Marginal posterior density for ρ for BALB/c females for all causes of death

4.5 SUMMARY

This chapter detailed the techniques used to obtain marginal posterior densities for each parameter. The marginal posterior density for the scale parameter λ was obtained by a three-dimensional Gauss-Legendre approximation to the integrals of α, β, and ρ. The location of the marginal posterior density for the time dependence parameter α was greater than one indicating an increasing lung tumor rate with time. The location of the marginal posterior density for the dose parameter β was greater than zero indicating that the lung tumor rate increases with dose when time is held fixed. Finally the location of the marginal posterior density for the dose-rate parameter ρ varied from less than one to greater than one depending upon the cause of death.

CHAPTER 5

SUMMARY AND CONCLUSIONS

This thesis described the techniques used to estimate dose-rate effectiveness factors using Bayesian techniques. The DREFs are necessary when determining human cancer risks after prolonged exposure to radiation.

The high dose-rate mice had radiation delivered at levels of 0.5 Gy and 2.0 Gy at 0.43 Gy/min. The low dose-rate mice were given radiation at 0.5 Gy, 1.0 Gy, and 2.0 Gy at a dose-rate of 0.083 Gy/day while the remaining mice were sham irradiated. All of the mice that were used in the data analysis were BALB/c females

The estimation began by plotting non-parametric estimates of the cumulative hazard versus time and the total time on test versus fraction failed. The software developed for the non-parametric analysis was written using FORTRAN on an IBM PC. Non-parametric estimation indicated an increasing hazard rate for every endpoint that was studied. Based on the non-parametric results, a relative risk Weibull model was chosen for the parametric analysis.

Bayes' Theorem was applied to the likelihood to a yield joint posterior density for the parameters. Uniform prior densities were used for the paremeters α, β, and ρ. The prior density for the parameter λ was taken to be λ^{-1}. This prior density may be considered locally uniform when the likelihood is sharply peaked. All of the marginal

posterior densities for the model parameters: λ, α, β, and ρ were calculated in a three step procedure using Gauss-Legendre numerical integration routines. The programs necessary for the numerical evaluations of the integrals were created using "Mathematica." The results show for the first time the distribution for the dose-rate effectiveness factor which quantifies the residual uncertainty about ρ. This probability density may be further updated if more data should become available.

The results from the parametric estimation indicated that the hazard rate is increasing with time for all of the causes looked at. The dose parameter β was clearly greater than zero indicating that as dose increases the cumulative hazard increases if time is held fixed. Finally, the analyses of ρ indicated that the DREF is dependent upon the cause of death.

Results from the analyses indicated that ρ is less than one for lung tumors, signifying that high dose-rate irradiation is less effective at causing lung tumors than low dose-rate radiation. The parametric estimate for ρ using breast cancer as the endpoint of interest was greater than one indicating that high dose-rate irradiation is more effective at causing breast cancer than low dose-rate irradiation for a fixed dose. Finally, the parametric estimation indicated that ρ was greater than one when all causes of death were chosen as the endpoint of interest. This indicates that high dose-rate irradiation is overall more effective at shortening the lives of the mice than low dose-rate irradiation.

REFERENCES

REFERENCES

1. National Council on Radiation Protection and Measurements. Report No. 64 "Influences of Dose and its Distribution in Time on Dose-Response Relationships for Low -LET Radiations." Washington D.C. 1980.

2. BEIR V. "Health Effects of Exposure to Low Levels of Ionizing Radiation," Commision on Life Sciences, National Research Council, National Academy Press, Washington D.C. 1990.

3. BEIR IV. "Health Risks of Radon and Other Internally Deposited Alpha-Emitters" Commision on Life Sciences, National Research Council, National Academy Press, Washington D.C. 1988.

4. Du Mouchel, W., Groer, P.G., "A Bayesian Methodology for Scaling Radiation Studies from Animal to Man." Health Physics 57, p. 411-418, 1989.

5. Storer, John B., Mitchell, T.J., Fry, R.J.M., "Extrapolation of the Relative Risk of Radiogenic Neoplasms Across Mouse Stains and to Man." Radiation Research, 114, p. 331-353, 1988.

6. Ullrich, R.L., Storer, J.B., "Influence of Gamma Irradiation on the Development of Neoplastic Disease in Mice. III Dose-Rate Effects." Radiation Research, 80, p. 325-342, 1979.

7. Nelson, W., "Hazard Plot Analysis of Incomplete Failure Data." IEEE Symposium. on Reliability, p. 391-403, 1969.

8. Barlow, R.E., Campo,R., "Total Time on Test Processes and Applications to Failure Data Analysis.", Reliability and Fault Tree Analysis, p. 451-481, Barlow, R.E. et al. eds., SIAM, Philidelphia, 1975.

9. Davis, Philip J., Rabinowitz, Philip., "Methods of Numerical Integration." Academic Press, New York, 1975.

10. Mathematica 2.2 for Sun Spark, Wolfram Research Inc., 100 Trade Center Drive Champaign, Il., 1988.

APPENDICES

APPENDIX 1

COMPUTER PROGRAMS

A1.1 INTRODUCTION

Appendix 1. contains all of the computer programs used in the non-parametric and parametric analysis. A1.2. contains the FORTRAN code used to determine the Nelson estimate of the cumulative hazard and standard deviation. A1.3 contains the FORTRAN code developed to determine the total time on test. A1.4. and A1.5. contain "Mathematica" programs used to obtain the weight-abscissa pairs for the n point Gauss-Legendre routine. These subsections also include the programs necessary to calculate the Gauss-Legendre approximations to the integrals.

A1.2 THE NELSON ESTIMAT0R

```
c     This program will do the calculations for the Nelson estimate
      CHARACTER*20 FILNAM
      REAL HZ,RR,NEL,USD,LSD,S,SD1,SD
      INTEGER J,N,TIM,IND
      WRITE(*,*)'NAME OF FILE (INCLUDE EXTENSION)'
      READ '(A)',FILNAM
      OPEN(10,FILE=FILNAM,STATUS='OLD')
      OPEN(20,FILE='RES.DAT',STATUS='UNKNOWN')
      REWIND(10)
c     This part of the program calculates reads how many data points there are
      N=0
555   READ(10,*,END=95)TIM,RR,IND
      N=N+1
      GOTO 555
95    REWIND(10)
      NEL=0
      SD=0
c     This part of the program calculates the cumulative hazard and the
c     standard deviation.
      DO 1 J=1,N
```

```
      READ (10,*,END=96)TIM,RR,IND
      IF (IND.EQ.1) THEN
      HZ=1/RR
      S=(1/RR)**2
      SD=SD+S
      NEL=NEL+HZ
      SD1=(SD)**0.5
      USD=NEL+SD1
      LSD=NEL-SD1
      WRITE(*,*)TIM,NEL,USD,LSD
      WRITE(20,60)TIM,NEL,USD,LSD
      END IF
60    FORMAT(1X,I4.4,E13.6,E13.6,E13.6,E13.6)
1     CONTINUE
      CLOSE(10)
      WRITE(*,*)'END OF PROGRAM'
96    WRITE(*,*)'FINAL RESULTS ARE IN RES.DAT'
      CLOSE(20)
      STOP
      END
```

A2.3 THE TOTAL TIME ON TEST PLOT

```
c     THIS PROGRAM WILL CALCULATE THE  TOLTAL TIME ON TEST

c     PART 1 READ IN THE DATA FILE
      CHARACTER*20 FILNAM
      INTEGER TTT,TIM,RNK
     WRITE(*,*)'NAME OF FILE (INCLUDE EXTENSION)'
     READ '(A)',FILNAM
     OPEN(10,FILE=FILNAM,STATUS='OLD')
     OPEN(20,FILE='TTT.DAT',STATUS='UNKNOWN')
     REWIND(10)
     N=0
 555  READ(10,*,END=97)TIM,RNK,IND
      N=N+1
      IF(IND.EQ.1)THEN
     nmk=RNK
     END IF
     GO TO 555
c     PART 2  CALCULATE THE TOTAL TIME ON TEST
 97   REWIND(10)
     TTT=0
```

```
      nxt=0
      ntim=0
     DO 1 J=1,N
     READ (10,*,END=96)TIM,RNK,IND
     IF (IND.EQ.0)THEN
     TTT=TIM+ttt
     ELSE
     ndif=nrnk-rnk
     TTT=TTT+tim*(ndif+1)-nxt+ntim
     ntim=tim
     nxt=tim*(ndif+1)
     WRITE(*,*)TTT
     WRITE(20,*)TTT
     ENDIF
1    continue
96     CLOSE(10)
     CLOSE(20)
     WRITE(*,*)'END PROGRAM'
     WRITE(*,*)'RESULTS ARE IN TTT.DAT'
     STOP
     END
```

A1.4 TWO-DIMENSIONAL GAUSS-LEGENDRE ROUTINE

Note: 1. a and b are the limits of integration for each dimension

2. n is the number of weight-abscissa pairs

3. pr[α, β, ρ] is the function for the 2-dimensional routine while varying the parameter ρ along the interval from a' to b' in increments of c'

Calculation of the weight-abscissa pairs

```
<<NumericalMath`GaussianQuadrature`

mx=GaussianQuadratureWeights[n,a,b];

h=Transpose[mx];

no=h[[1]];

wt=h[[2]];

Do[d[i]=n[[i]],{i,1,n}];

Do[c[i]=w[[i]],{i,1,n}];

mx=GaussianQuadratureWeights[n,a,b];

ht=Transpose[mx];

no=ht[[1]];

wt=ht[[2]];
```

The Gauss-Legendre routine for 2-dimensions

```
Do[For[i=1,i<n+1,i++,z[i]=Apply[Plus,

(pr[d[i],no,ρ ]*wt)*c[i]]];Print[FortranForm[Sum[

z[i],{i,1,n}]]],{ρ, a', b' c'}]
```

A1.5. 3-DIMENSIONAL GAUSS-LEGENDRE ROUTINE

Note: 1. a and b are the limits of integration for each dimension

2. n is the number of weight-abscissa pairs

3. s[α, β, λ, ρ] is the function that is integrated in the 3-dimensional routine while varying the parameter ρ over the range of a' to b' in increments of c'

Calculation of the weight-abscissa pairs

```
<<NumericalMath`GaussianQuadrature`
nx=GaussianQuadratureWeights[n,a,b];
h=Transpose[nx];
ab=h[[1]];
w=h[[2]];
Do[d[i]=n[[i]],{i,1,n}];
Do[c[i]=w[[i]],{i,1,n}];
mx=GaussianQuadratureWeights[n,a,b];
ht=Transpose[mx];
no=ht[[1]];
we=ht[[2]];
Do[g[j]=no[[j]],{j,1,n}];
Do[e[j]=we[[j]],{j,1,n}];
mx=GaussianQuadratureWeights[n,a,b];
```

```
ht=Transpose[mx];

nd=ht[[1]];

wt=ht[[2]];
```

The Gauss-Legendre routine for 3-dimensions

```
Do[For[j=1,j<n,j++,For[i=1,i<n,i++,z[j,i]=Apply[Plus,

(s[d[i],nd,g[j]]*wt)*c[i]*e[j]]]];Print[FortranForm[Sum[

z[j,i],{j,1,n},{i,1,n}]]],{ρ, a', b', c' }]
```

APPENDIX 2.

NON-PARAMETRIC ESTIMATES

A2.1. INTRODUCTION

Appendix 2 contains the figures for all of the non-parametric estimates not covered in the main section of the thesis. A2.2 contains all of the lung tumor hazard plots not presented in chapter two. A2.3 contains the lung tumor total time on test plots not covered in chapter two. A2.4 and A2.5 contains all the breast cancer hazard and total time on test plots for Balb/c females. A2.6 and A2.7 contains all the life shortening hazard and total time on test plots for Balb/c females.

A2.2 NELSON'S ESTIMATE OF THE CUMULATIVE HAZARD FOR LUNG TUMORS

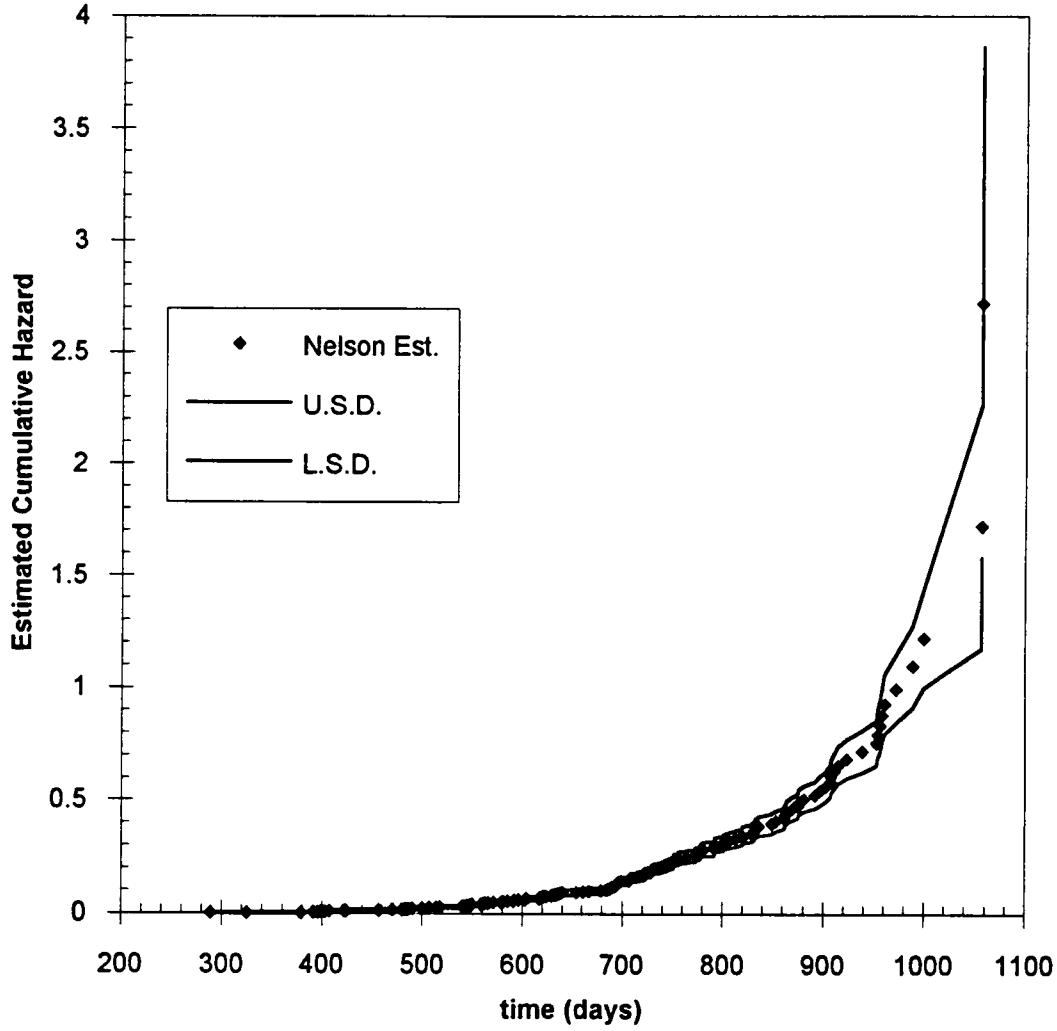

Figure A2.1 Nelson's estimate of the cumulative hazard vs. time for BALB/c females with lung tumors: 0.5 Gy @ 0.4 Gy/min

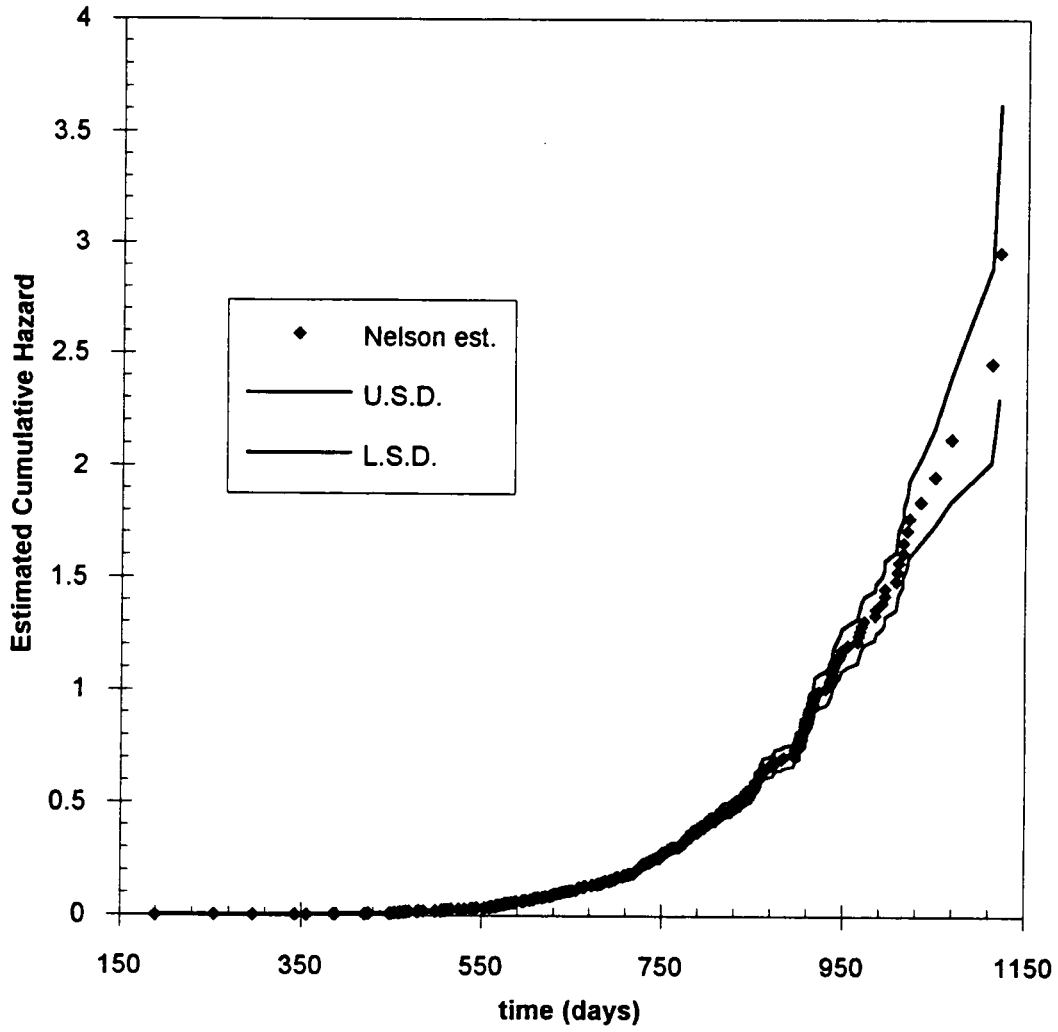

Figure A2.2 Nelson's estimate of the cumulative hazard vs. time for BALB/c females with lung tumors: 0.5 Gy @ 0.083 Gy/day

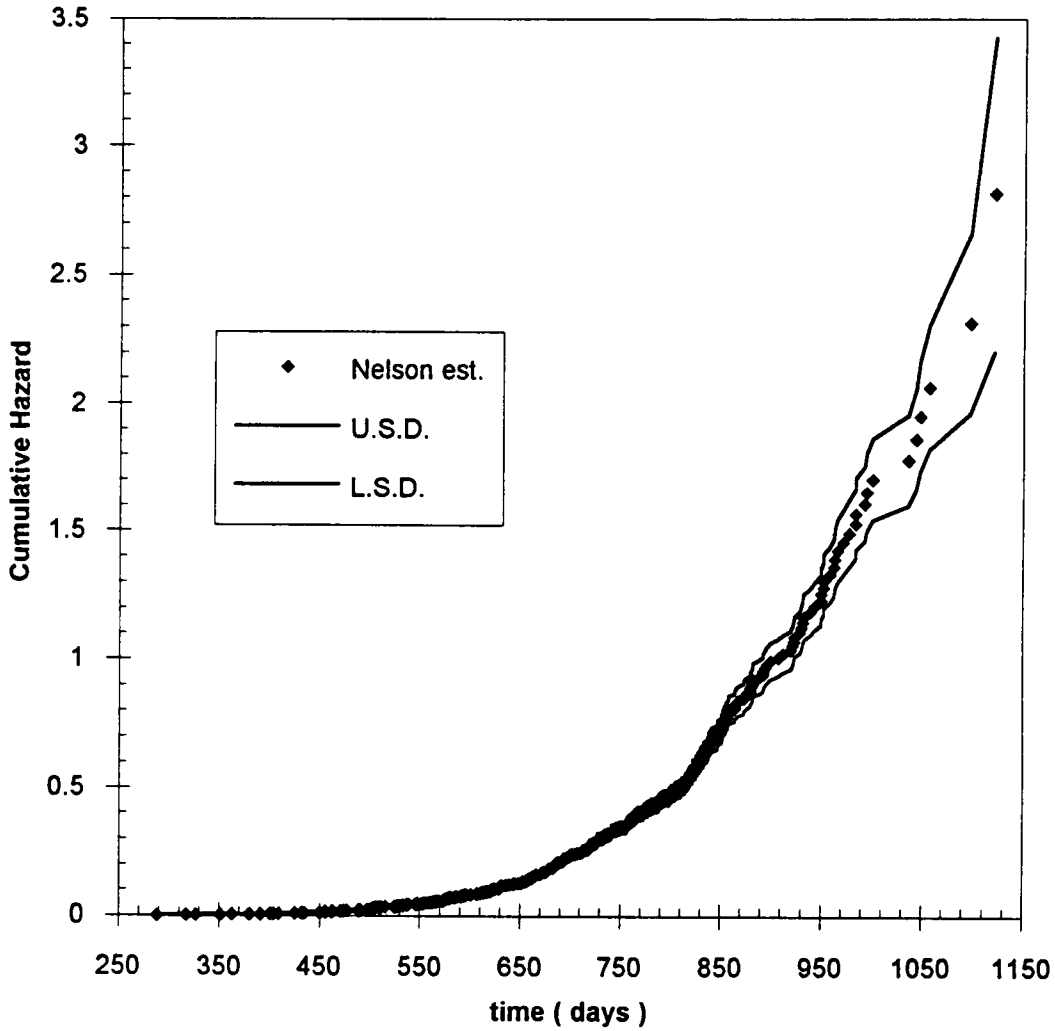

Figure A2.3 Nelson's estimate of the cumulative hazard vs. time for Balb/c females with lung tumors: 1.0 Gy @ 0.083 Gy/day

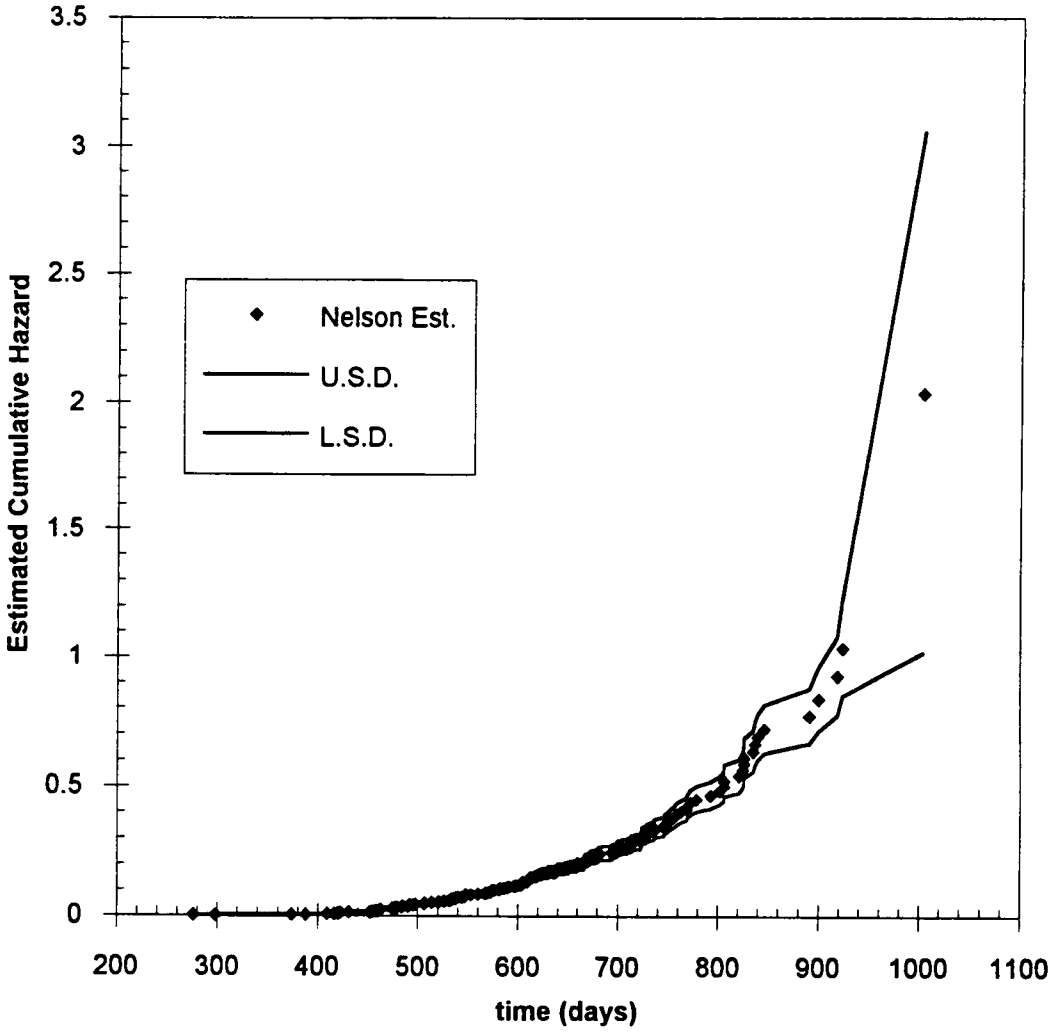

Figure A2.4 Nelson's estimate of the cumulative hazard vs. time for BALB/c females with lung tumors: 2.0 Gy @ 0.4 Gy/min

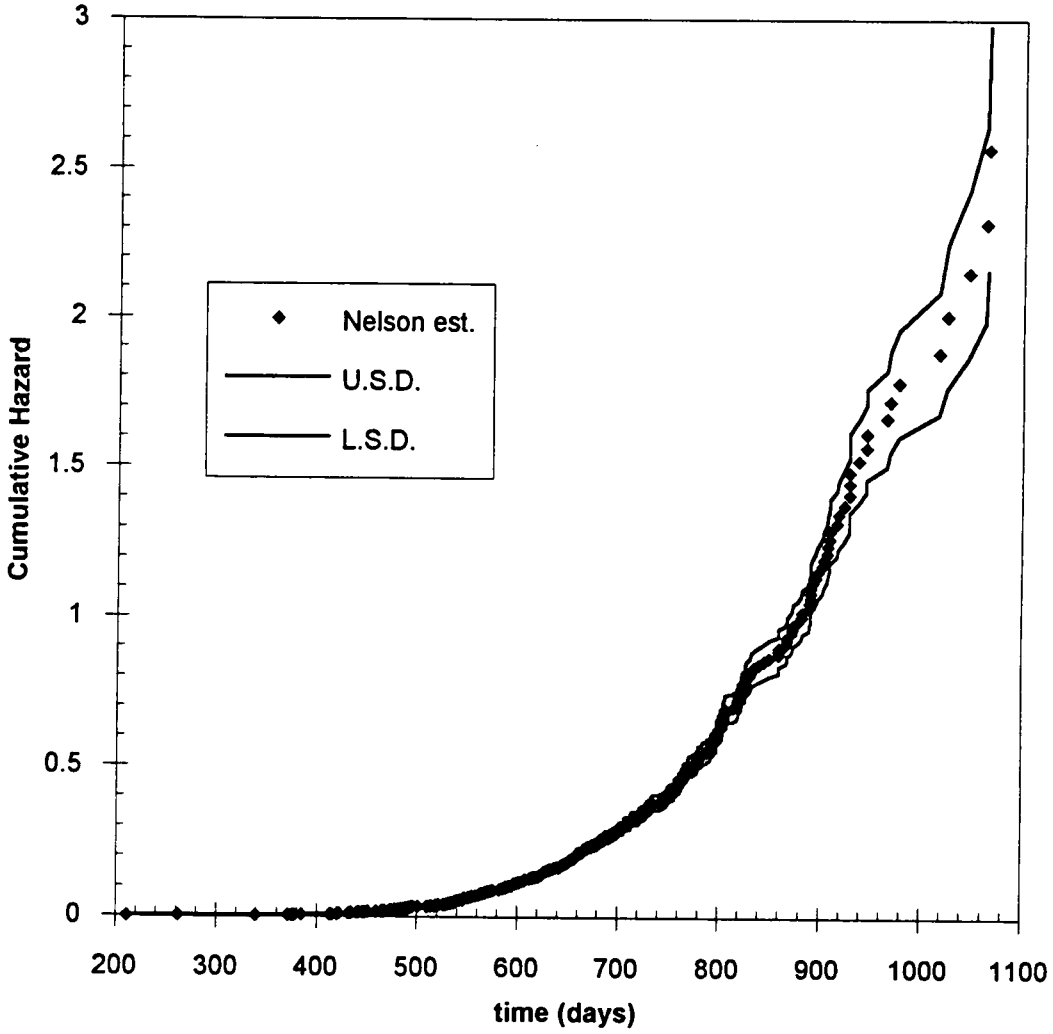

Figure A2.5 Nelson's estimate of the cumulative hazard vs. time for BALB/c females with lung tumors: 2.0 Gy @ 0.083 Gy/day

A2.3 TOTAL TIME ON TEST PLOTS FOR LUNG TUMORS

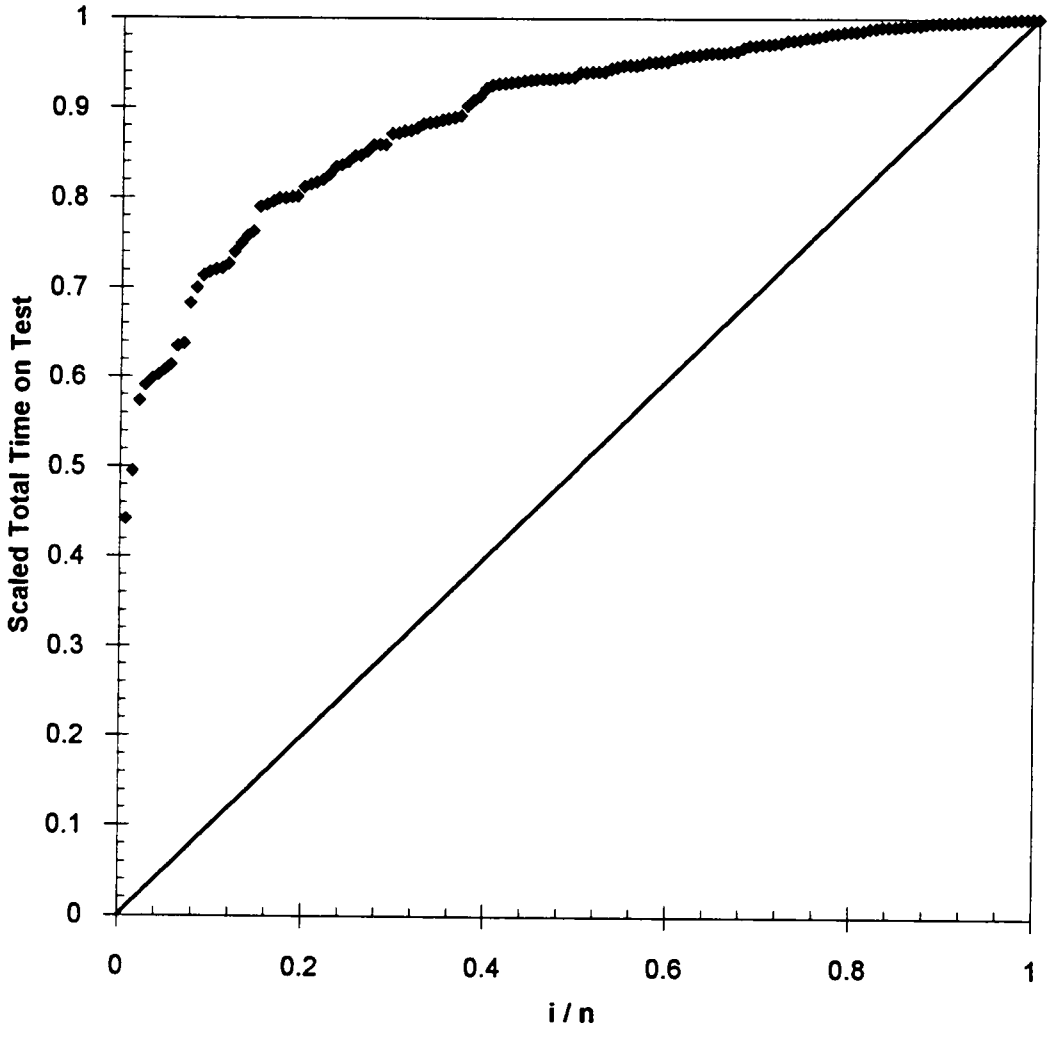

Figure A2.6 Scaled total time on test vs. fraction failed for BALB/c females with lung tumors: 0.5 Gy @ 0.4 Gy/min

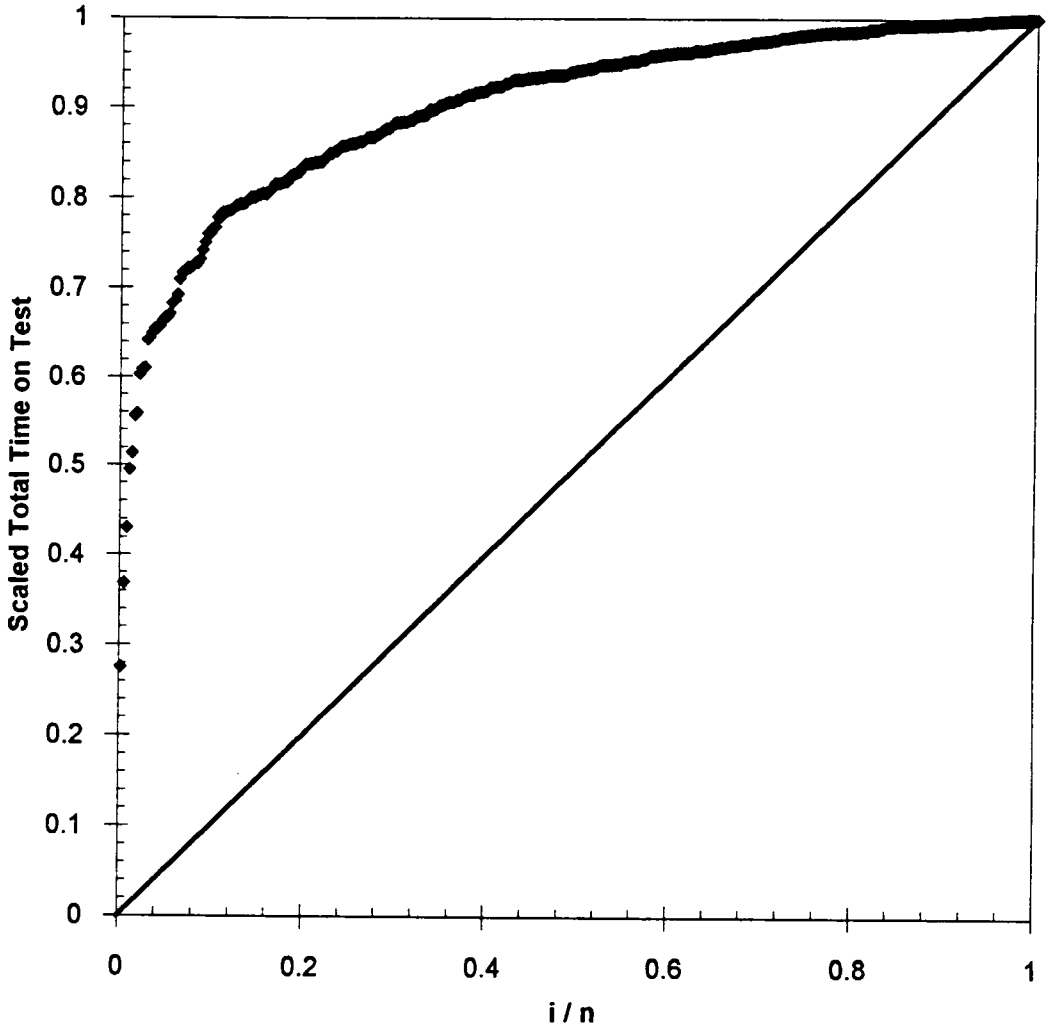

Figure A2.7 Scalced Total Time on Test vs. fraction failed for BALB/c females with lung tumors: 0.5 Gy, 0.083 Gy/day

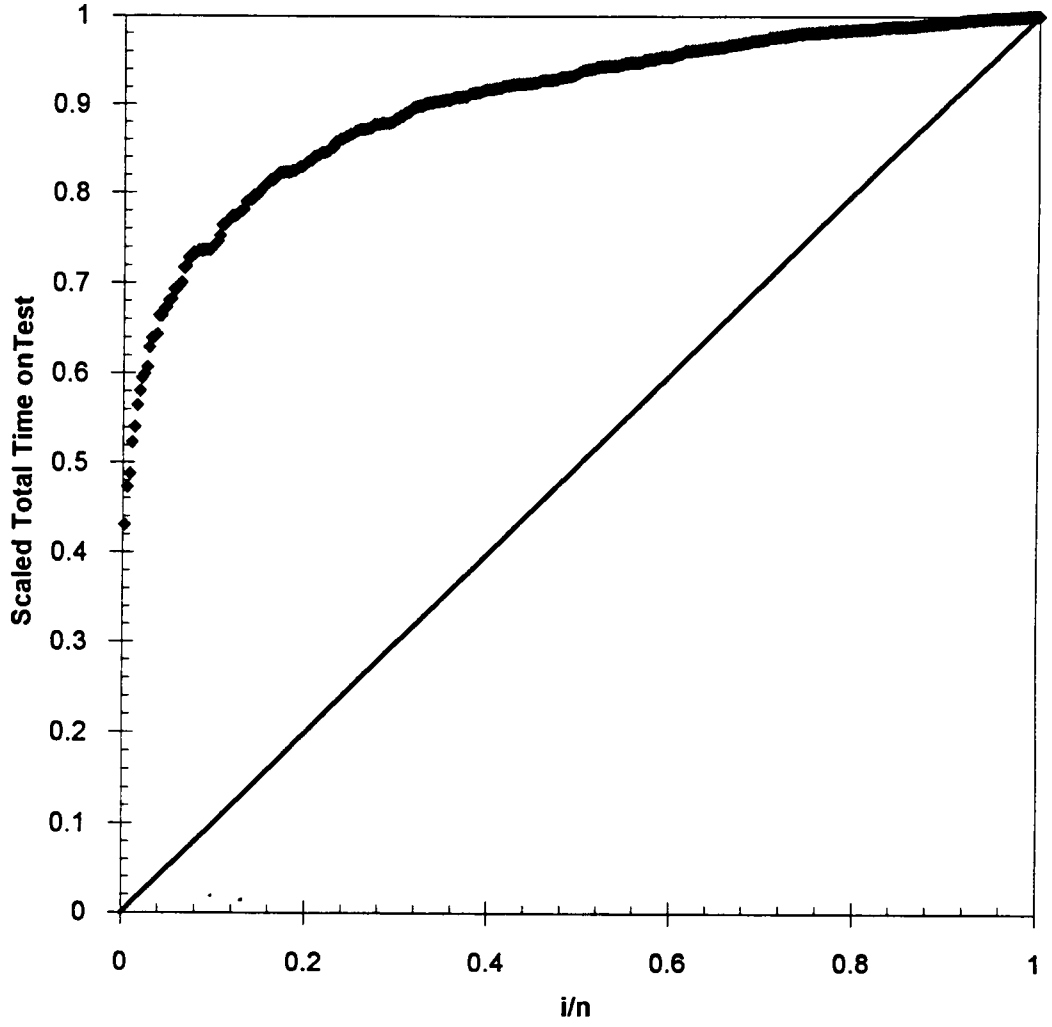

Figure A2.8 Scaled total time on test vs. fraction failed for BALB/c females with lung tumors: 1.0 Gy, 0.083 Gy/day

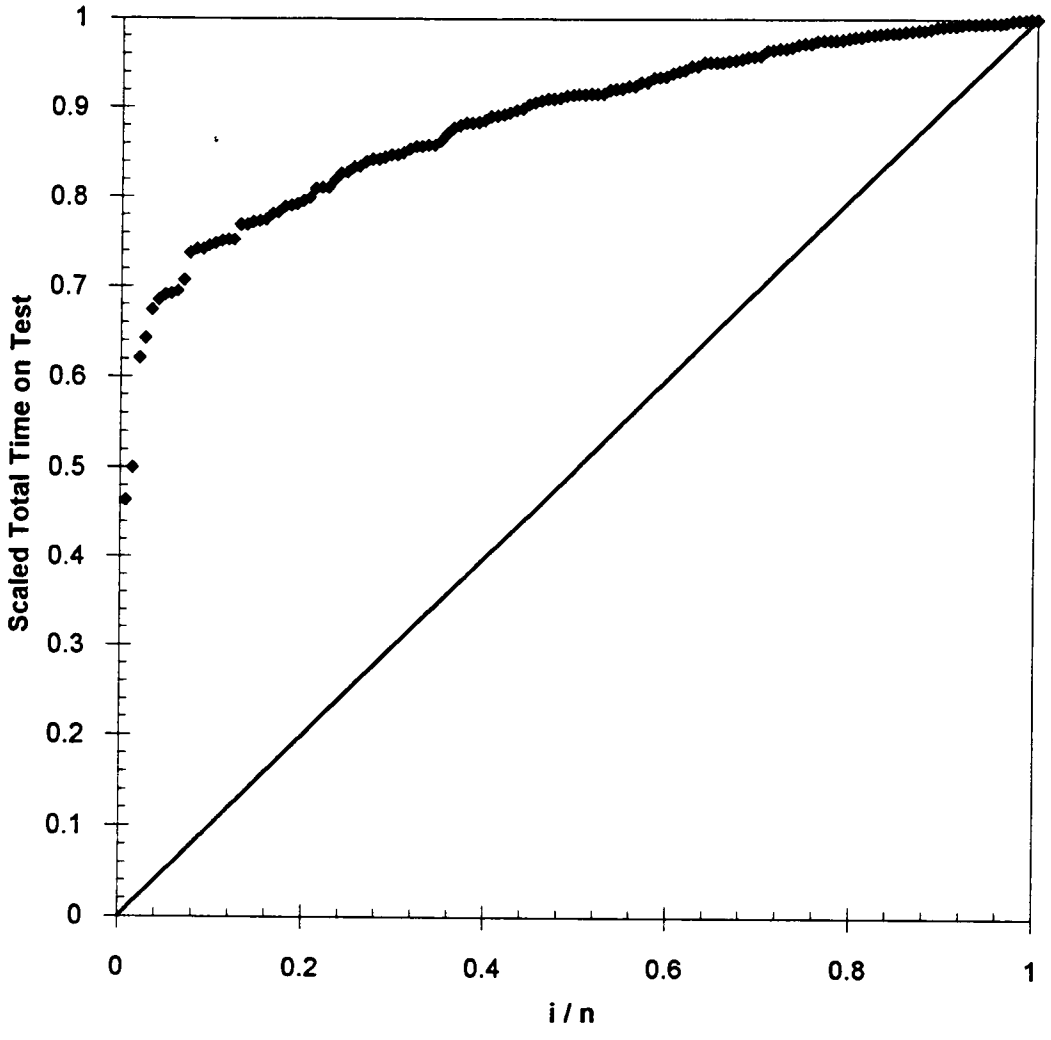

Figure A2.9 Scaled total time on test vs. fraction failed for BALB/c females with lung tumors: 2.0 Gy, 0.4 Gy/min

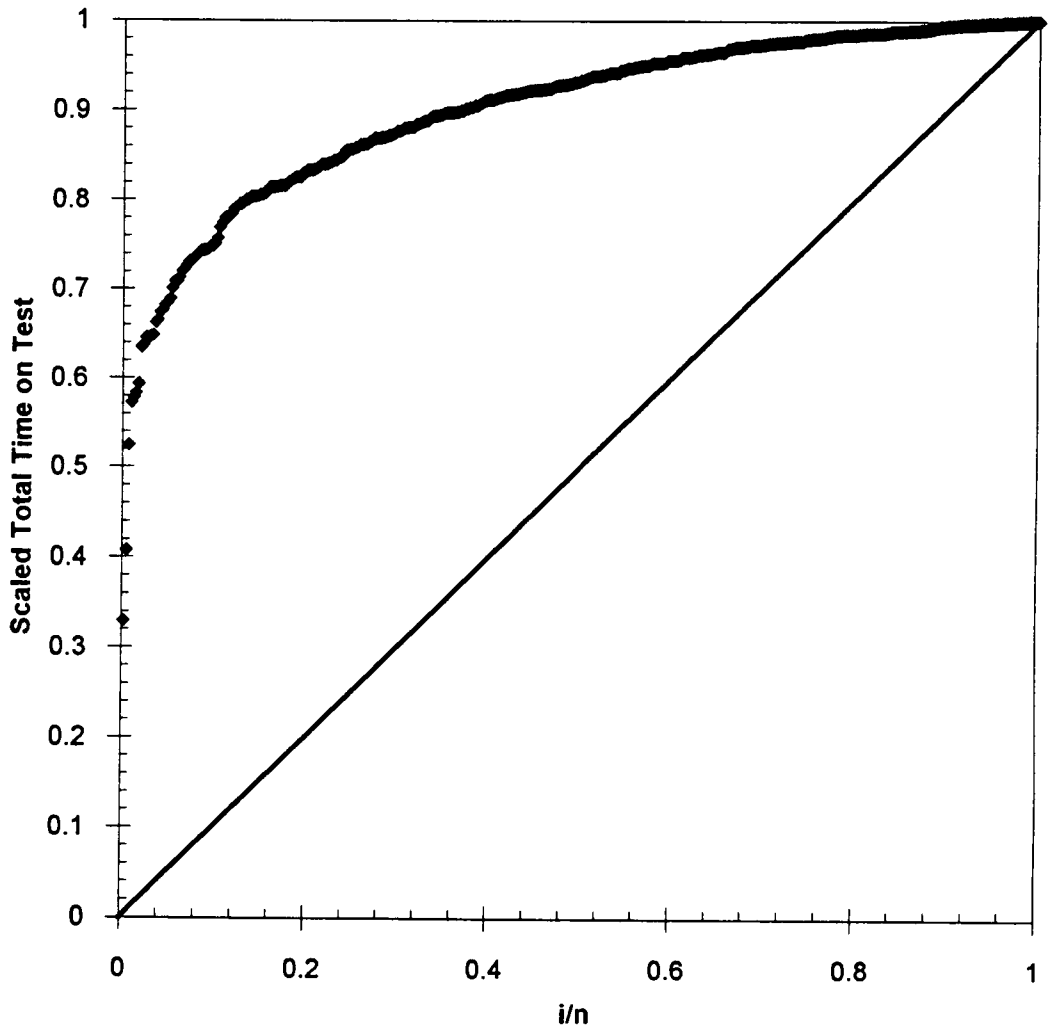

Figure A2.10 Scaled total time on test vs. fraction failed for BALB/c females with lung tumors: 2.0 Gy, 0.083 Gy/day

A2.4 NELSON'S ESTIMATE OF THE CUMULATIVE HAZARD FOR BREAST CANCER

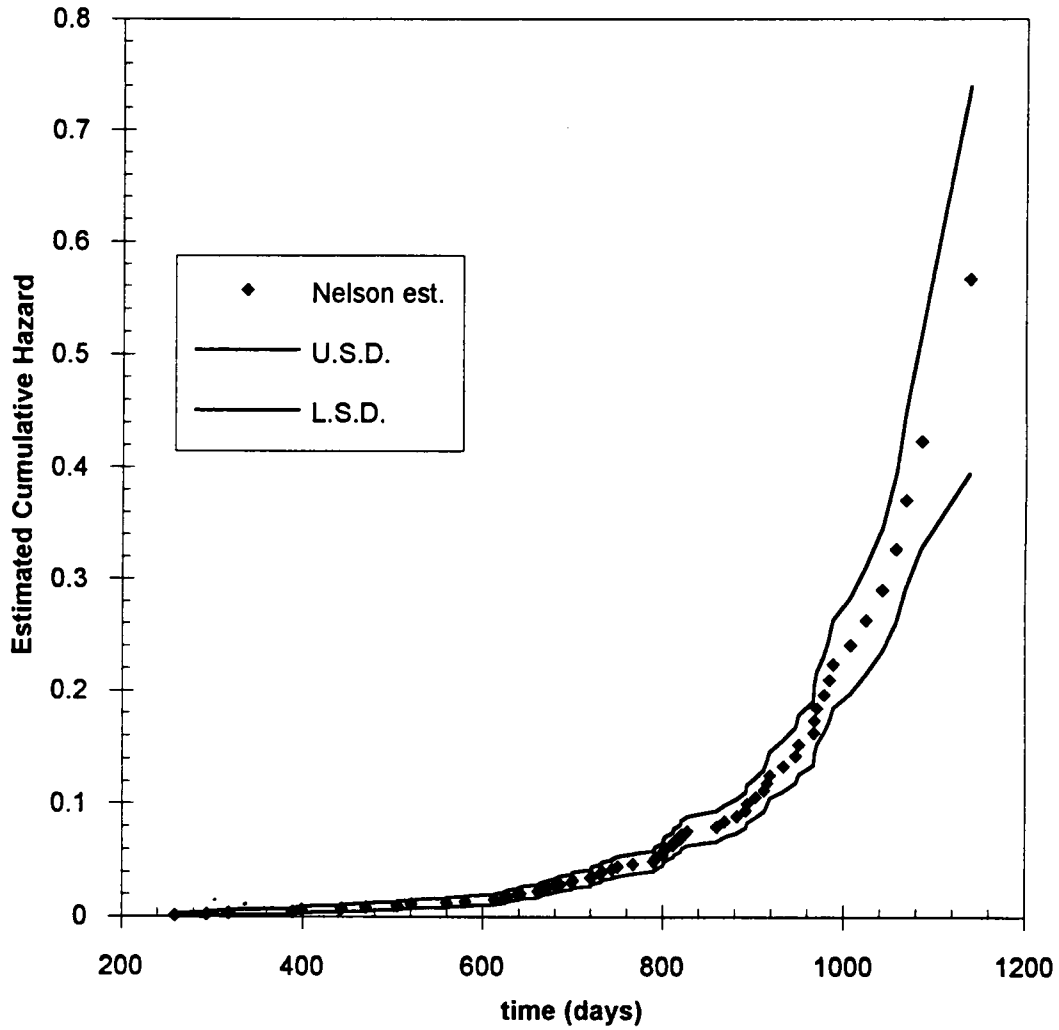

Figure A2.11 Nelson's estimate of the cumulative hazard vs time for BALB/c females with breast cancer: Unexposed

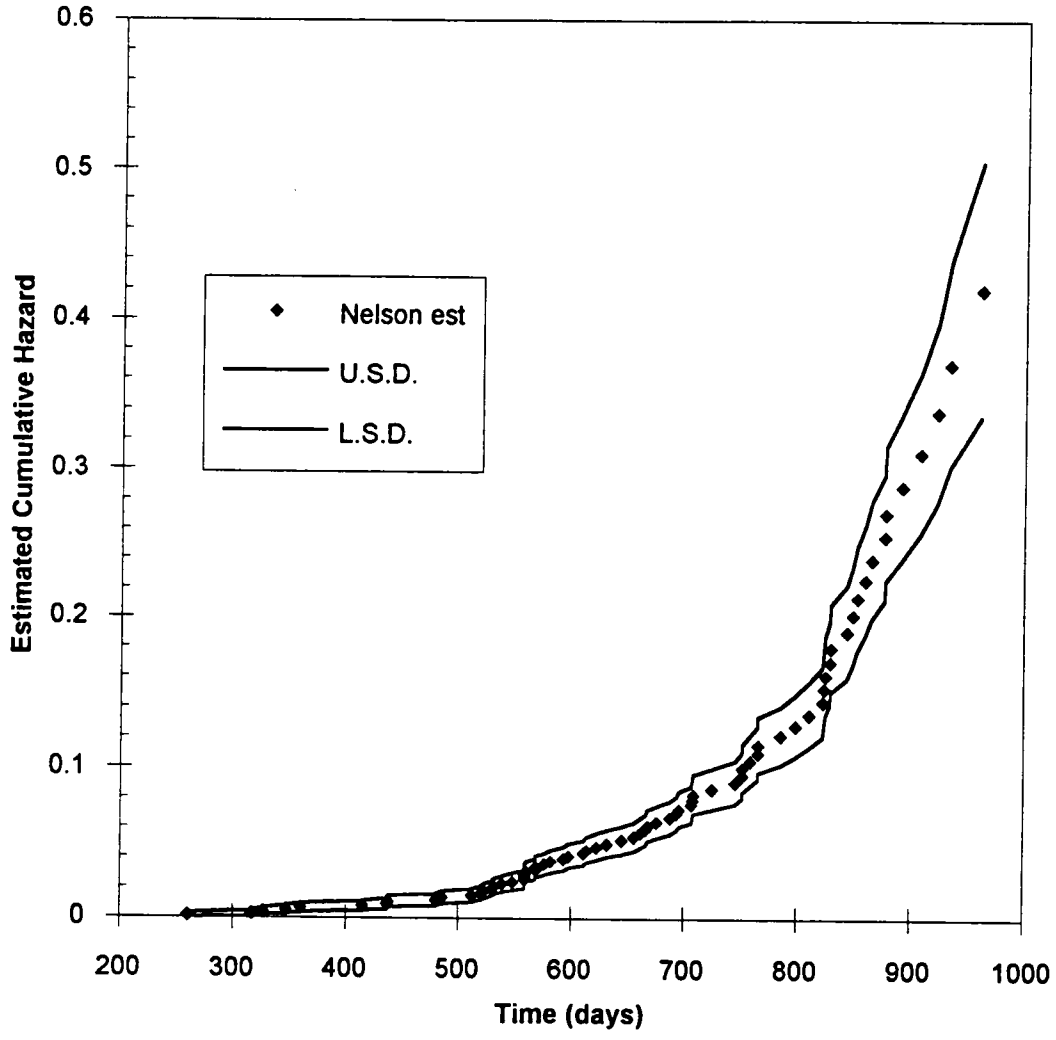

Figure A2.12 Nelson's estimate of the cumulative hazard vs time for BALB/c females with breast cancer: 0.5 Gy, 0.4 Gy/min

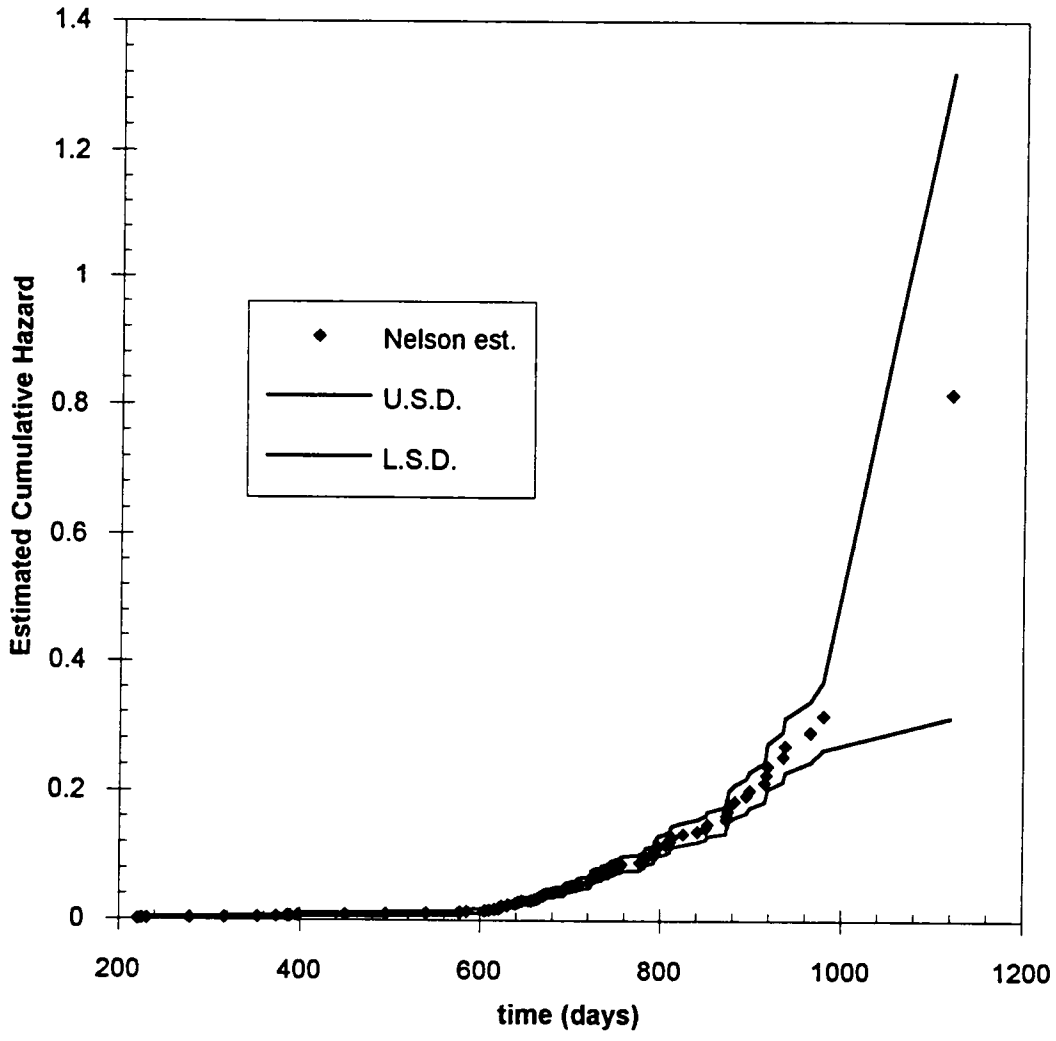

Figure A2.13 Nelson's estimate of the cumulative hazard vs time for BALB/c females with breast cancer: 0.5 Gy, 0.083 Gy/day

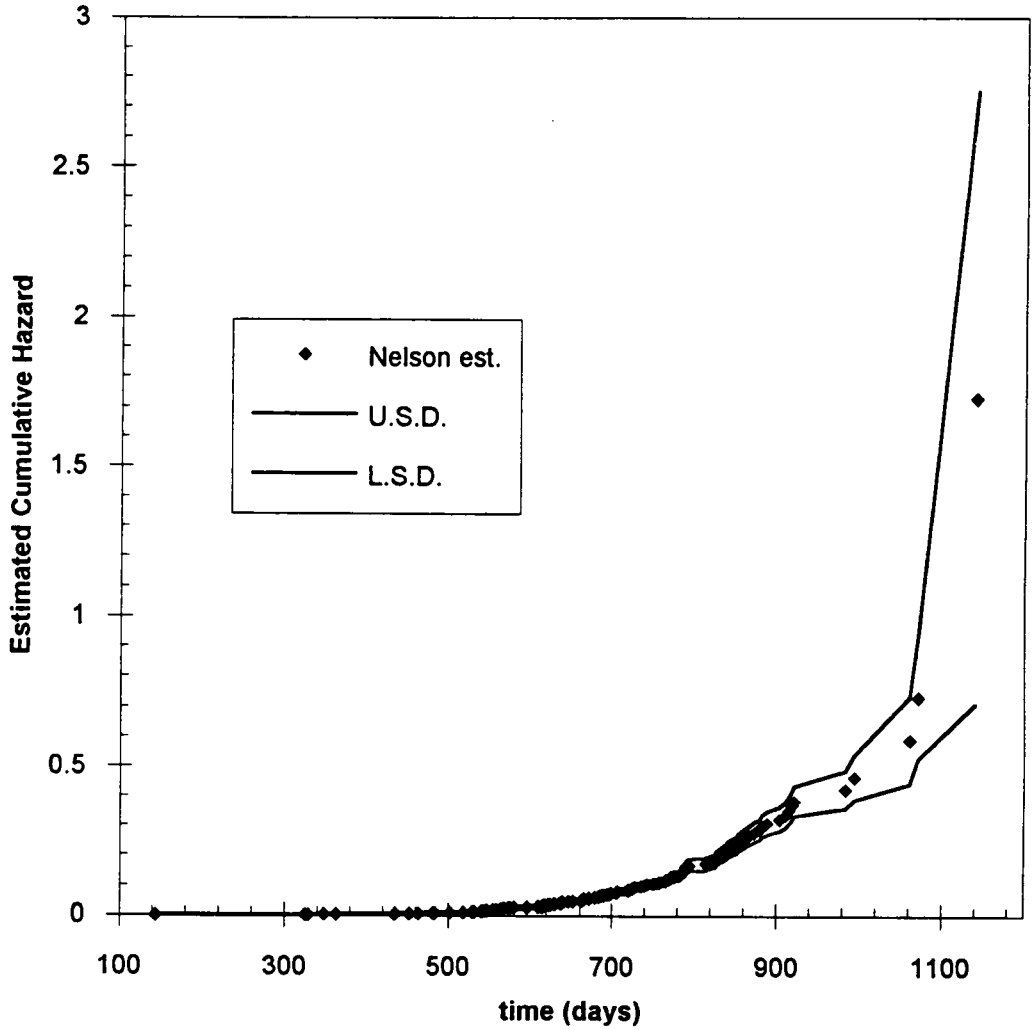

Figure A2.14 Nelson's estimate of the cumulative hazard vs time for BALB/c females with breast cancer: 1.0 Gy, 0.083 Gy/day

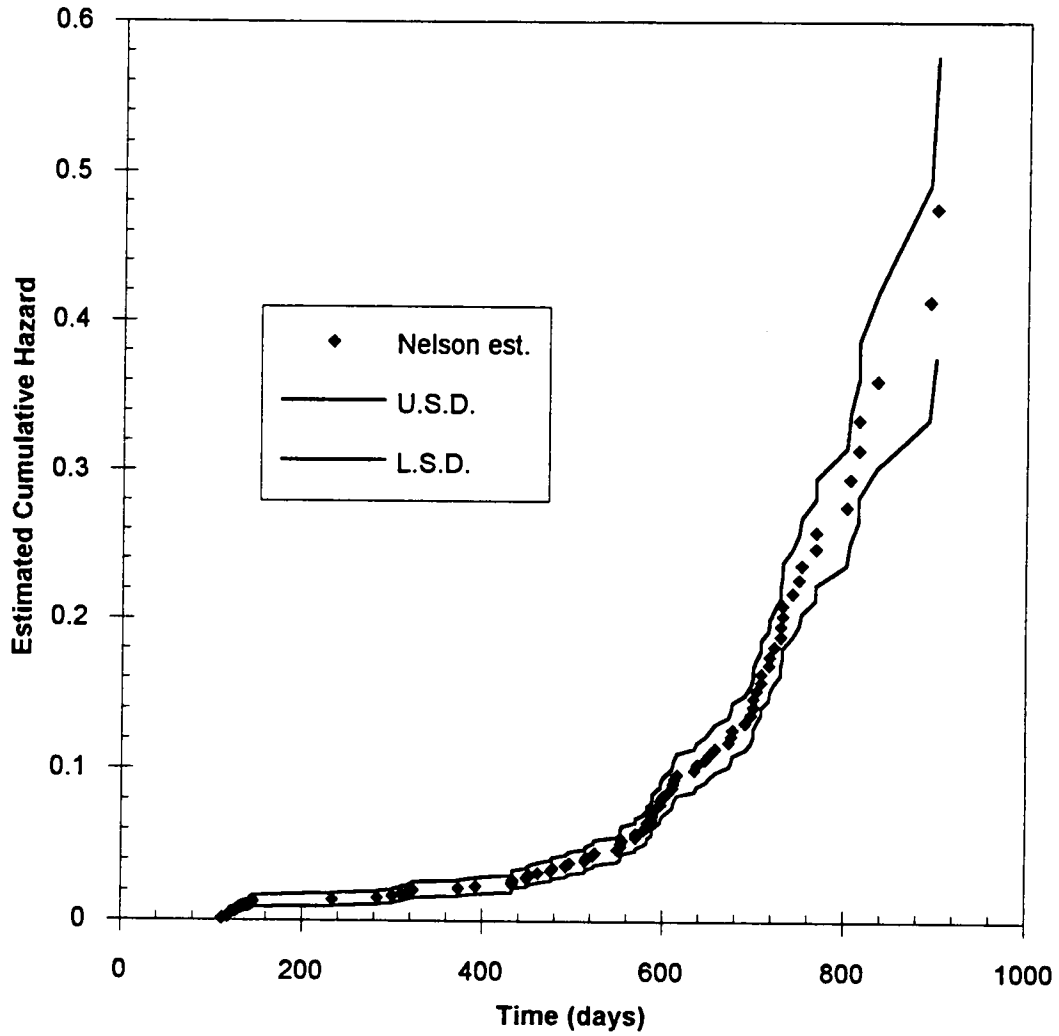

Figure A2.15 Nelson's estimate of the cumulative hazard vs time for BALB/c females with breast cancer: 2.0 Gy, 0.4 Gy/min

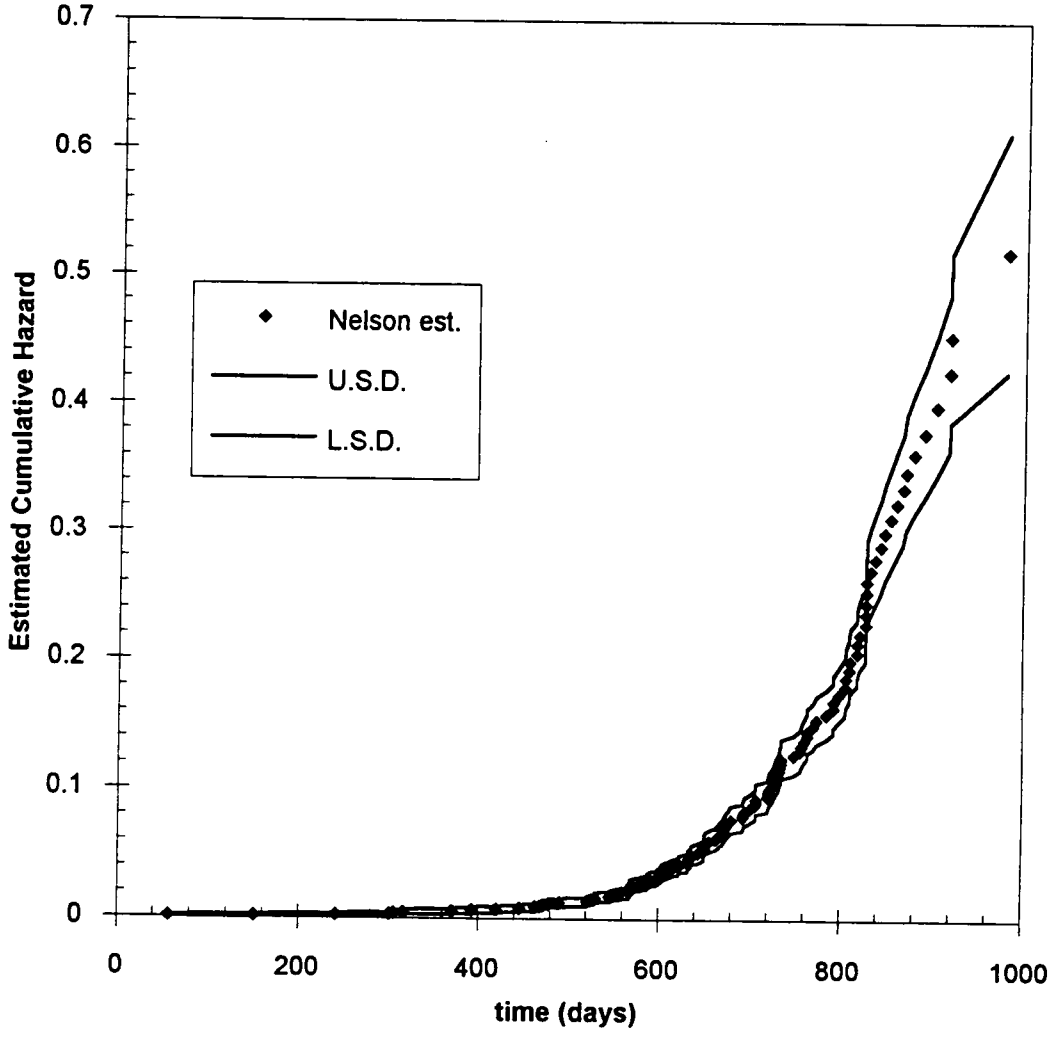

Figure A.2.16 Nelson's estimate of the cumulative hazard vs time for BALB/c females with breast cancer: 2.0 Gy @ 0.083 Gy/day

A2.5 TOTAL TIME ON TEST PLOTS FOR BREAST CANCER

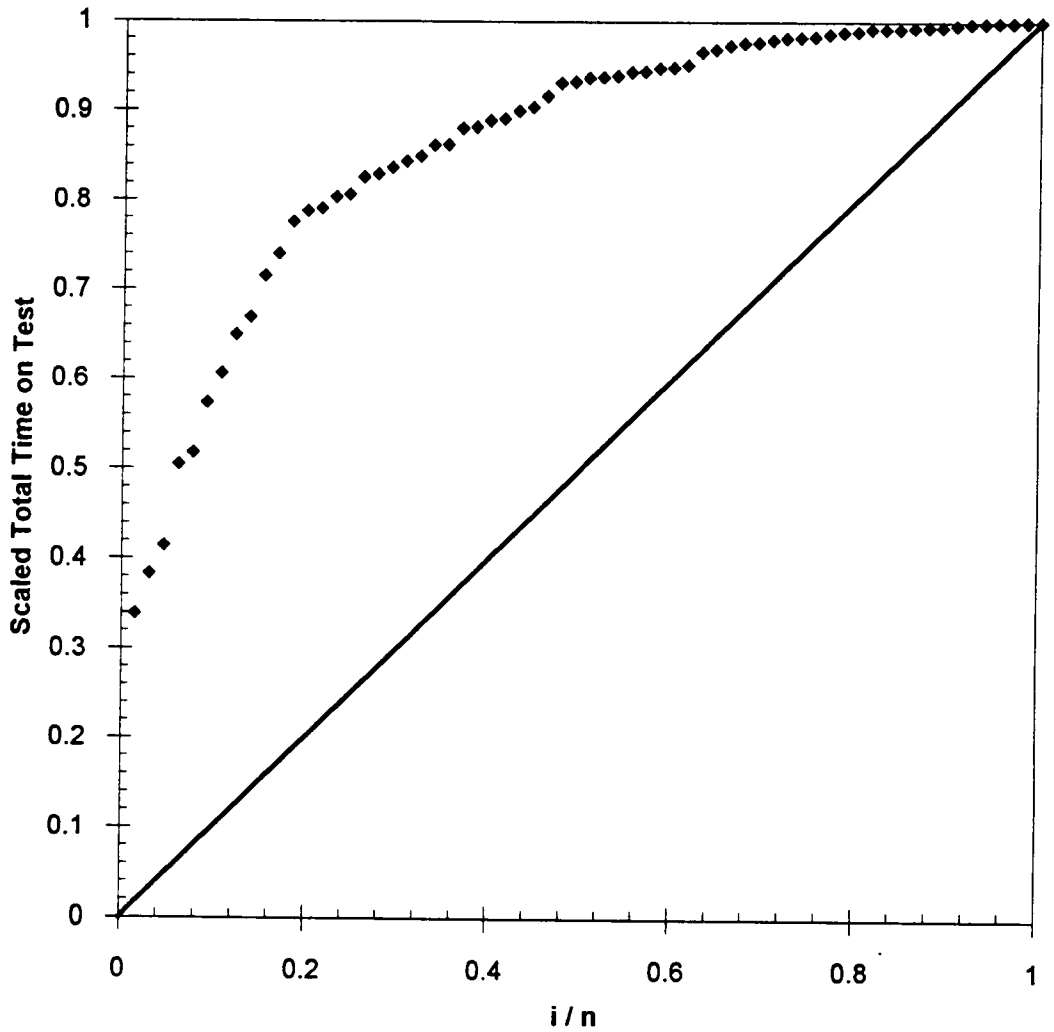

Figure A2.17 Scaled total time on test vs. fraction failed for BALB/c females with breast cancer: Unexposed

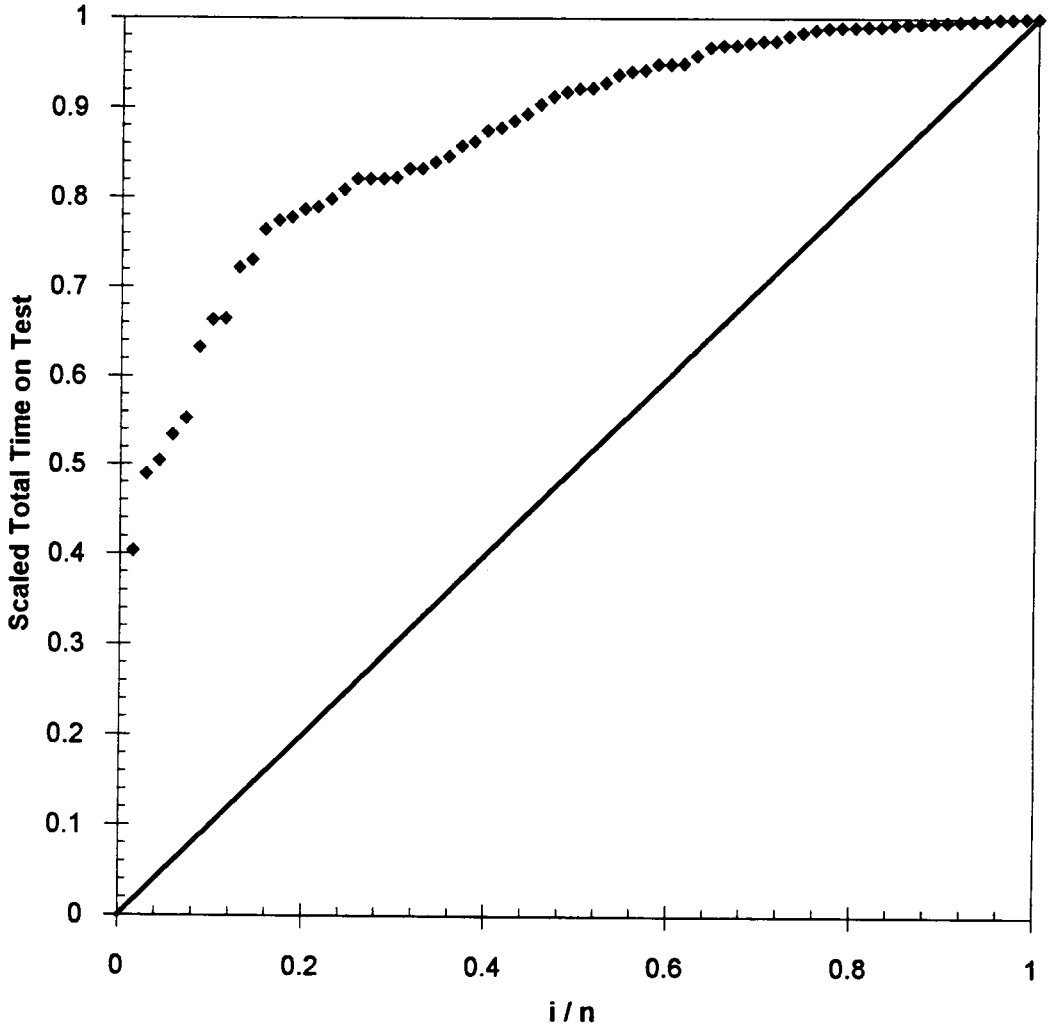

Figure A2.18 Scaled total time on test vs. fraction failed for BALB/c females with breast cancer: 0.5 Gy @ 0.4 Gy/min

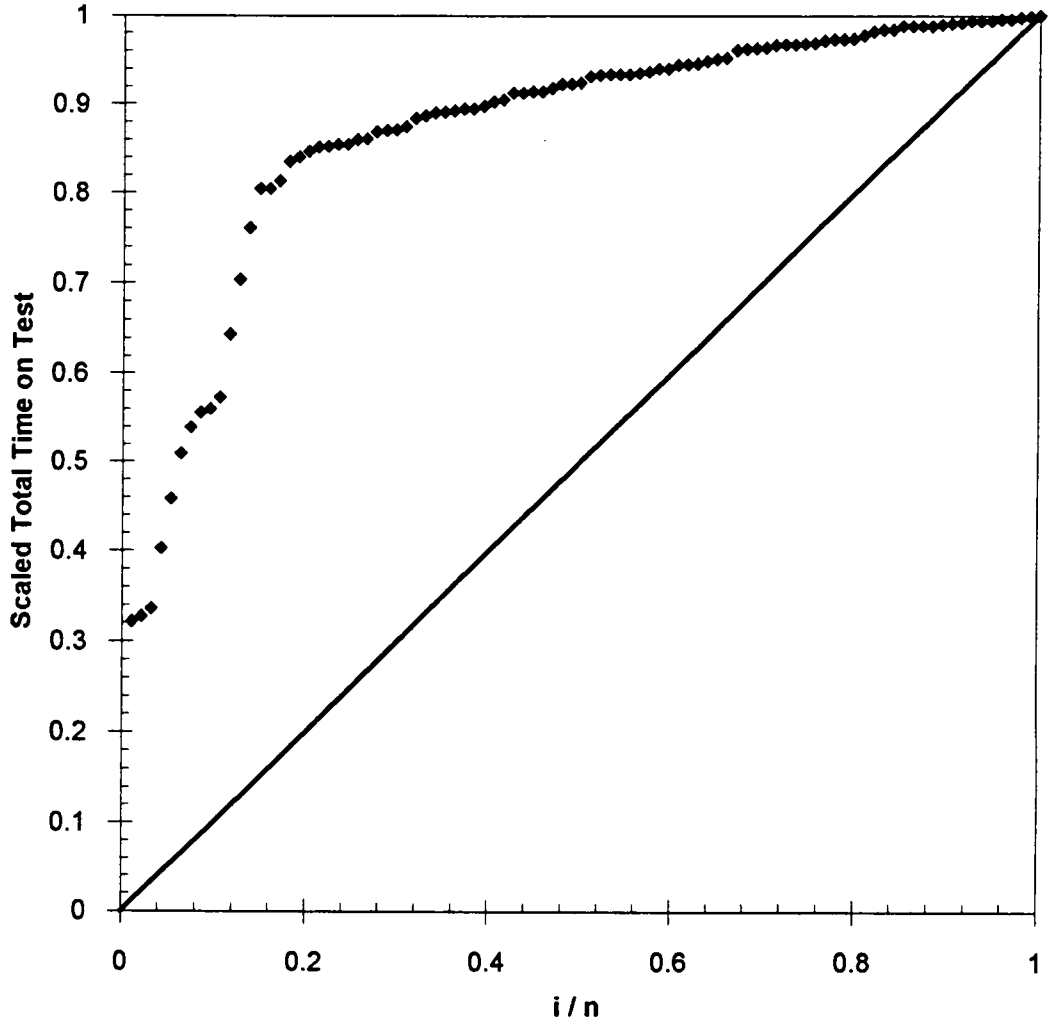

Figure A2.19 Scaled total time on test vs. fraction failed for BALB/c females with breast cancer: 0.5 Gy @ 0.083 Gy/day

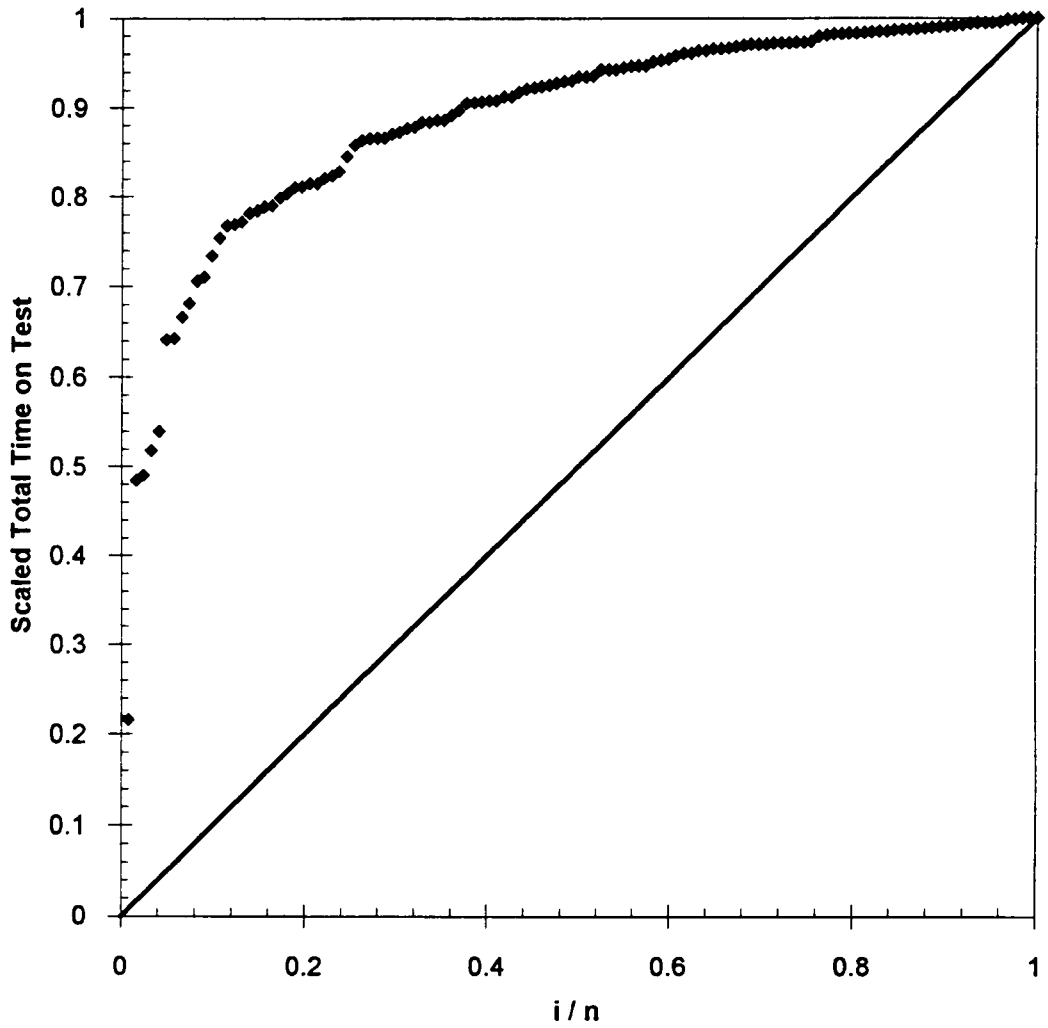

Figure A2.20 Scaled total time on test vs. fraction failed for BALB/c females with breast cancer: 1.0 Gy @ 0.083 Gy/day

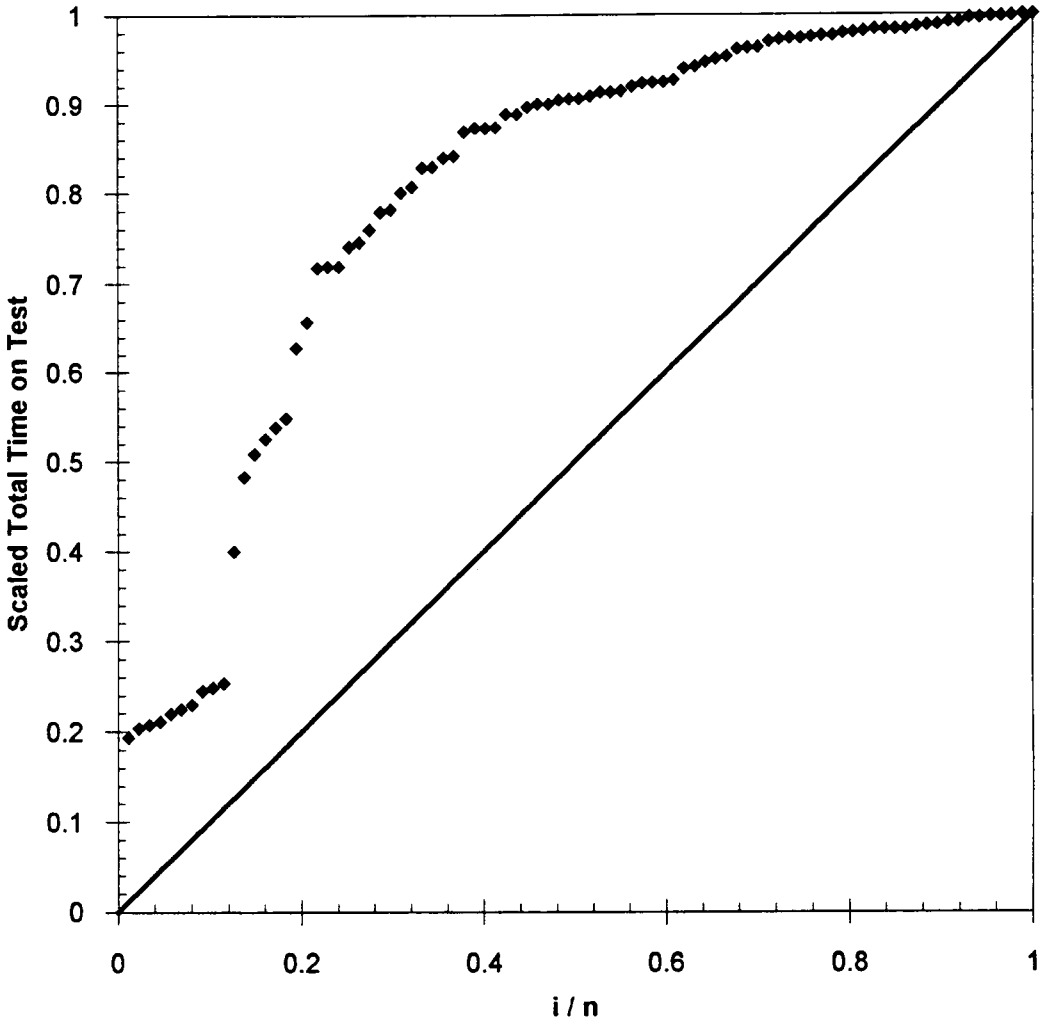

Figure A2.21 Scaled total time on test vs. fraction failed for BALB/c females with breast cancer: 2.0 Gy @ 0.4 Gy/min

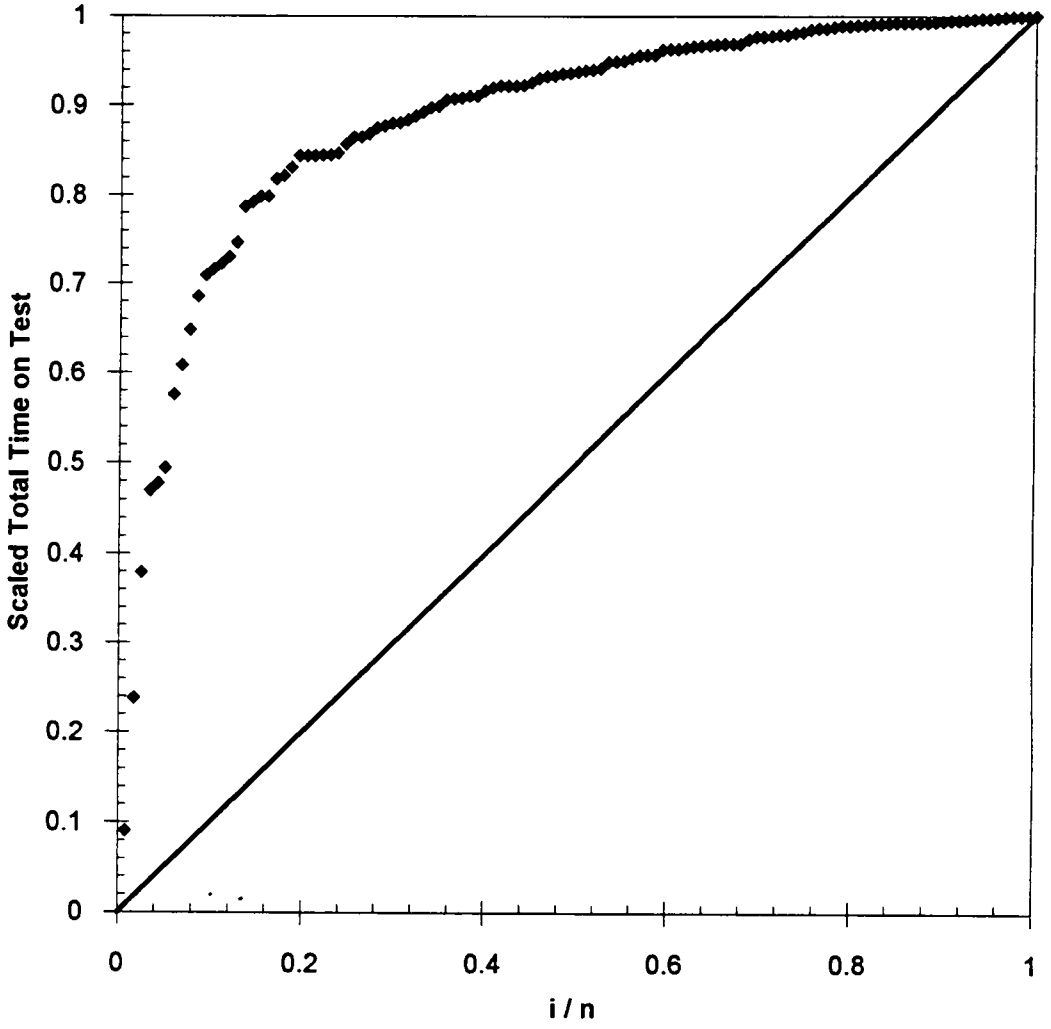

Figure A2.22 Scaled total time on test vs. fraction failed for BALB/c females with breast cancer: 2.0 Gy @ 0.083 Gy/day

A2.6 NELSON'S ESTIMATE OF THE CUMULATIVE HAZARD FOR ALL CAUSES OF DEATH

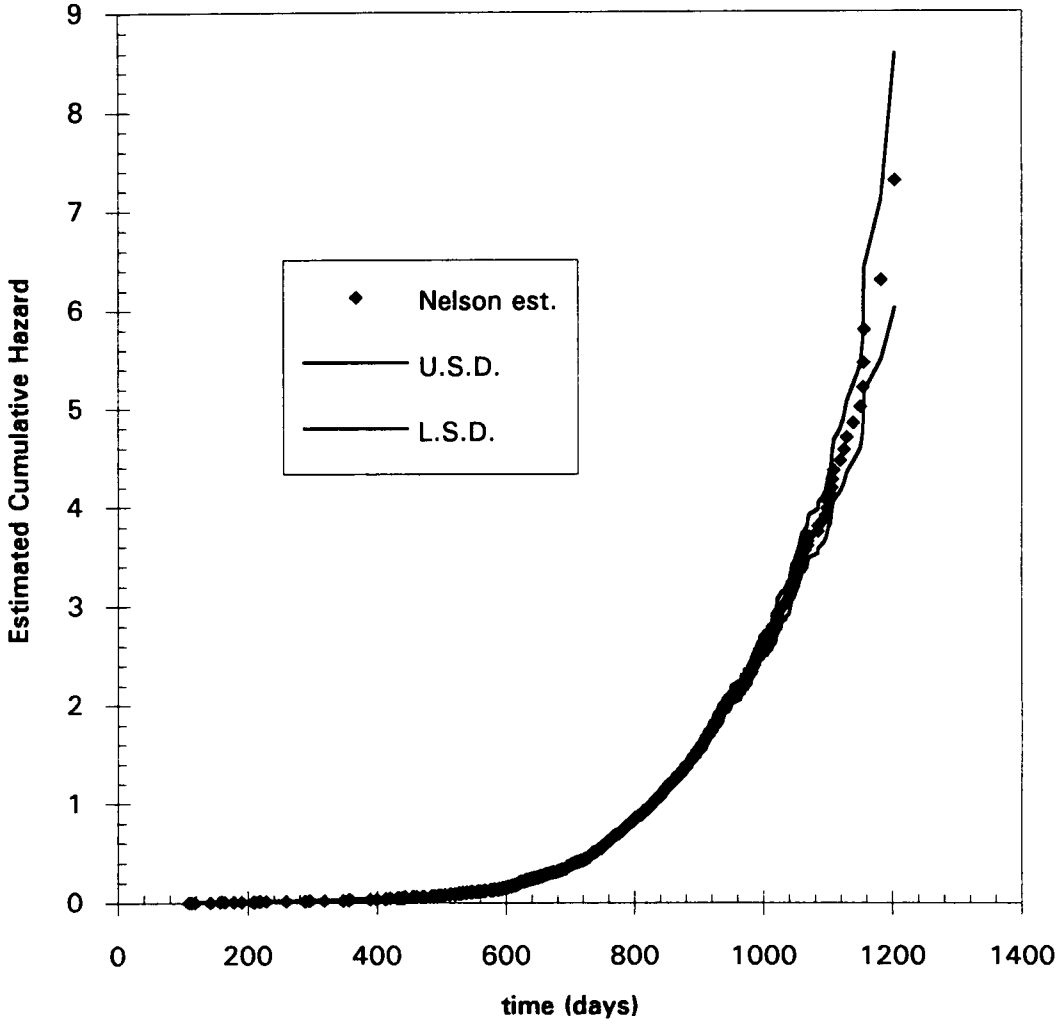

Figure A2.23 Nelson's estimate of the cumulative hazard vs time for BALB/c females using all causes of death : Unexposed

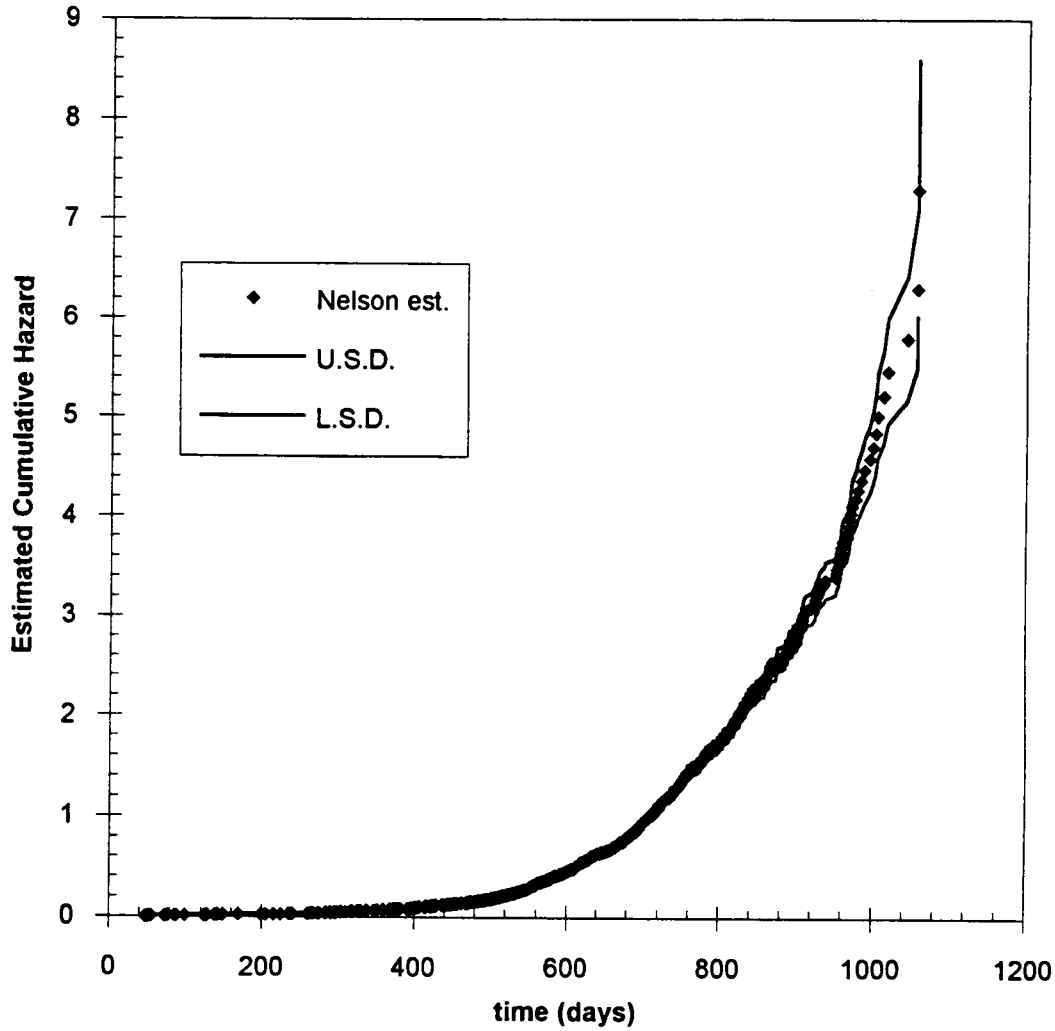

Figure A2.24 Nelson's estimate of the cumulative hazard vs time for BALB/c females using all causes of death : 0.5 Gy @ 0.4 Gy/min

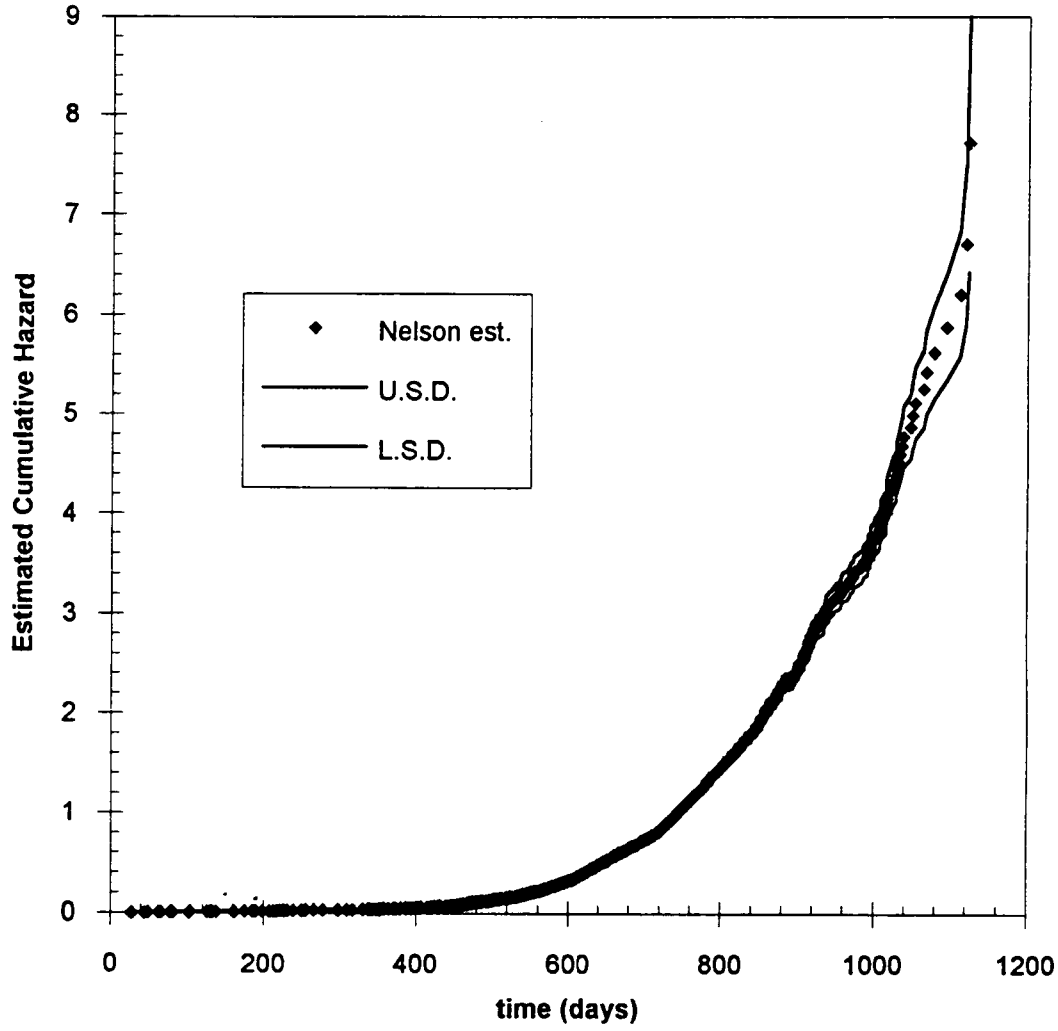

Figure A2.25 Nelson's Estimate Of The Cumulative Hazard vs Time For BALB/c females using all causes of death : 0.5 Gy @ 0.083 Gy/day

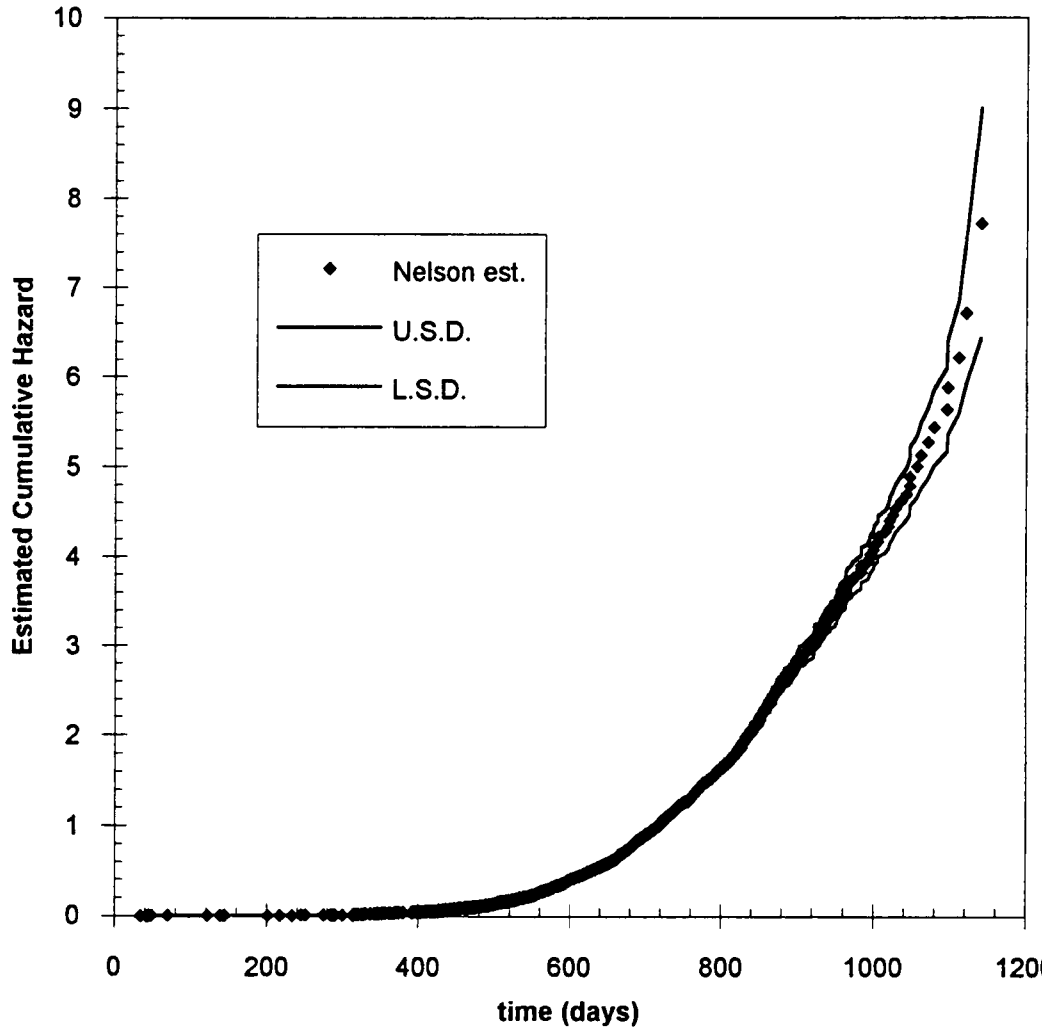

Figure A2.26 Nelson's estimate of the cumulative hazard vs time for BALB/c females using all causes of death : 1.0 Gy @ 0.083 Gy/day

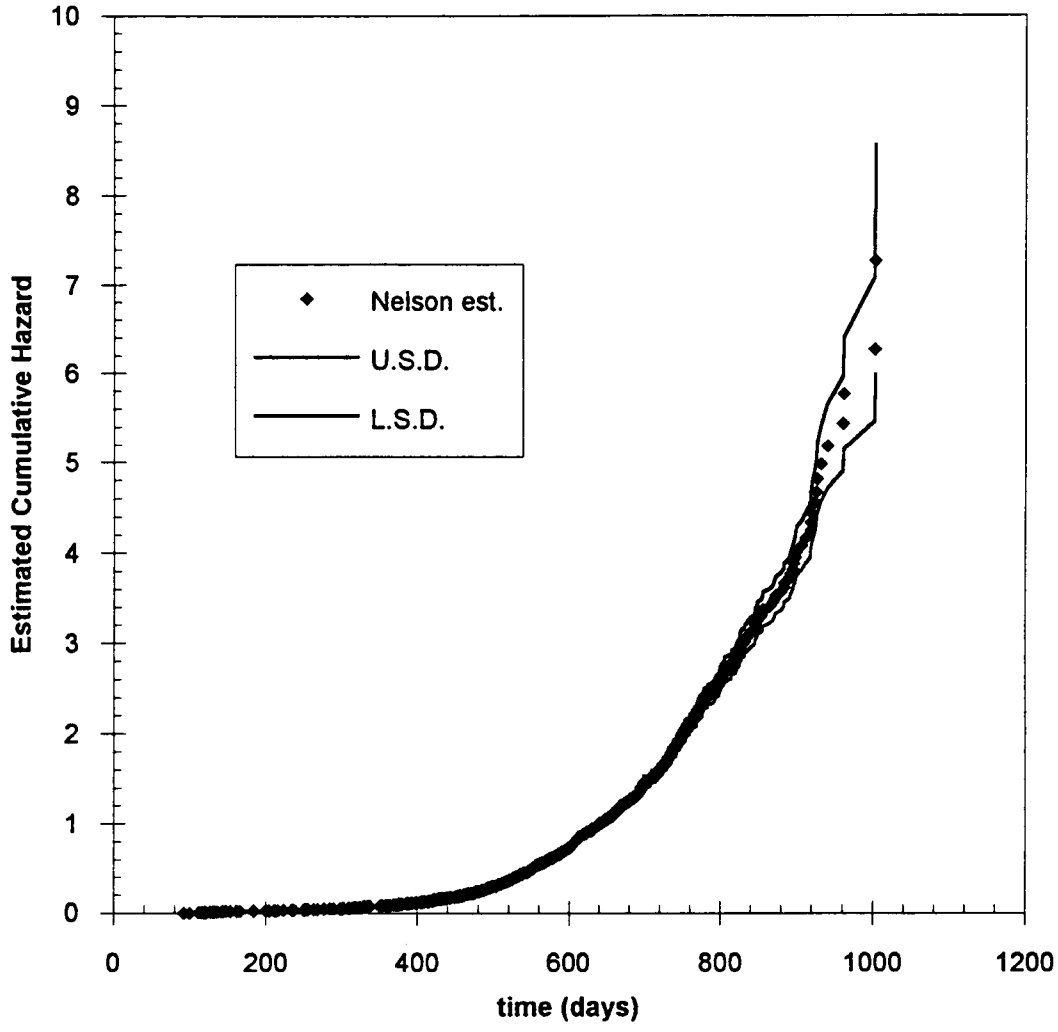

Figure A2.27 Nelson's estimate of the cumulative hazard vs time for BALB/c females using all causes of death : 2.0 Gy @ 0.4 Gy/min

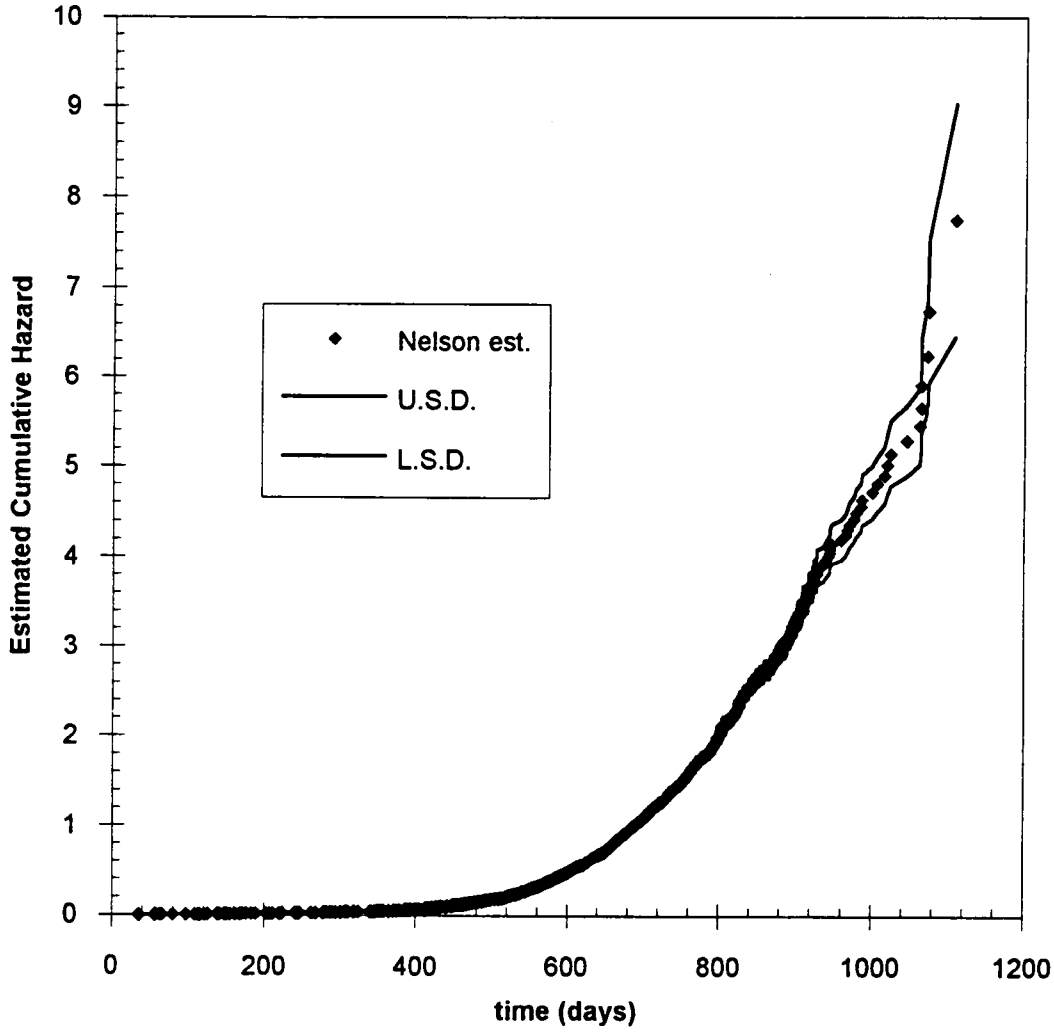

Figure A2.28 Nelson's estimate of the cumulative hazard vs time for BALB/c females using all causes of death : 2.0 Gy @ 0.083 Gy/day

A2.7 TOTAL TIME ON TEST PLOTS FOR ALL CAUSES OF DEATH

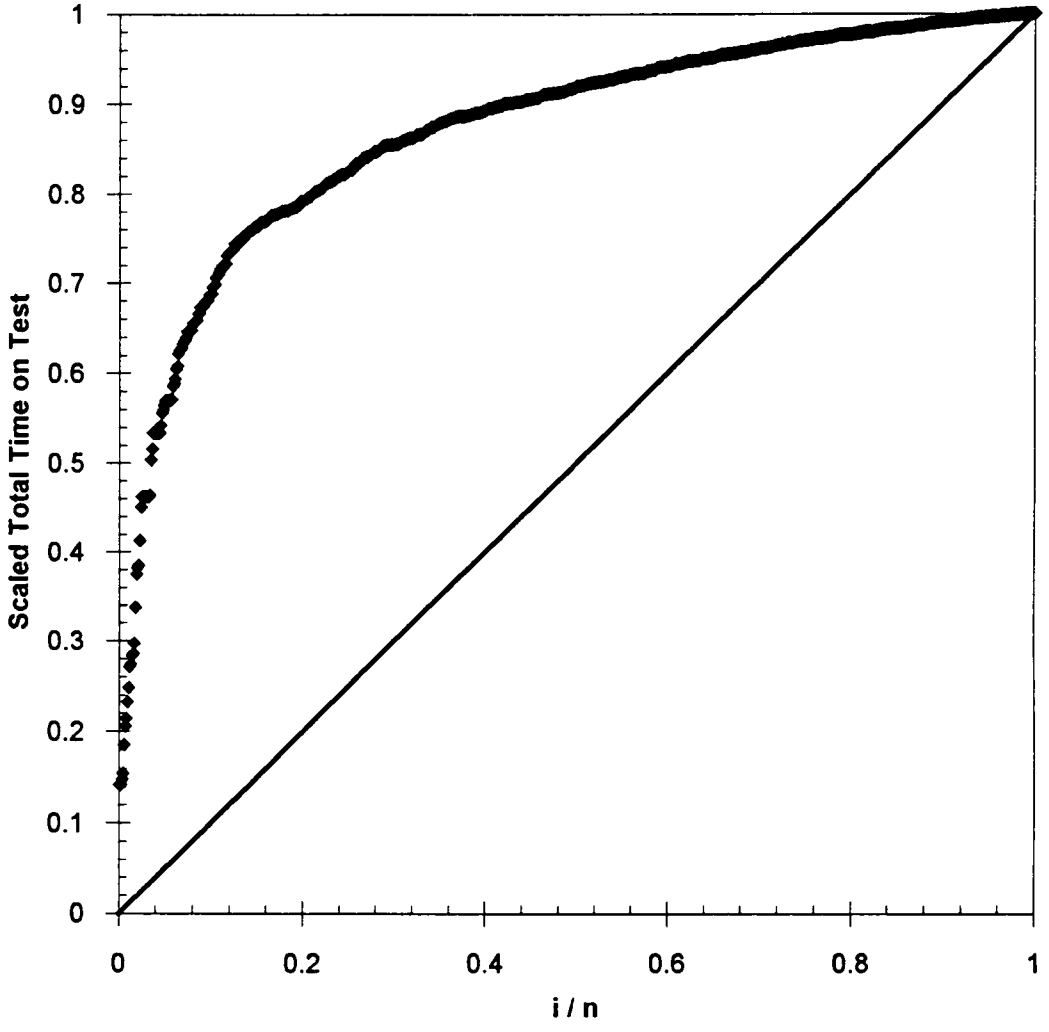

Figure A2.29 Scaled total time on test vs. fraction failed for BALB/c females using all causes of death: Unexposed

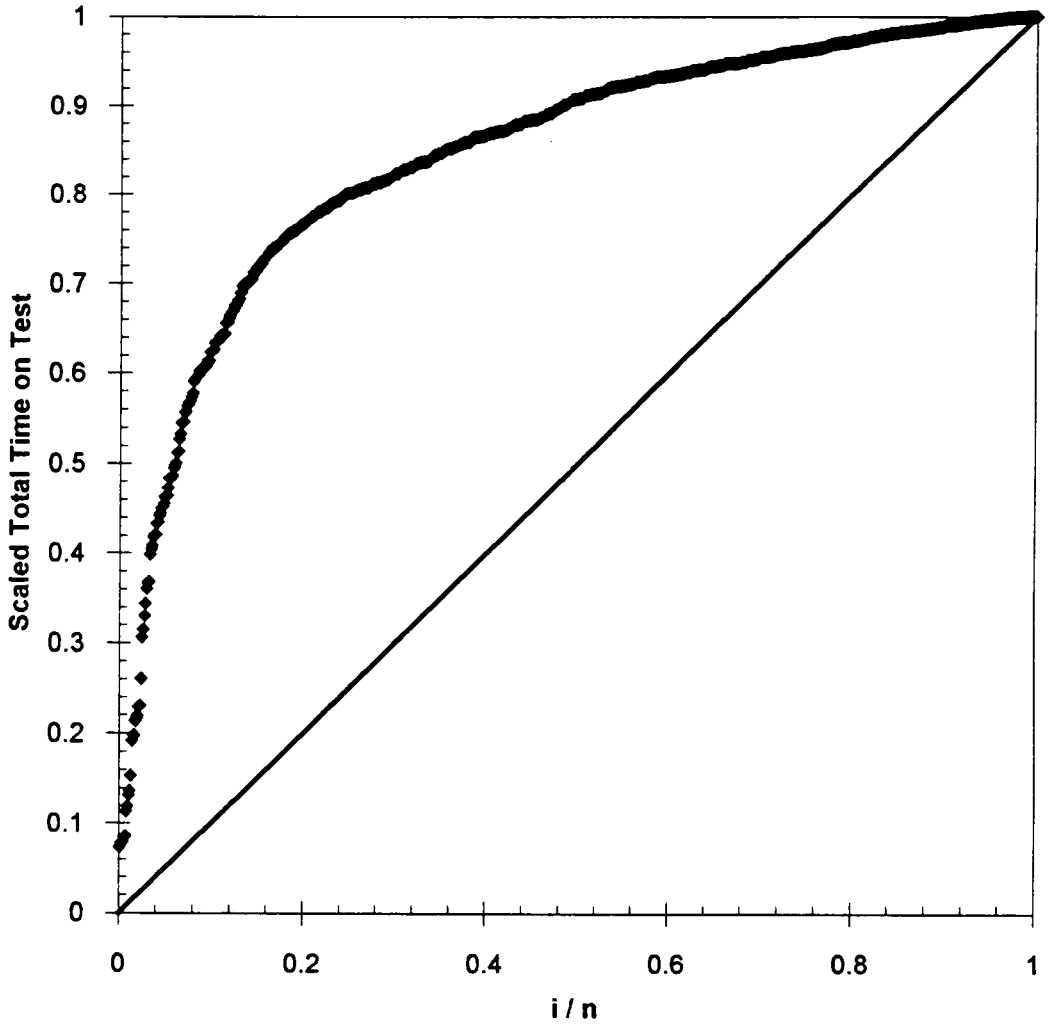

Figure A2.30. Scaled total time on test vs. fraction failed for BALB/c females using all causes of death: 0.5 Gy @ 0.4 Gy/min

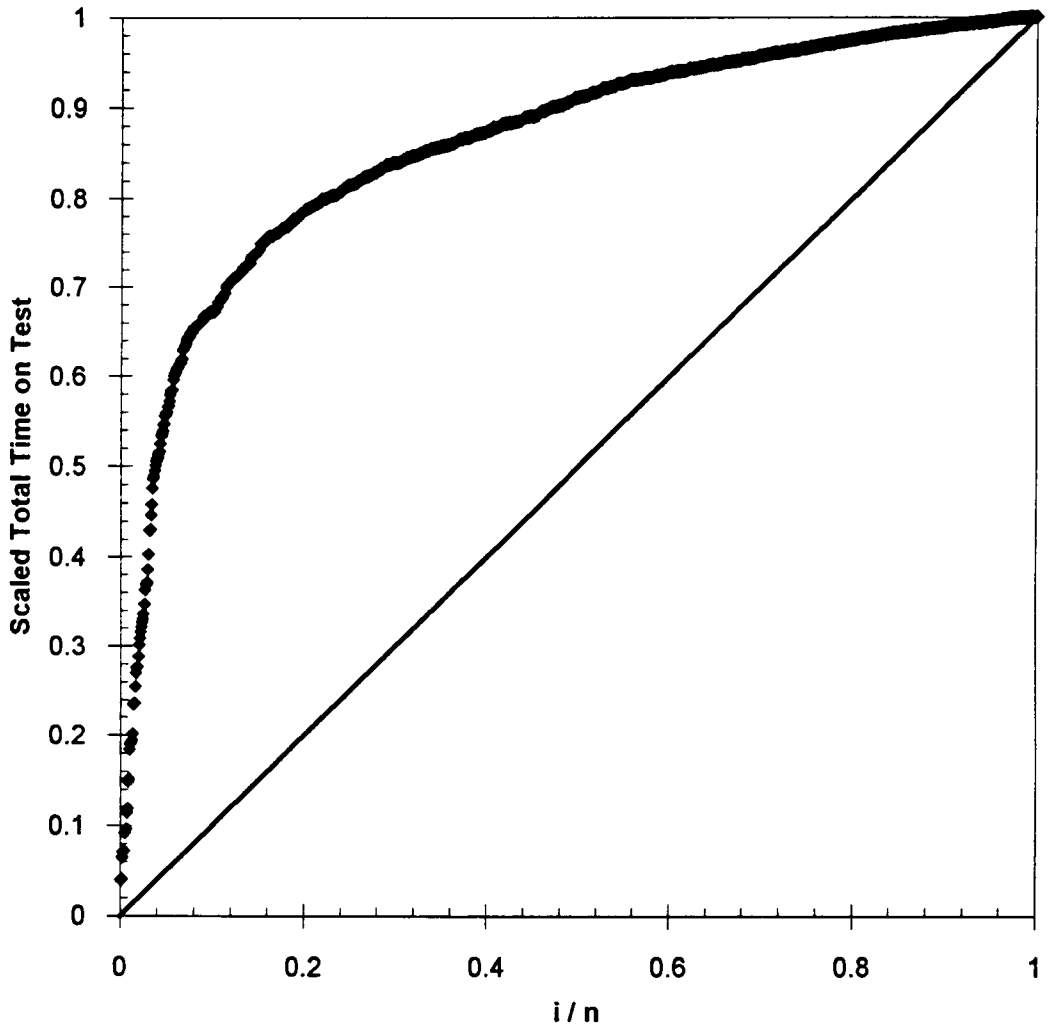

Figure A2.31 Scaled total time on test vs. fraction failed for BALB/c females using all causes of death: 0.5 Gy @ 0.083 Gy/day

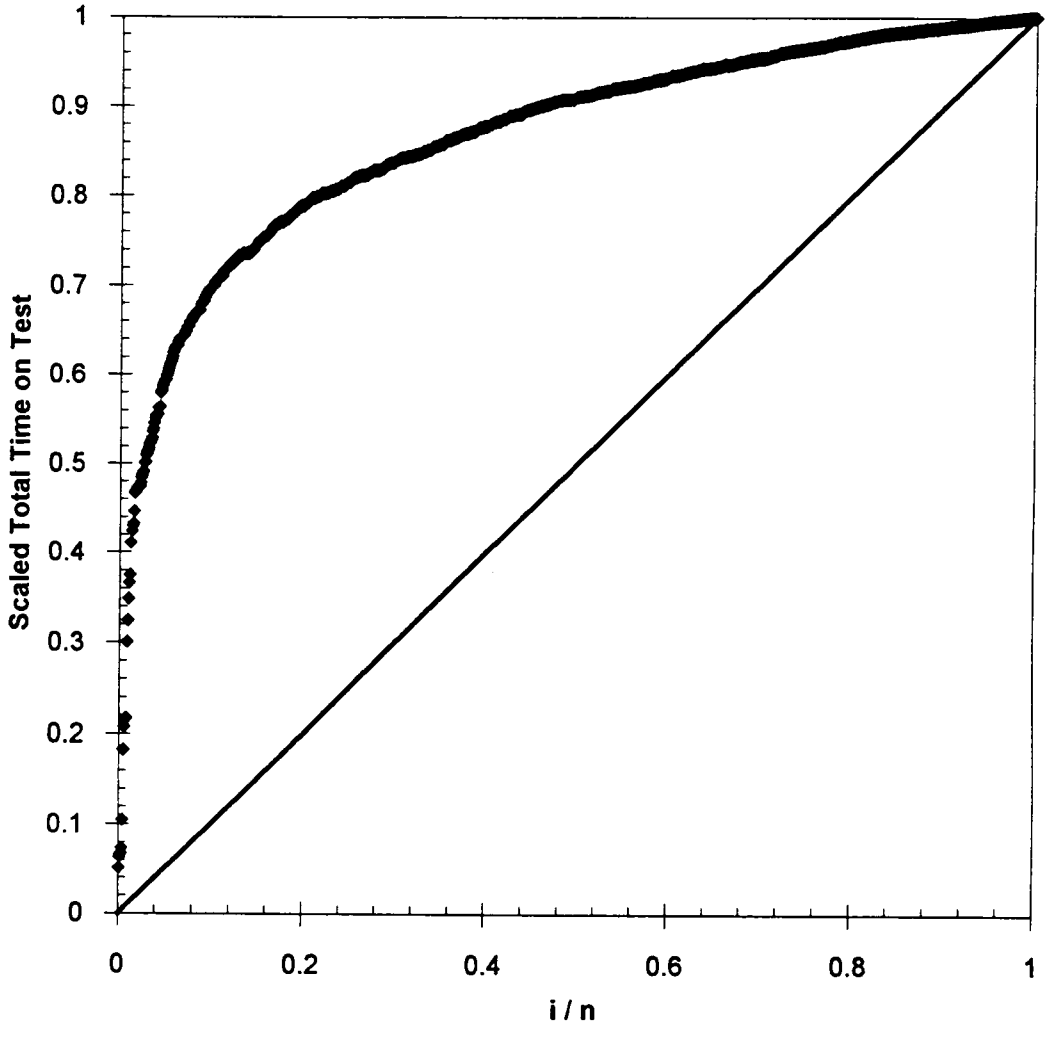

Figure A2.32 Scaled total time on test vs. fraction failed for BALB/c females using all causes of death: 1.0 Gy @ 0.083 Gy/day

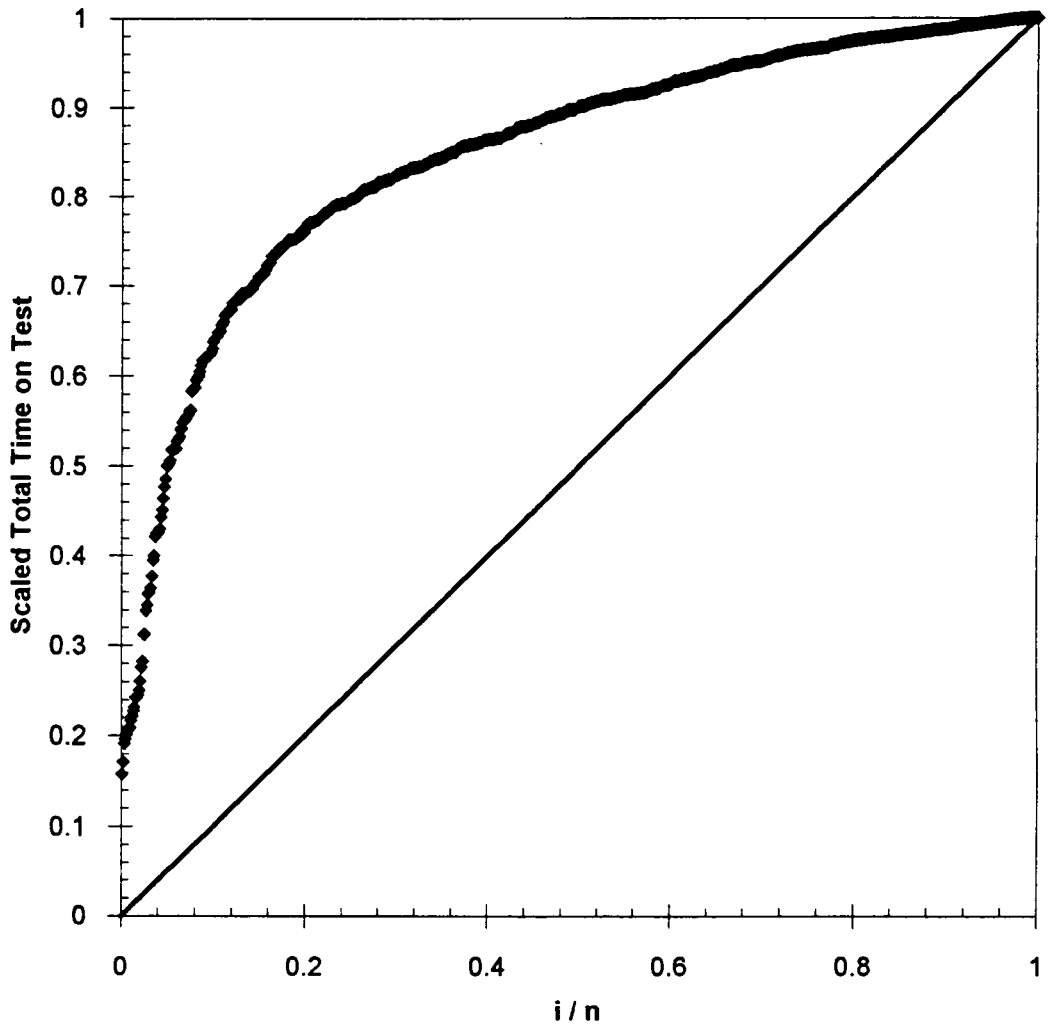

Figure A2.33 Scaled total time on test vs. fraction failed for BALB/c females Using All Causes Of Death: 2.0 Gy @ 0.4 Gy/min

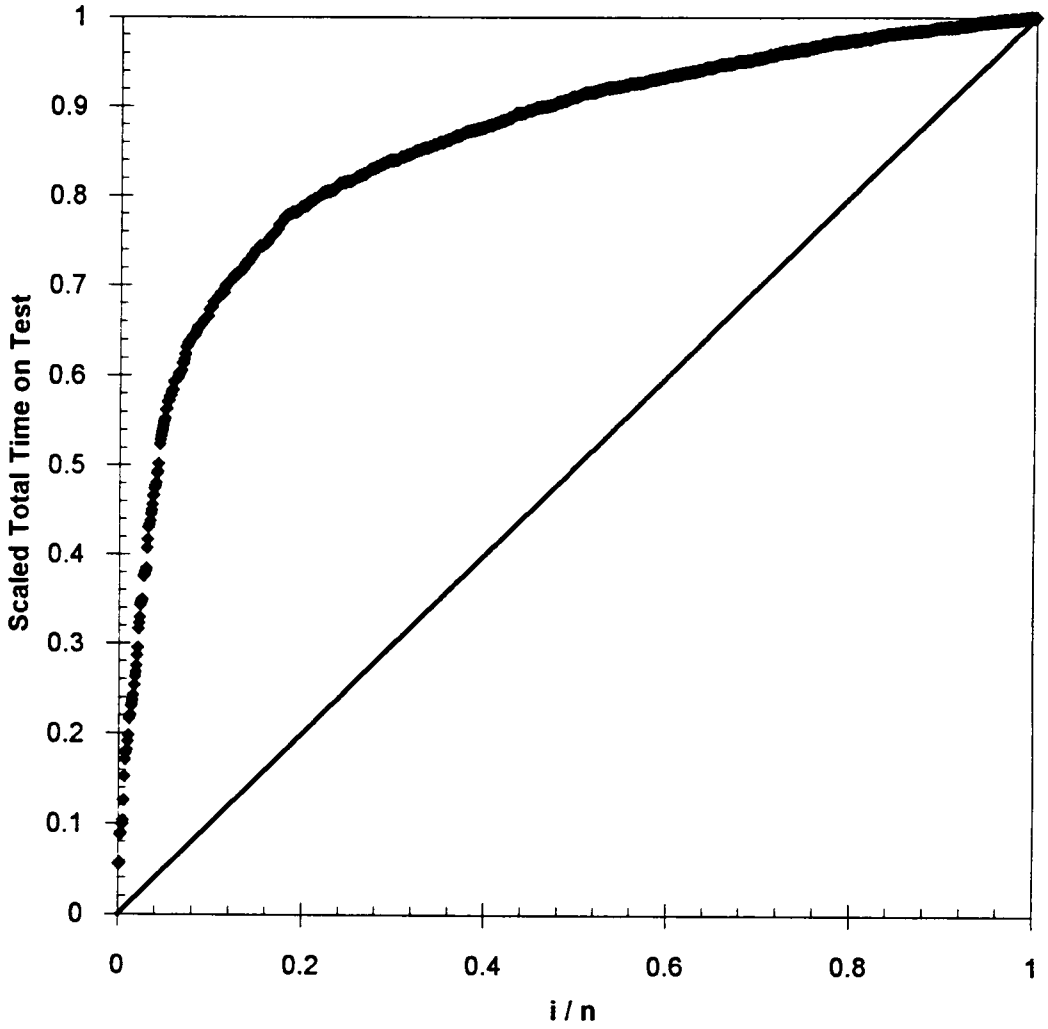

Figure A2.34 Scaled total time on test vs. fraction failed for BALB/c females Using All Causes Of Death: 2.0 Gy @ 0.083 Gy/day

APPENDIX 3

PARAMETRIC ESTIMATES

A3.1 INTRODUCTION

Appendix 3 contains the marginal posterior densities for the parameters α, β, and λ that were not included in the main body of the thesis. Appendix 3.2 contains the marginal posterior densities for the parameters with breast cancer as the endpoint of interest. Appendix 3.3 contains the marginal posterior densites for the parameters using all causes of death as the endpoint of interest.

A3.2 MARGINAL POSTERIOR DENSITES for α, β, AND λ

BREAST CANCER

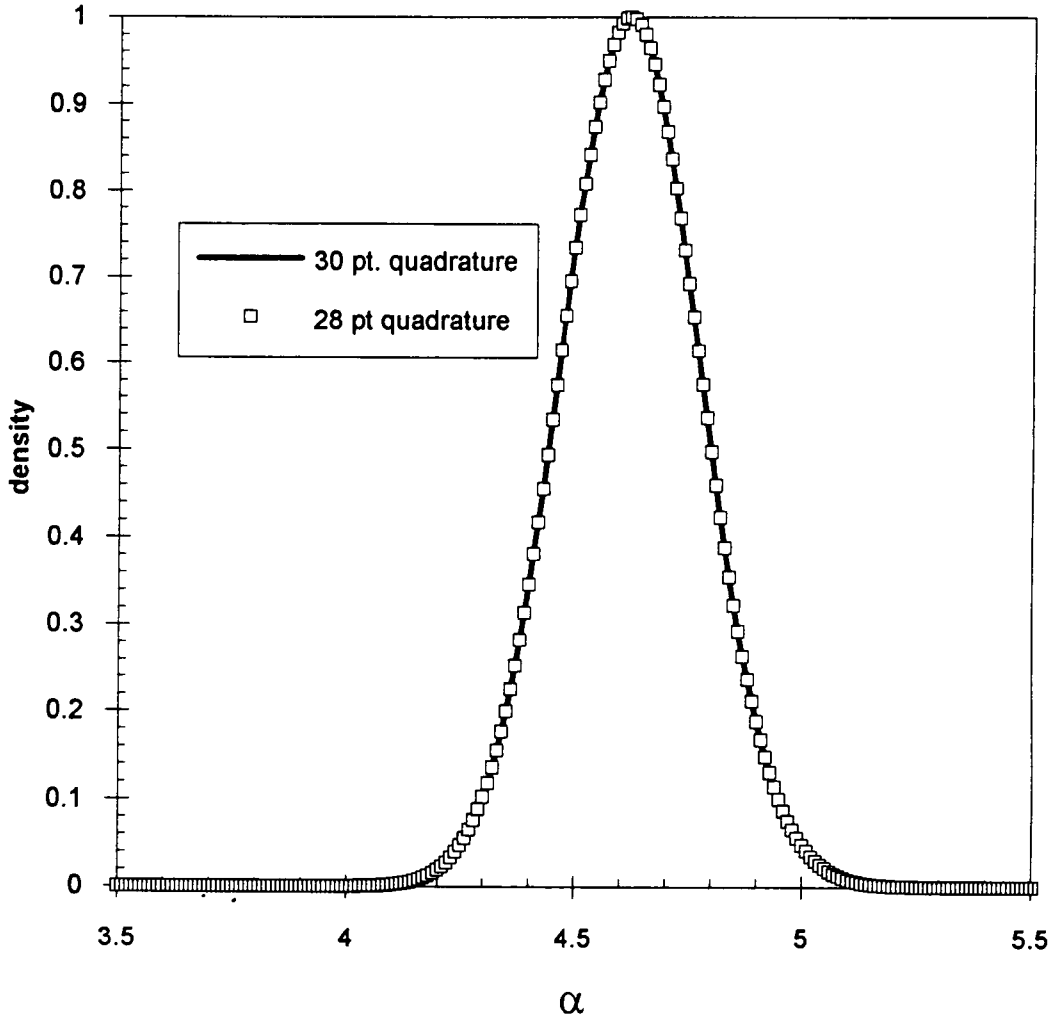

Figure A3.1 Marginal posterior density for α for BALB/c females with breast cancer

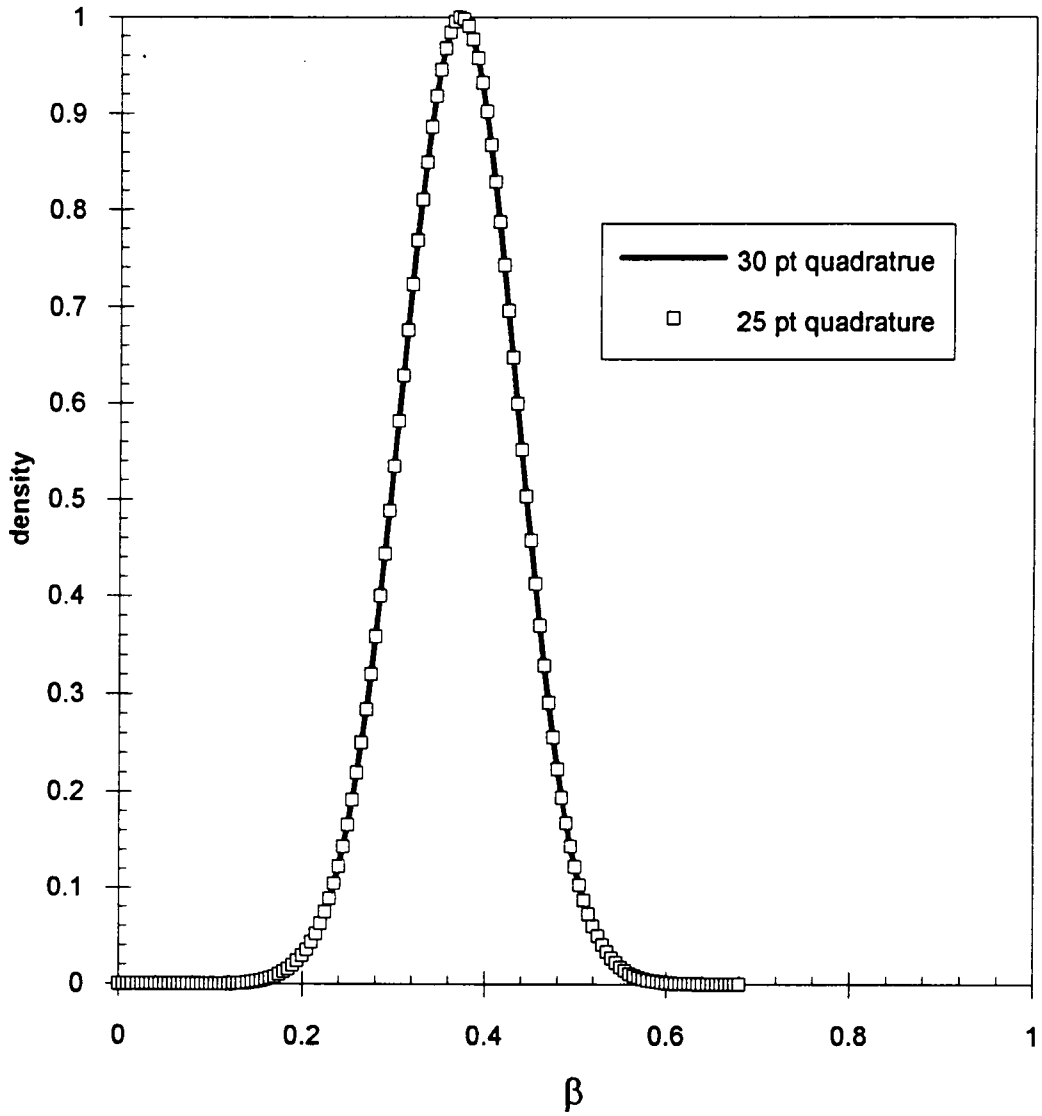

Figure A3.2 Marginal posterior desity for β for BALB/c females with breast cancer

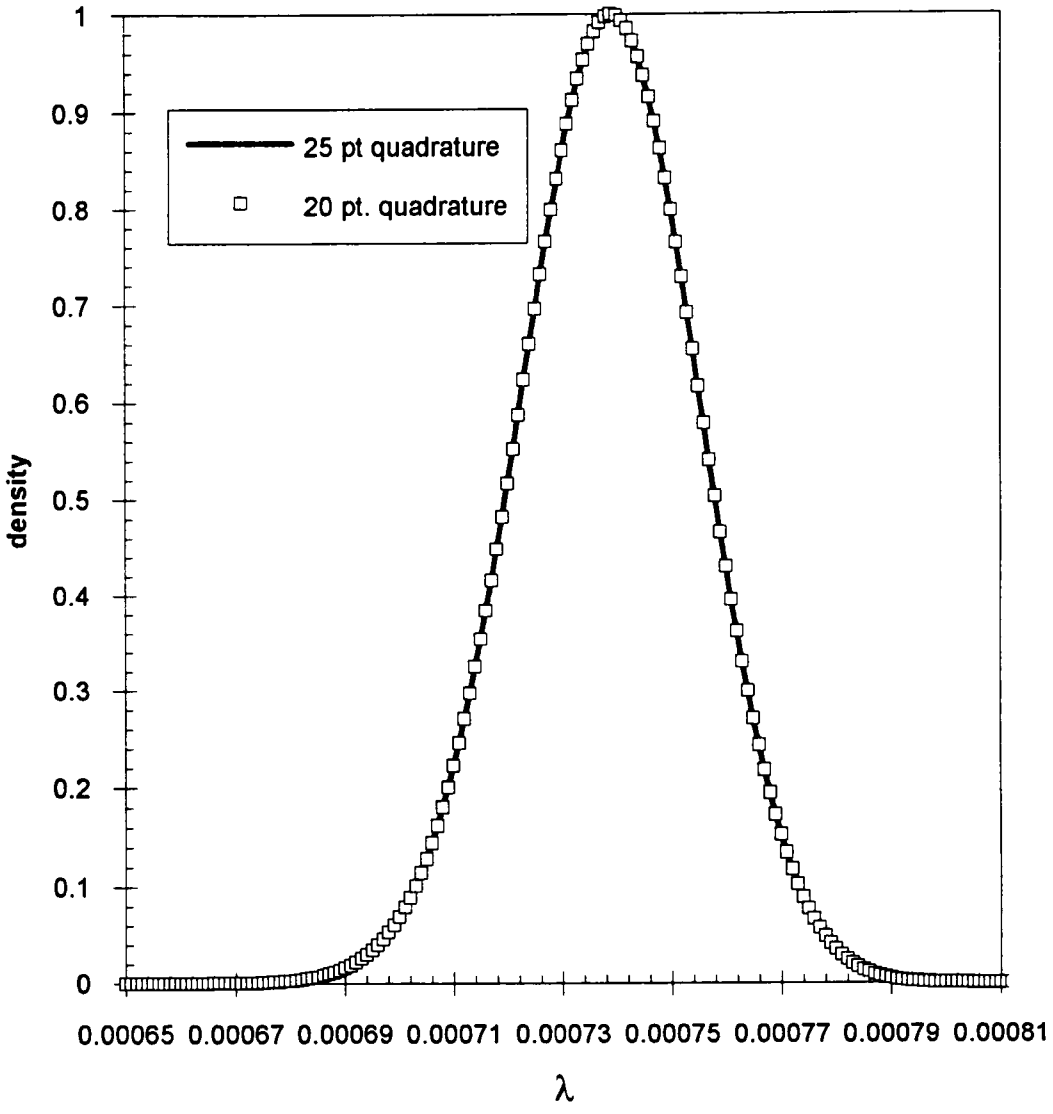

Figure A3.3 Marginal posterior desity for λ for BALB/c females with breast cancer

A3.3 MARGINAL POSTERIOR DENSITIES for α, β, AND λ

ALL CAUSES OF DEATH

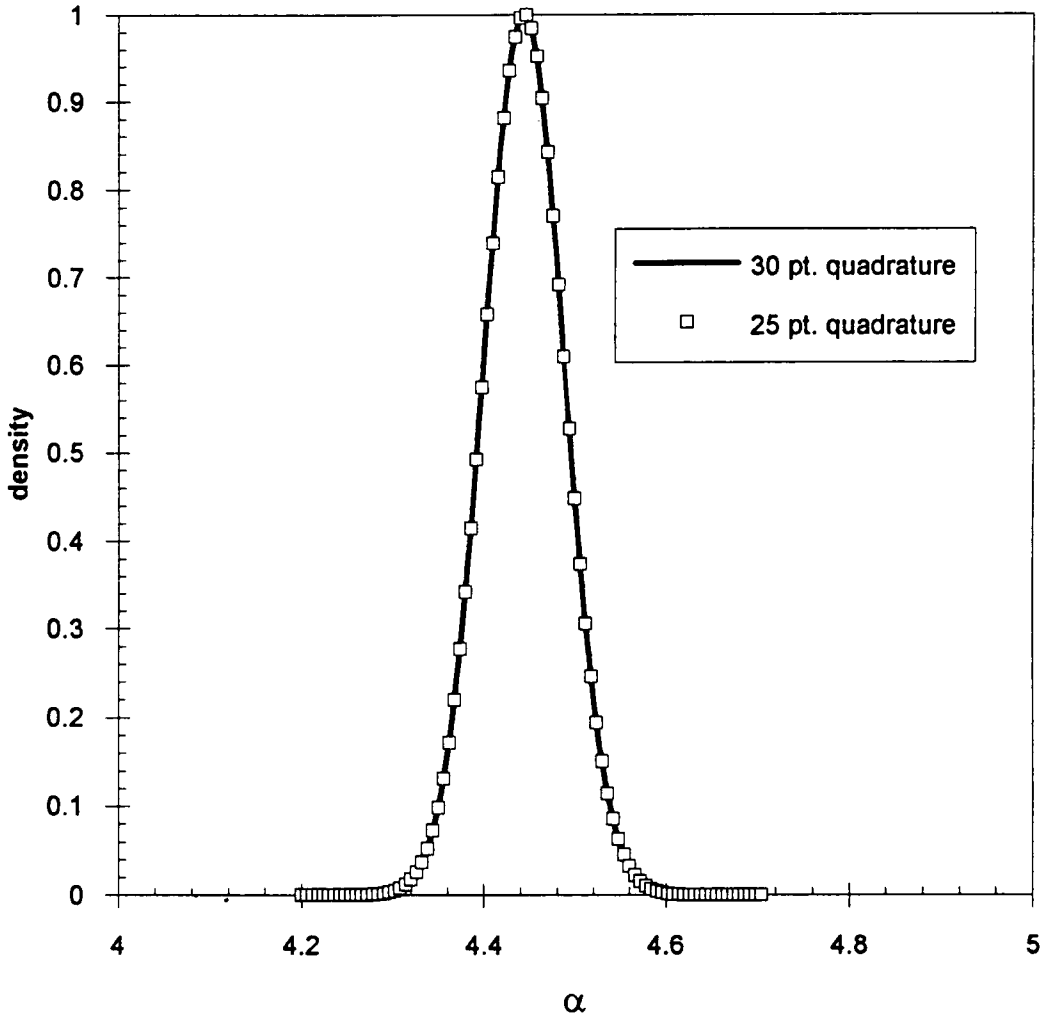

Figure A3.4 Marginal posterior desity for α for BALB/c females using all causes of death

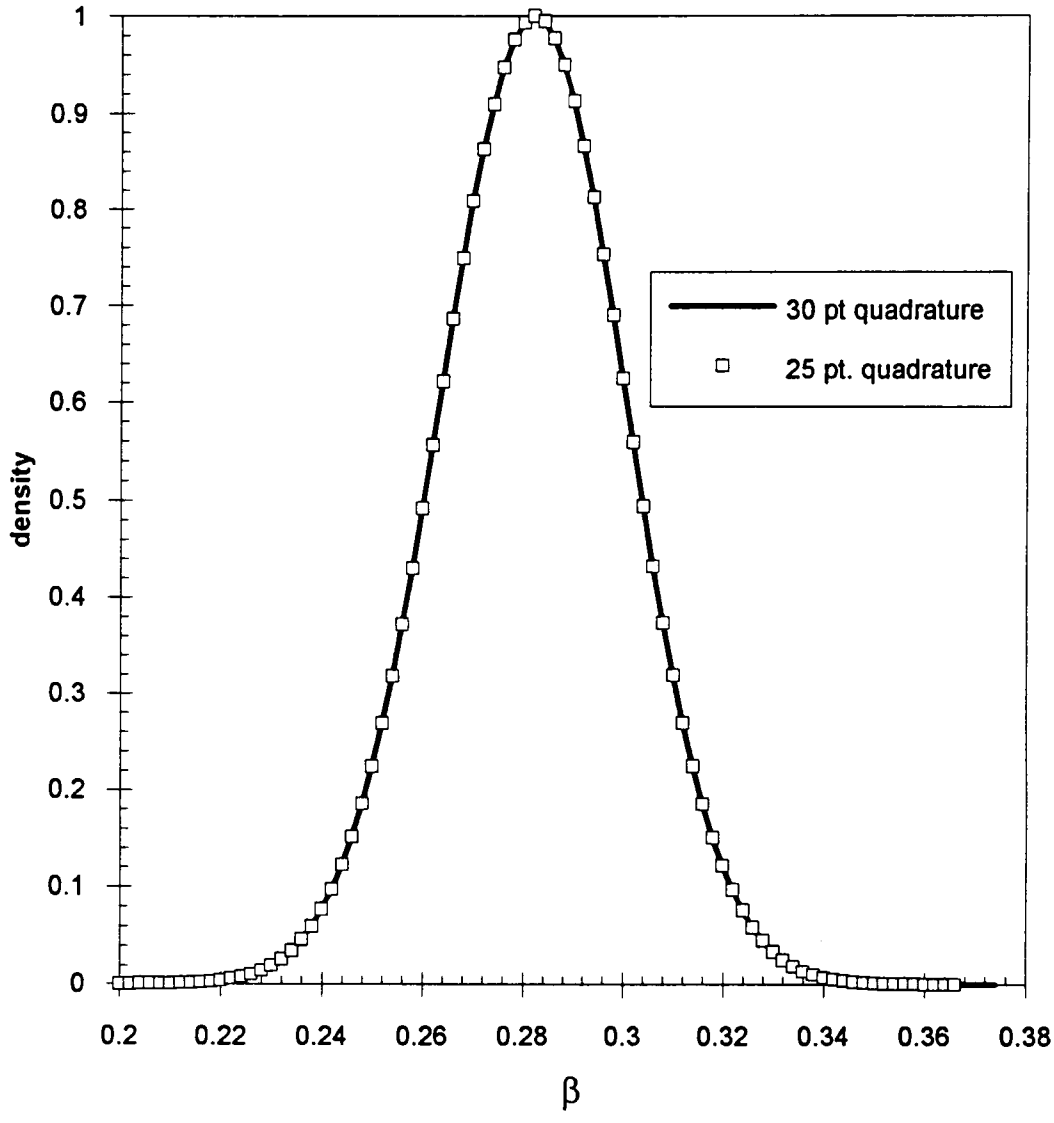

Figure A3.5 Marginal posterior desity for β for BALB/c females using all causes of death

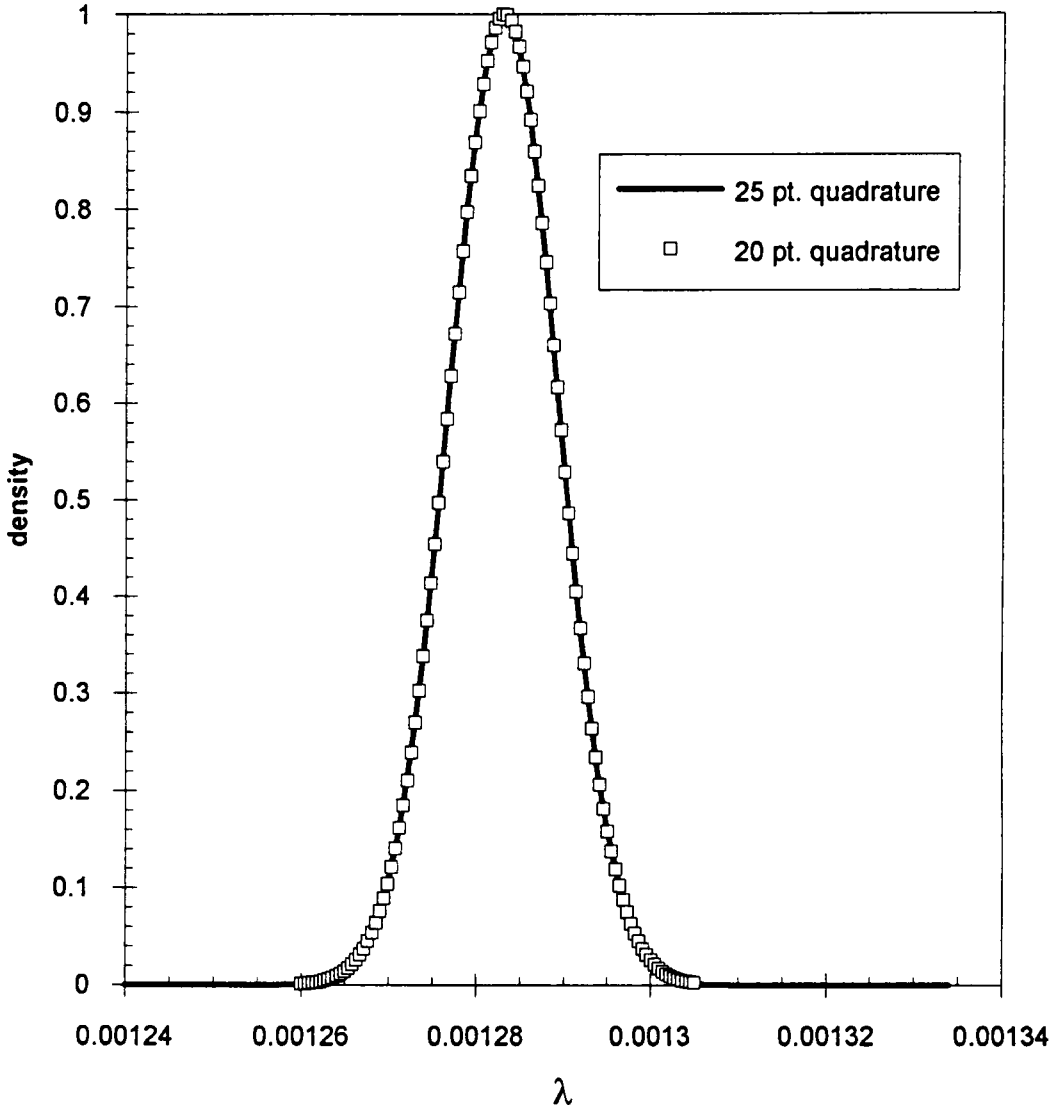

Figure A3.7 Marginal posterior desity for λ for BALB/c females using all causes of death

APPENDIX 4

PARAMETRIC VS. NON-PARAMETRIC ESTIMATES

A4.1 INTRODUCTION

Comparisons between the parametric and non-parametric estimates are made by inserting point estimates of the parameters into the formula for the cumulative hazard. The cumulative hazard using the point estimates is plotted versus time and overlaid over the non-parametric estimate. The point estimate is made by selecting the mode of the marginal posterior density. This procedure is repeated for each parameter. Since most of the prior densities were uniform prior densities, the posterior modes coincide with the maximum likelihood estimates. The maximum likelihood estimates for the cumulative hazard using a relative risk Weibull model are given below:

$$\hat{H}(t)=(\hat{\lambda}t)^{\hat{\alpha}} \quad \textit{unexposed group} \qquad (A4.1)$$

$$\hat{H}(t,d)=(\hat{\lambda}t)^{\hat{\alpha}}e^{\hat{\beta}d} \quad \textit{low dose-rate group} \qquad (A4.2)$$

$$\hat{H}(t,d)=(\hat{\lambda}t)^{\hat{\alpha}}e^{\hat{\beta}\hat{\rho}d} \quad \textit{high dose-rate group} \qquad (A4.3)$$

where the ^ represents the maximum likelihood estimate of the parameter.

A4.2 PARAMETRIC VS. NON-PARAMETRIC ESTIMATES USING LUNG TUMORS

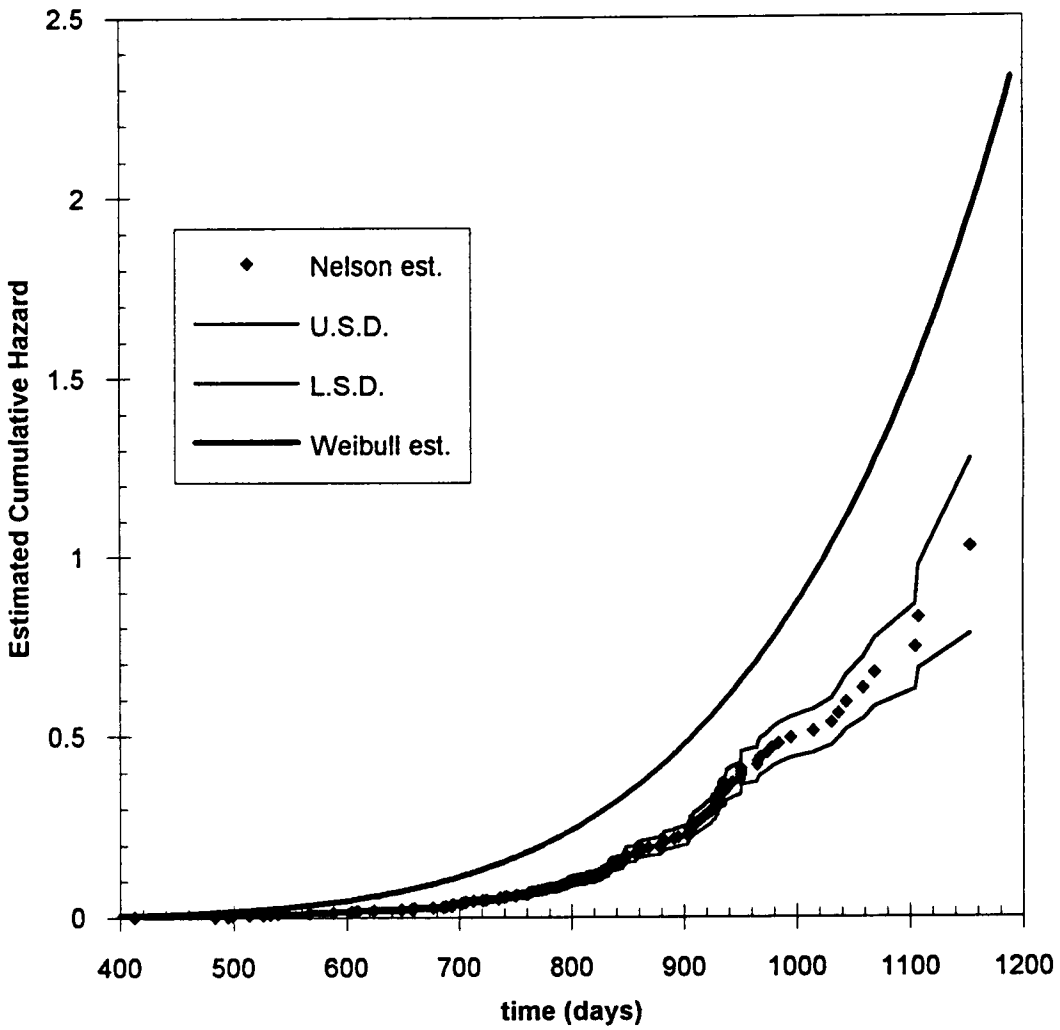

Figure A4.1 Estimated cumulative hazard vs time for BALB/c females with lung tumors: Unexposed

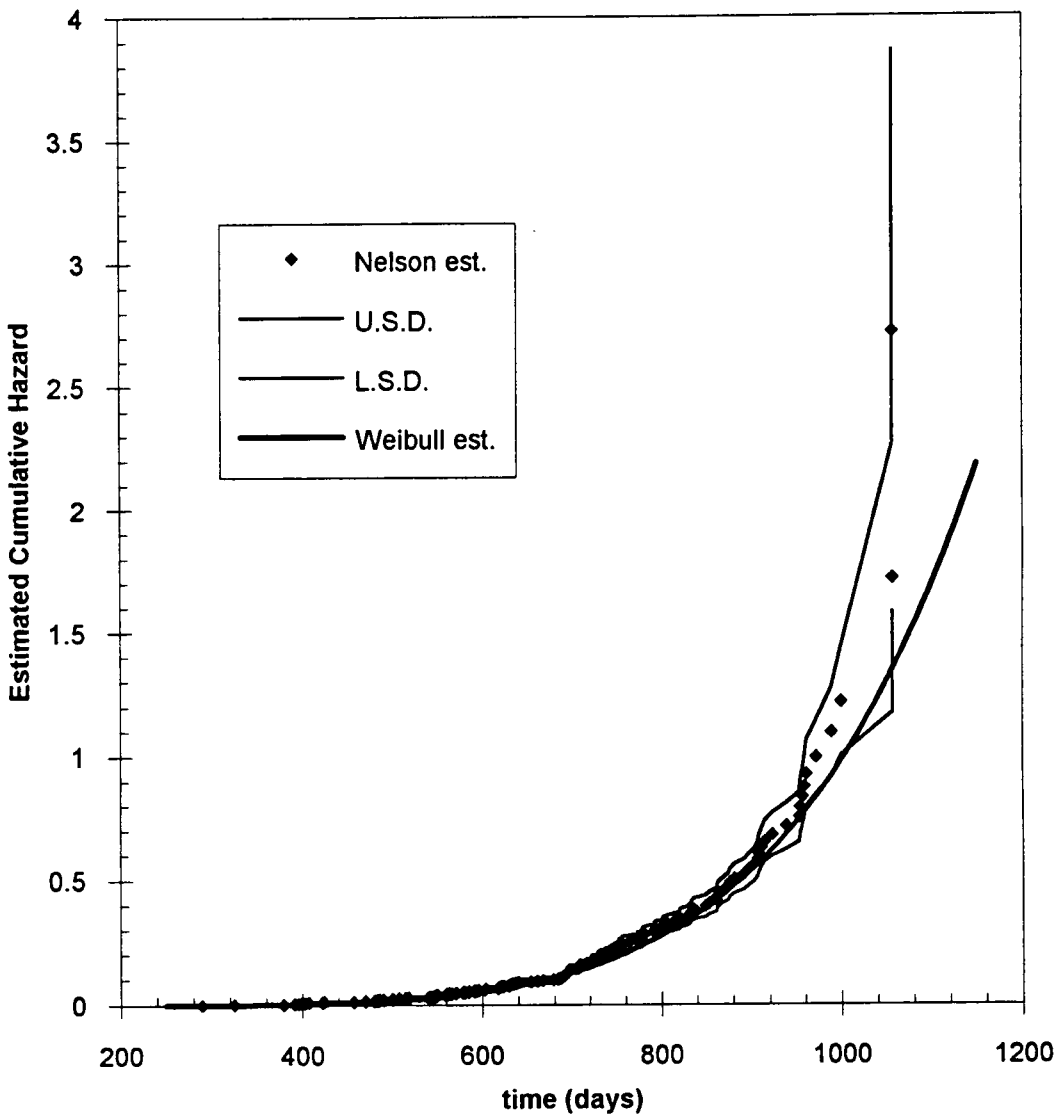

Figure A4.2 Estimated cumulative hazard vs time for BALB/c females with lung tumors: 0.5 Gy @ 0.4 Gy/min

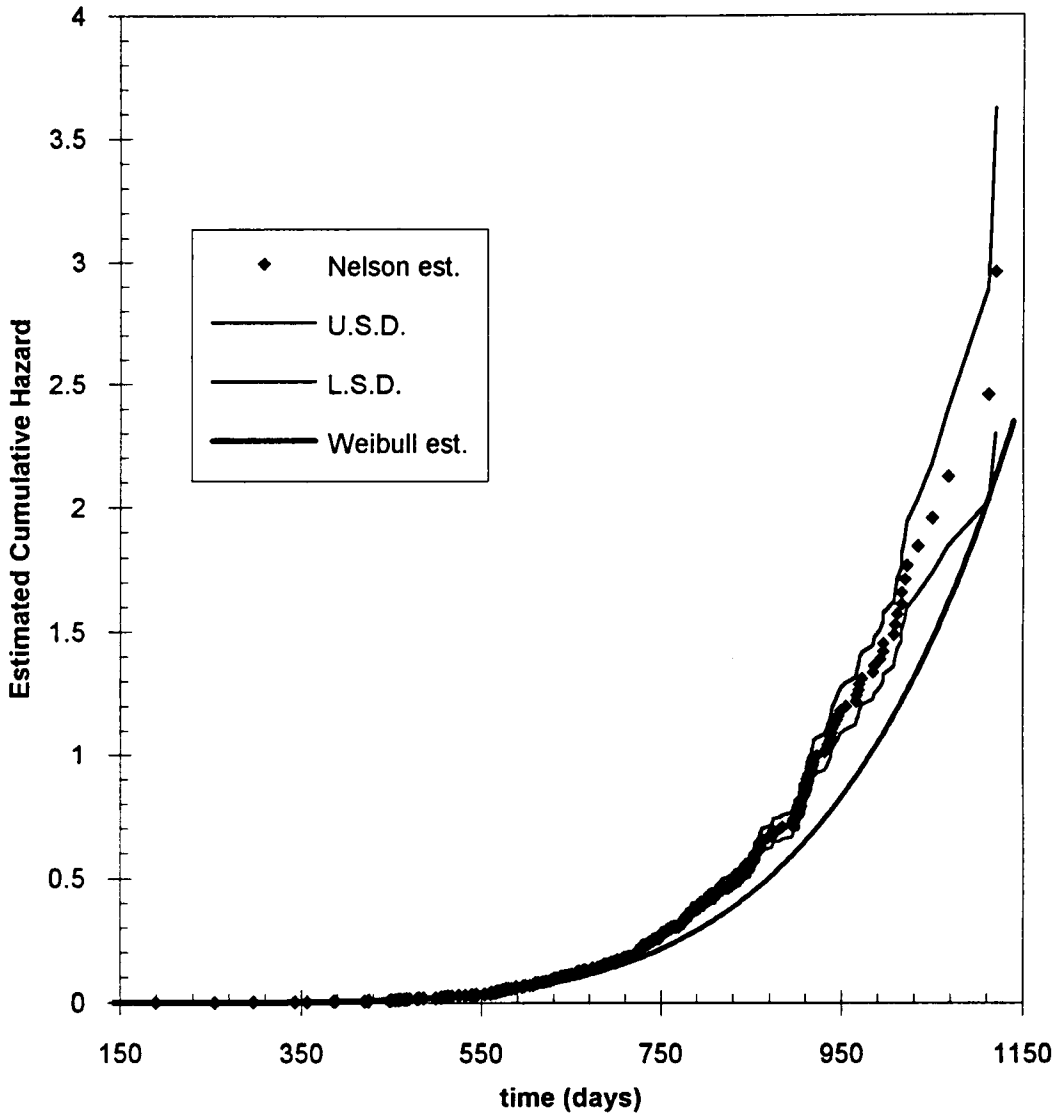

Figure A4.3 Estimated cumulative hazard vs time for BALB/c females with lung tumors: 0.5 Gy @ 0.083 Gy/day

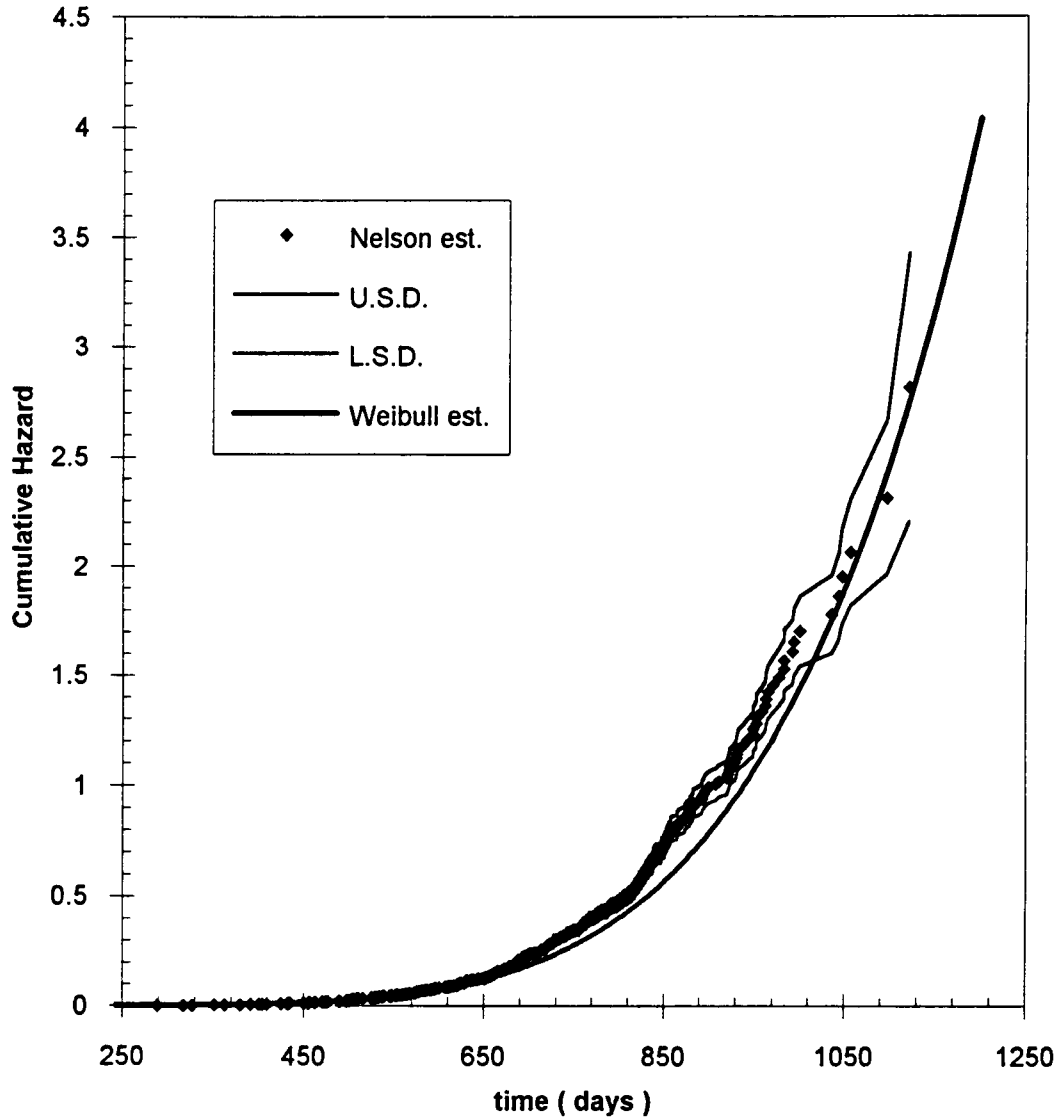

Figure A4.4 Estimated cumulative hazard vs time for BALB/c females with lung tumors: 1.0 Gy @ 0.083 Gy/day

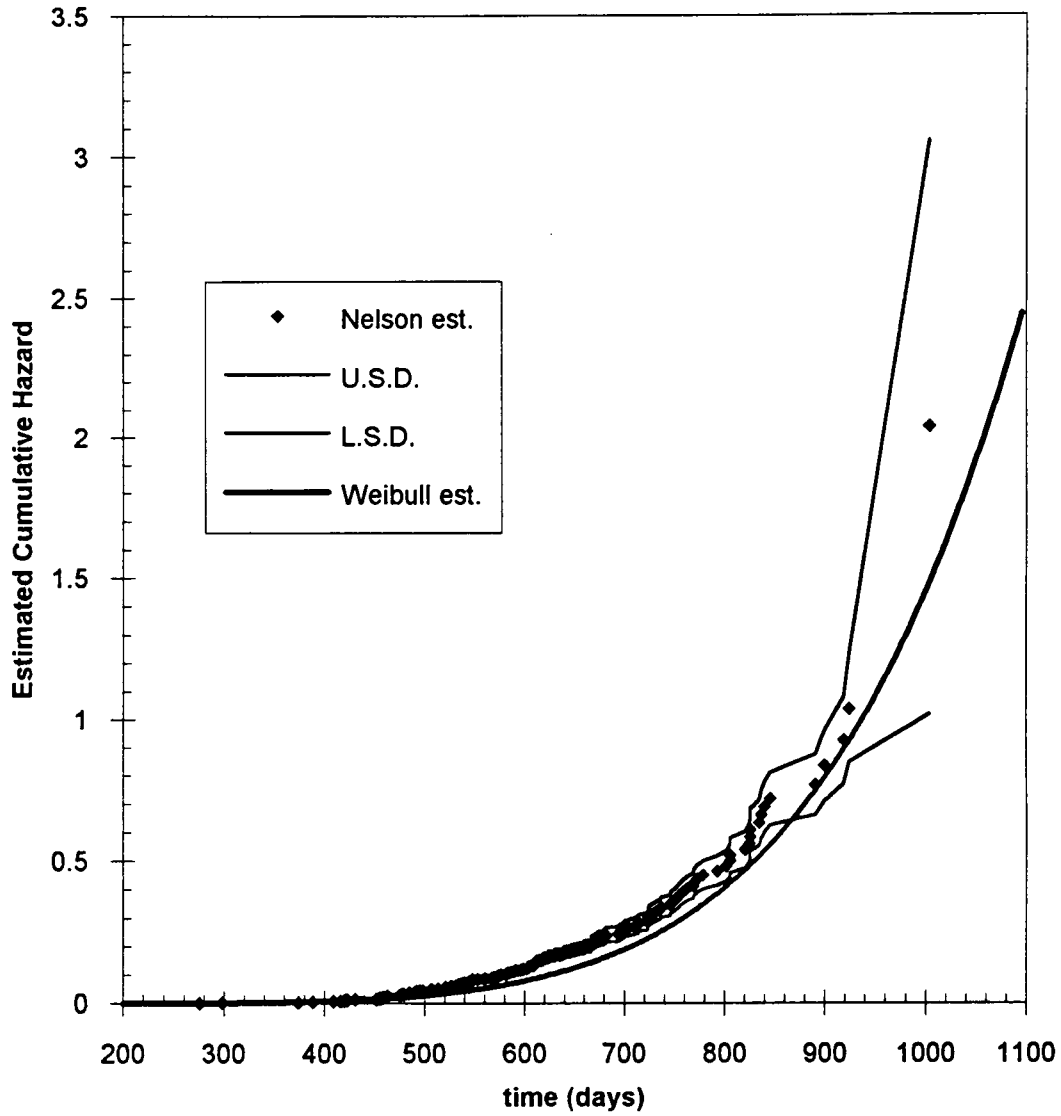

Figure A4.5 Estimated cumulative hazard vs time for BALB/c females with lung tumors: 2.0 Gy @ 0.4 Gy/min

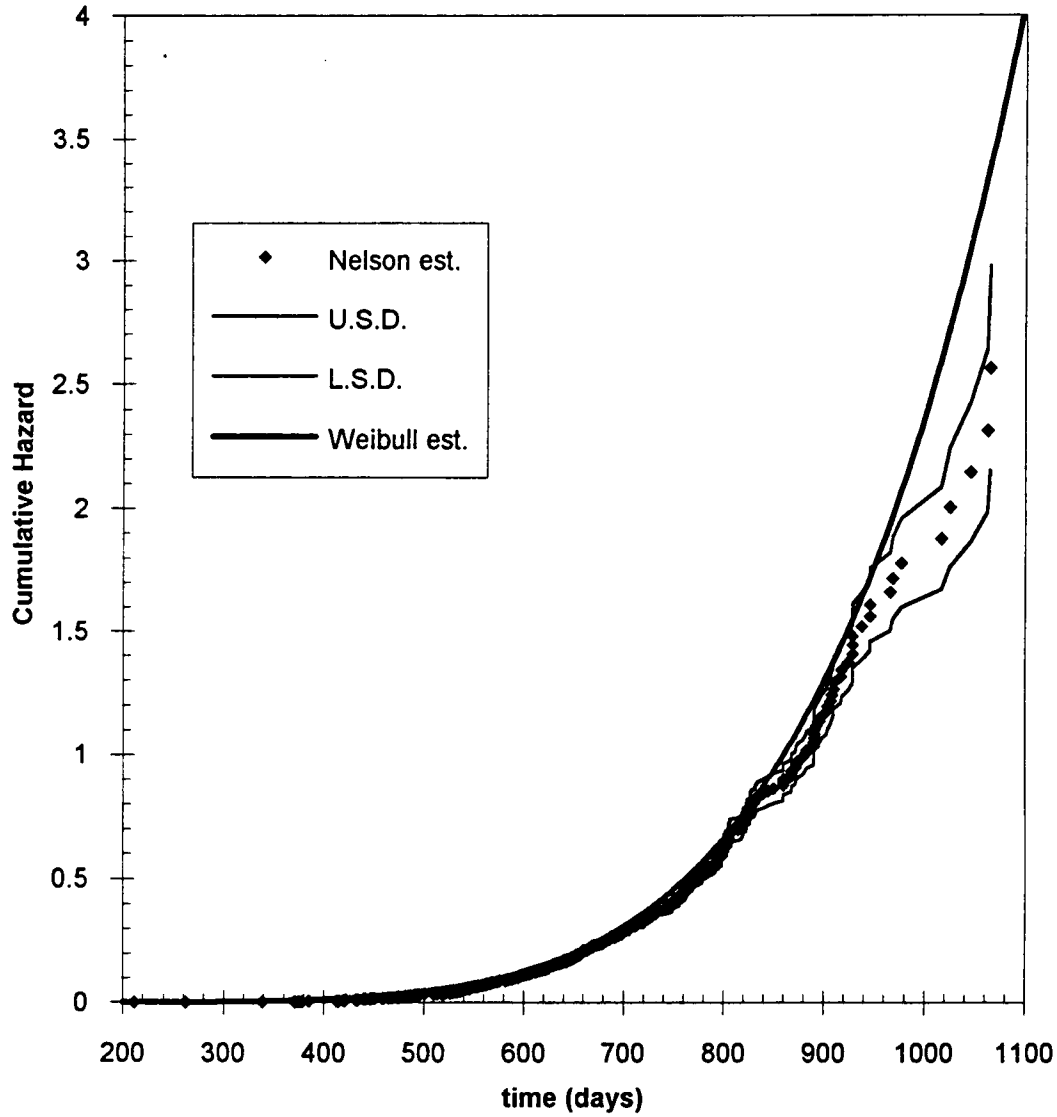

Figure A4.6 Estimated cumulative hazard vs time for BALB/c females with lung tumors: 2.0 Gy @ 0.083 Gy/day

A4.3 PARAMETRIC VS NON-PARAMETRIC ESTIMATES USING BREAST CANCER

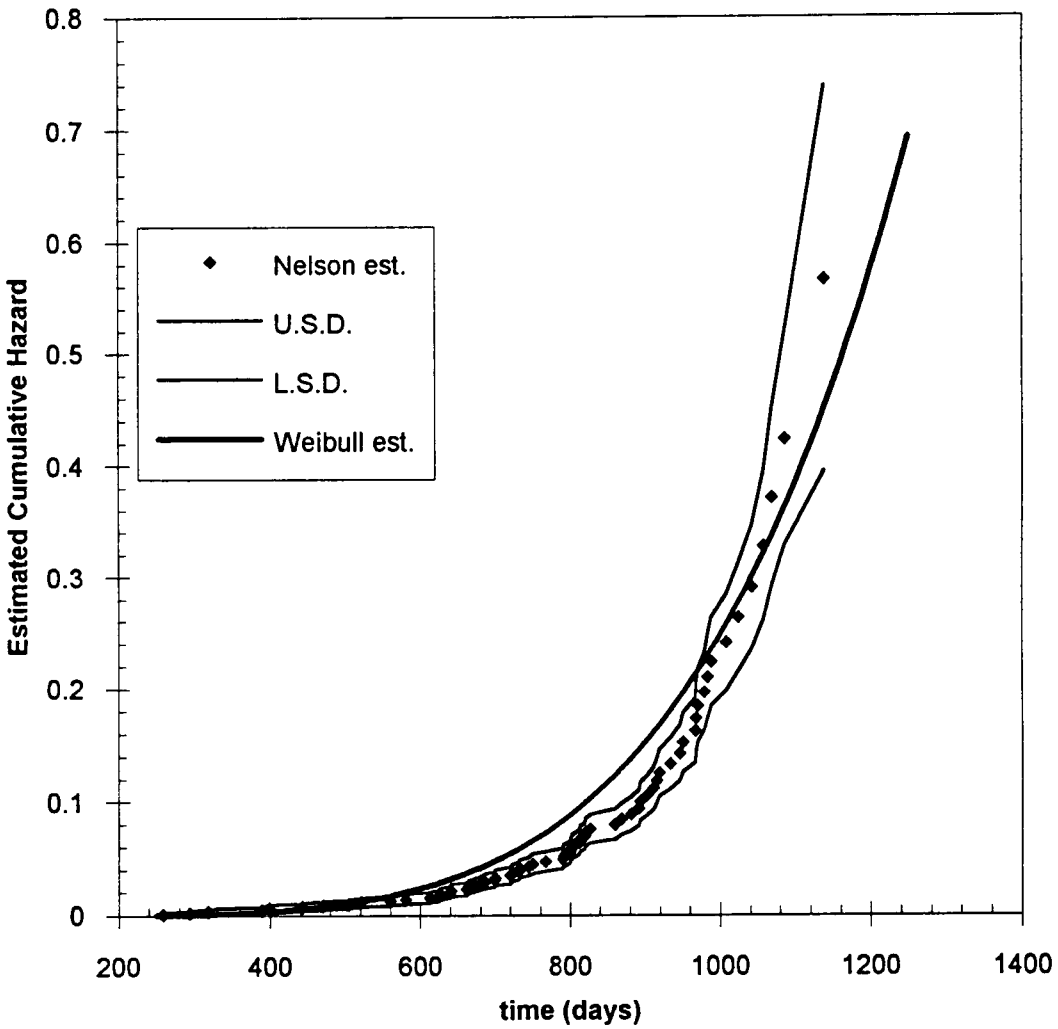

Figure A4.7 Estimated cumulative hazard vs time for BALB/c females with breast cancer: Unexposed

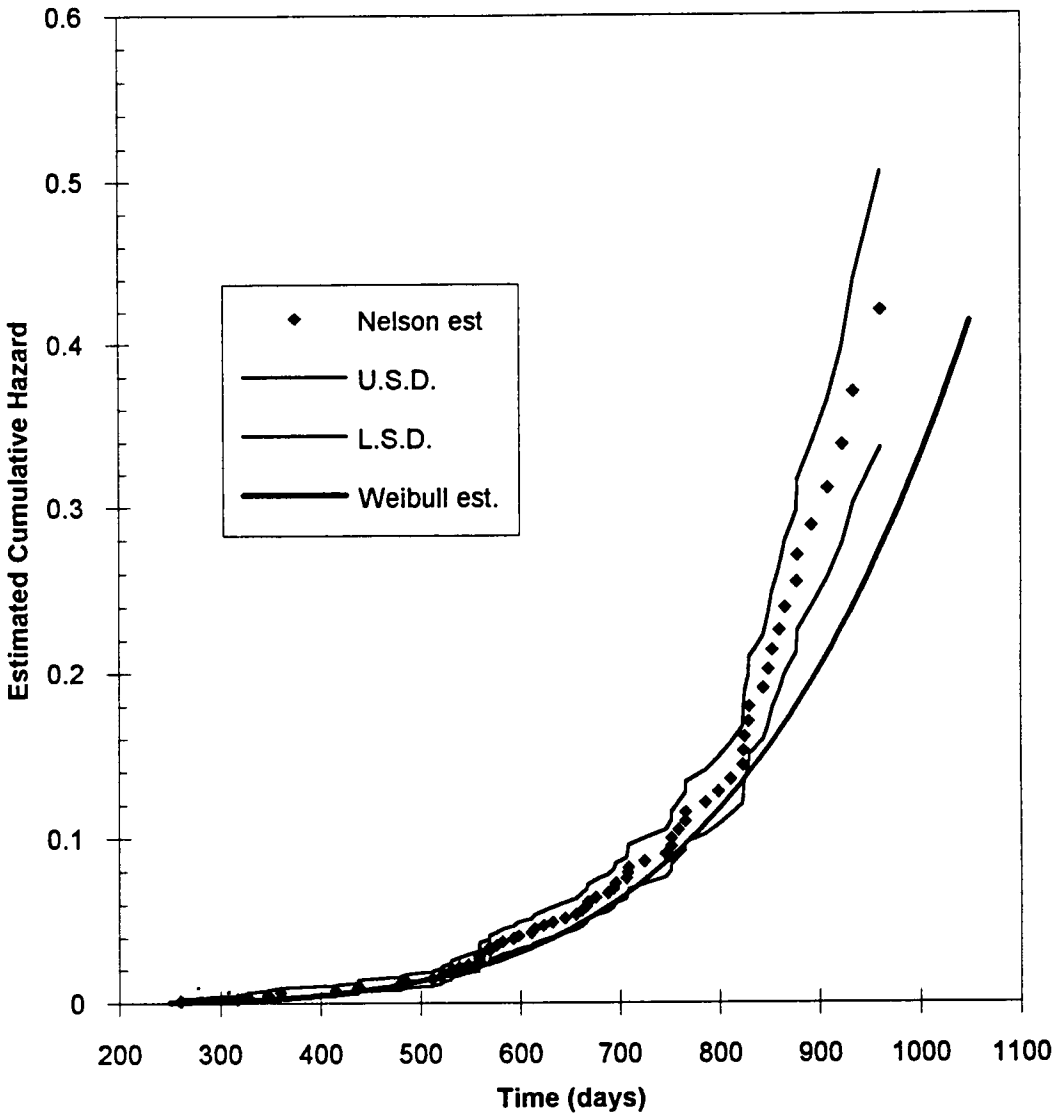

Figure A4.8 Estimated cumulative hazard vs time for BALB/c females with breast cancer: 0.5 Gy @ 0.4 Gy/min

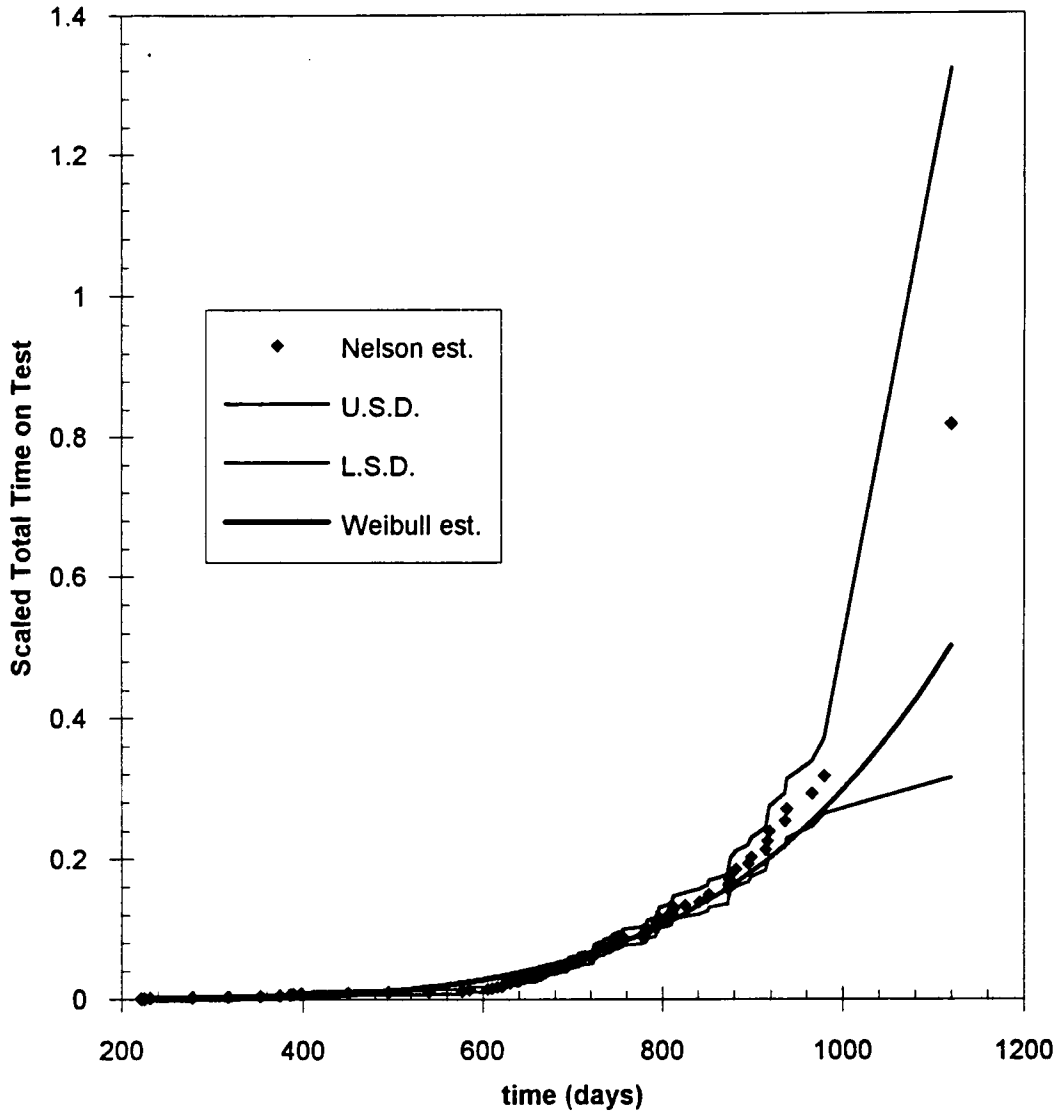

Figure A4.9 Estimated cumulative hazard vs time for BALB/c females with breast cancer: 0.5 Gy @ 0.083 Gy/day

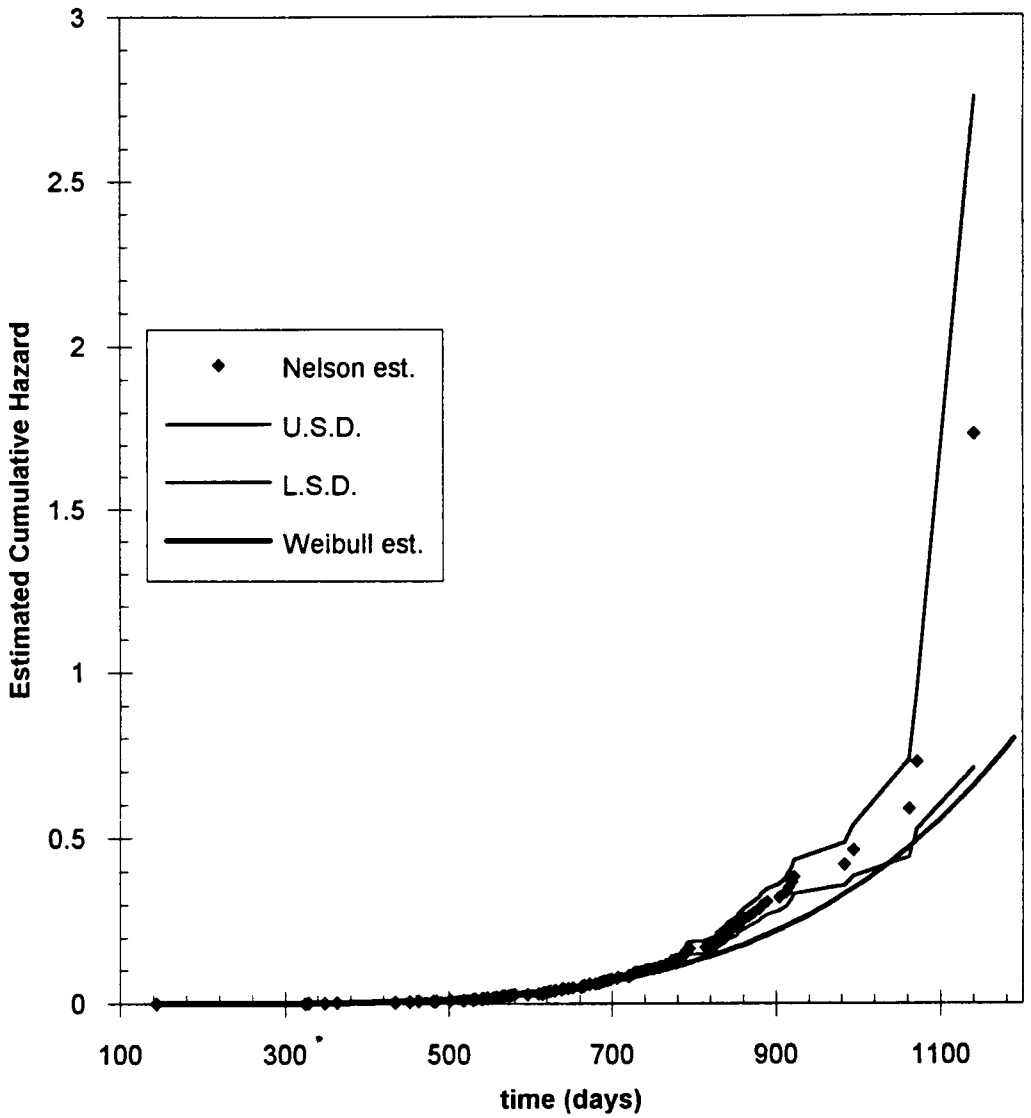

Figure A4.10 Estimated cumulative hazard vs time for BALB/c females with breast cancer: 1.0 Gy @ 0.083 Gy/day

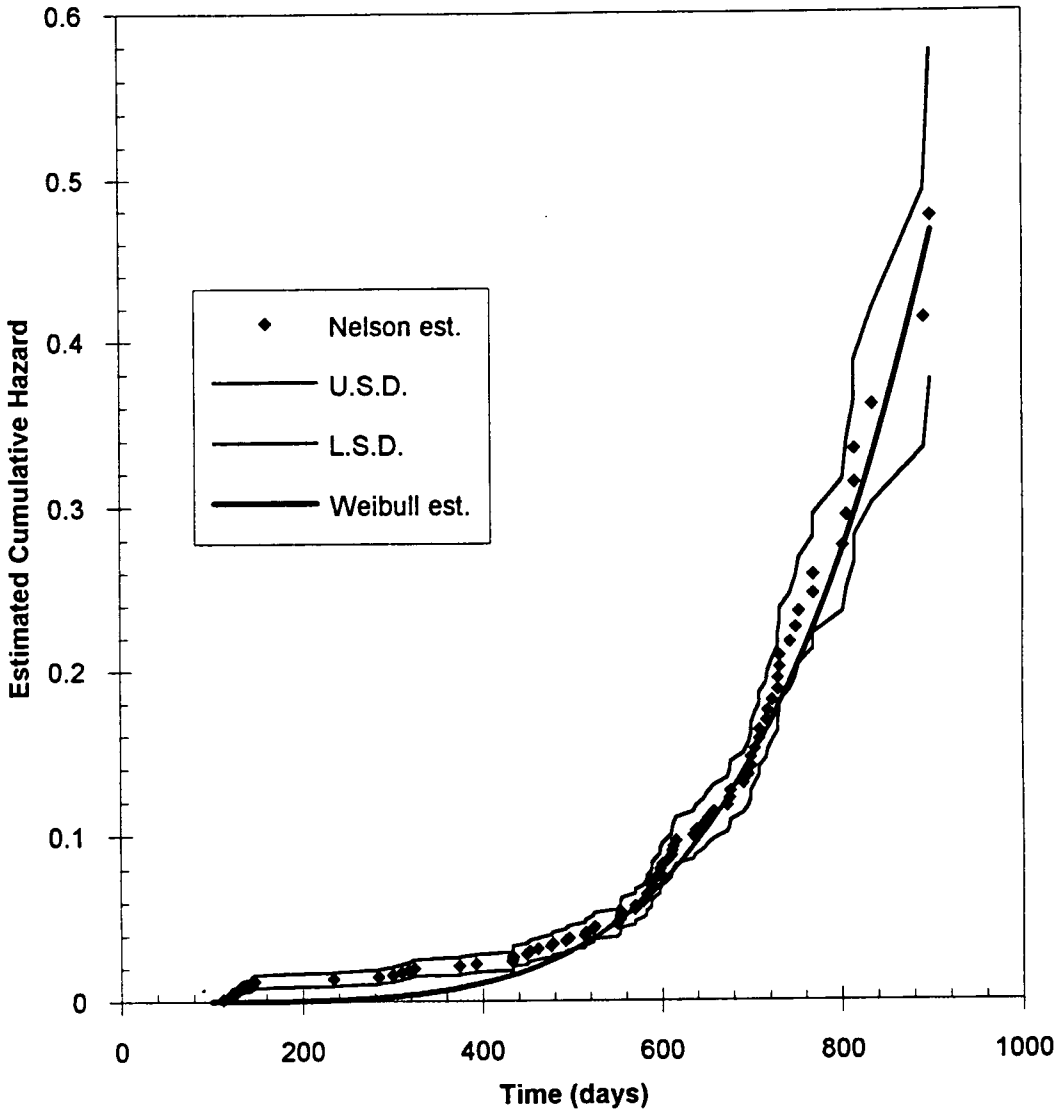

Figure A4.11 Estimated cumulative hazard vs time for BALB/c females with breast cancer: 2.0 Gy @ 0.4 Gy/min

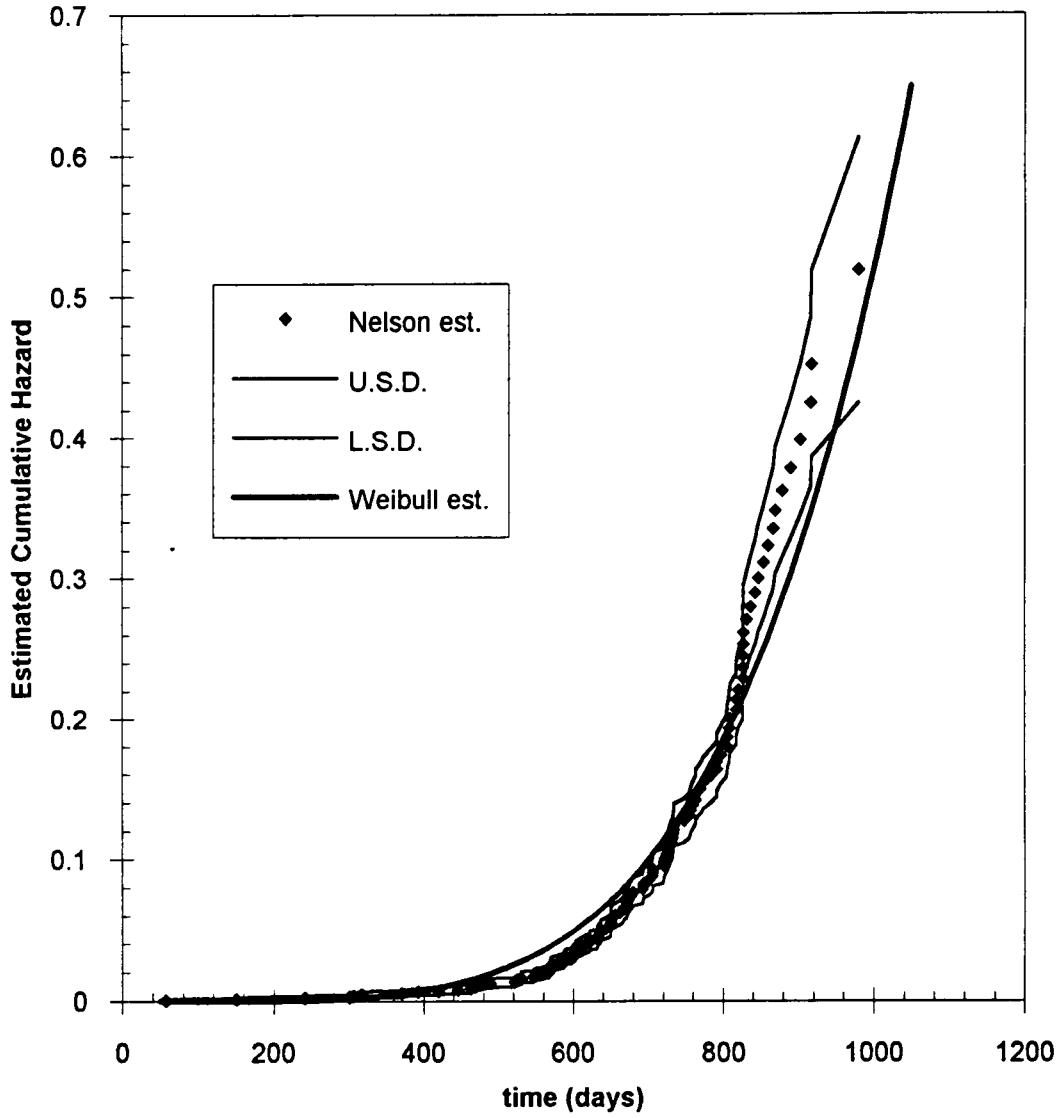

Figure A4.12 Estimated cumulative hazard vs time for BALB/c females with breast cancer: 2.0 Gy @ 0.083 Gy/day

A4.3 PARAMETRIC VS. NON-PARAMETRIC ESTIMATES FOR ALL CAUSES OF DEATH

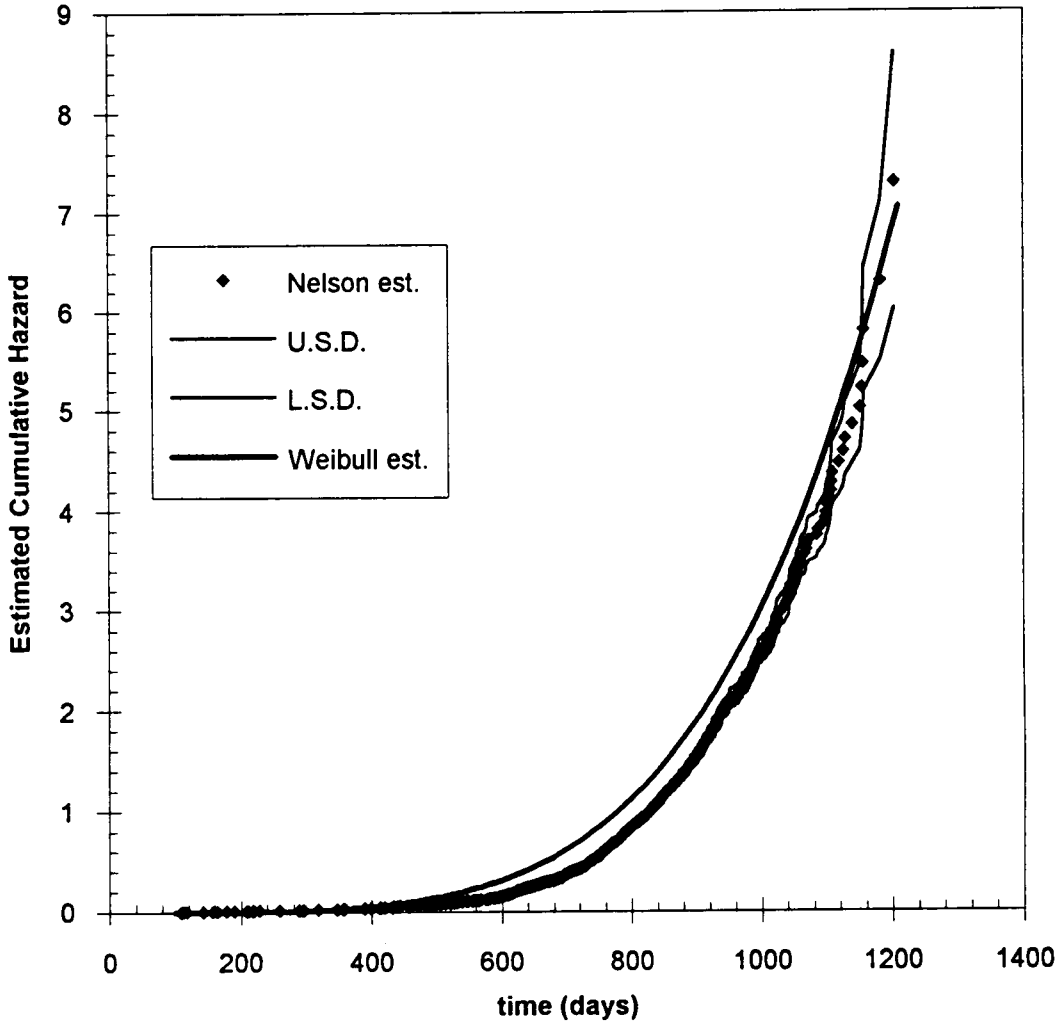

Figure A4.13 Estimated cumulative hazard vs time for BALB/c females using all causes of death: Unexposed

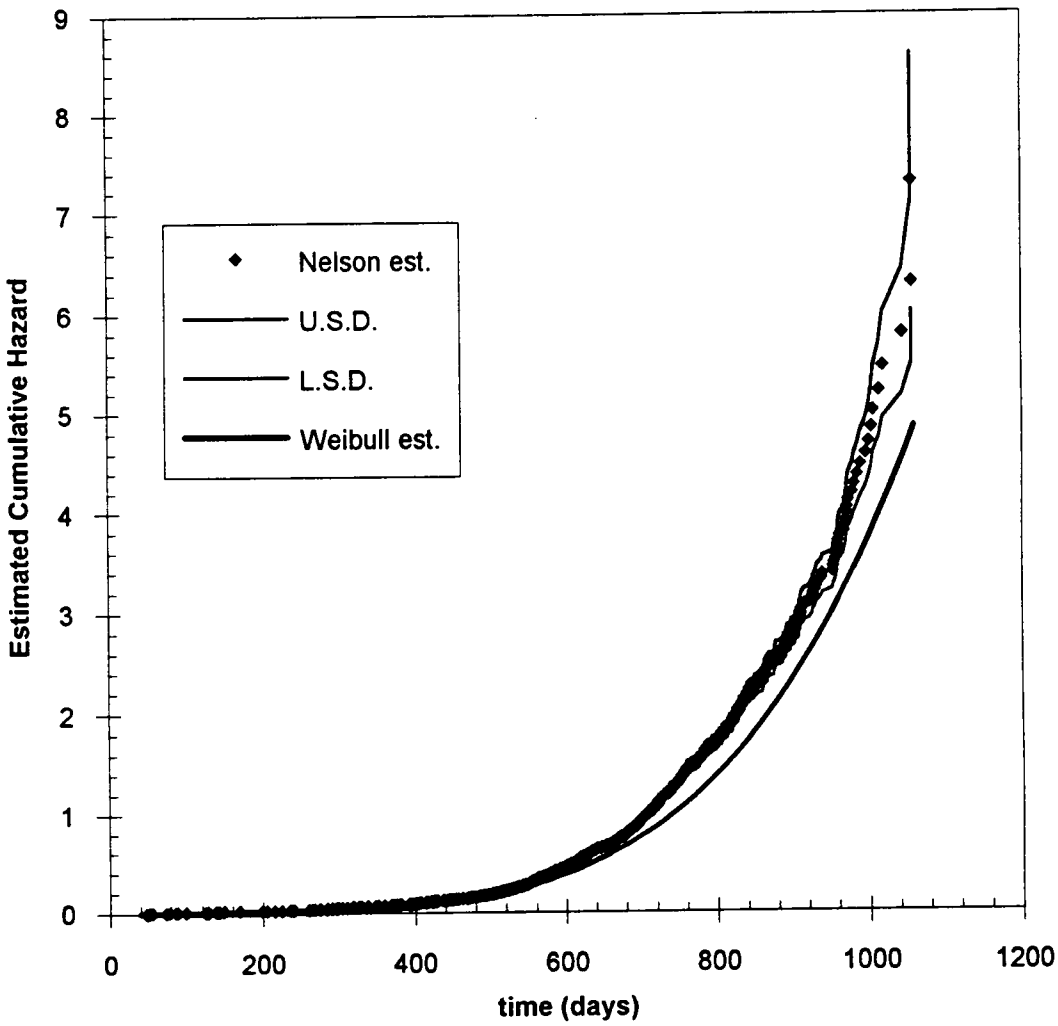

Figure A4.14 Estimated cumulative hazard vs time for BALB/c females using all causes of death: 0.5 Gy @ 0.4 Gy/min

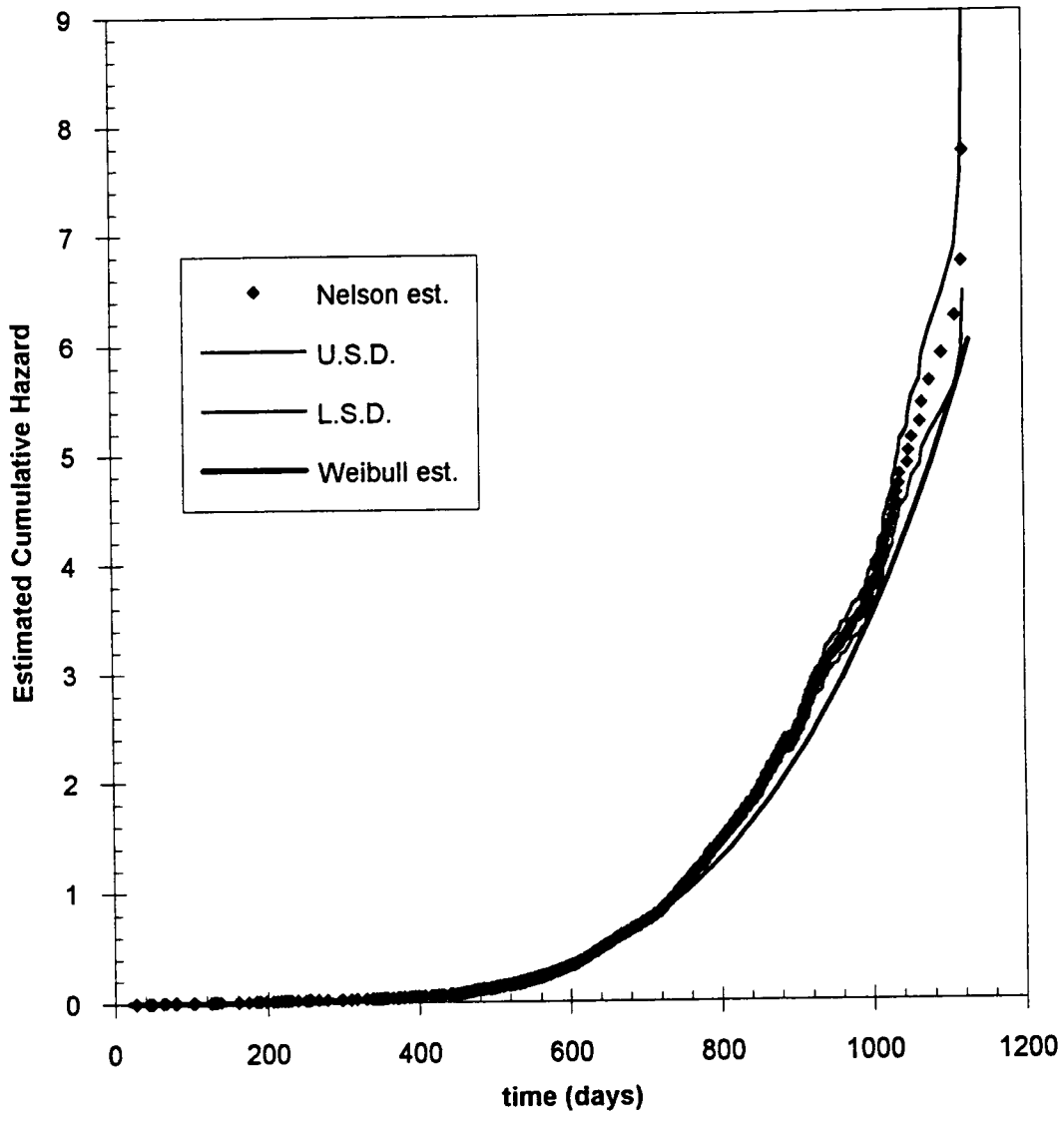

Figure A4.15 Estimated cumulative hazard vs time for BALB/c females using all causes of death: 0.5 Gy @ 0.083 Gy/day

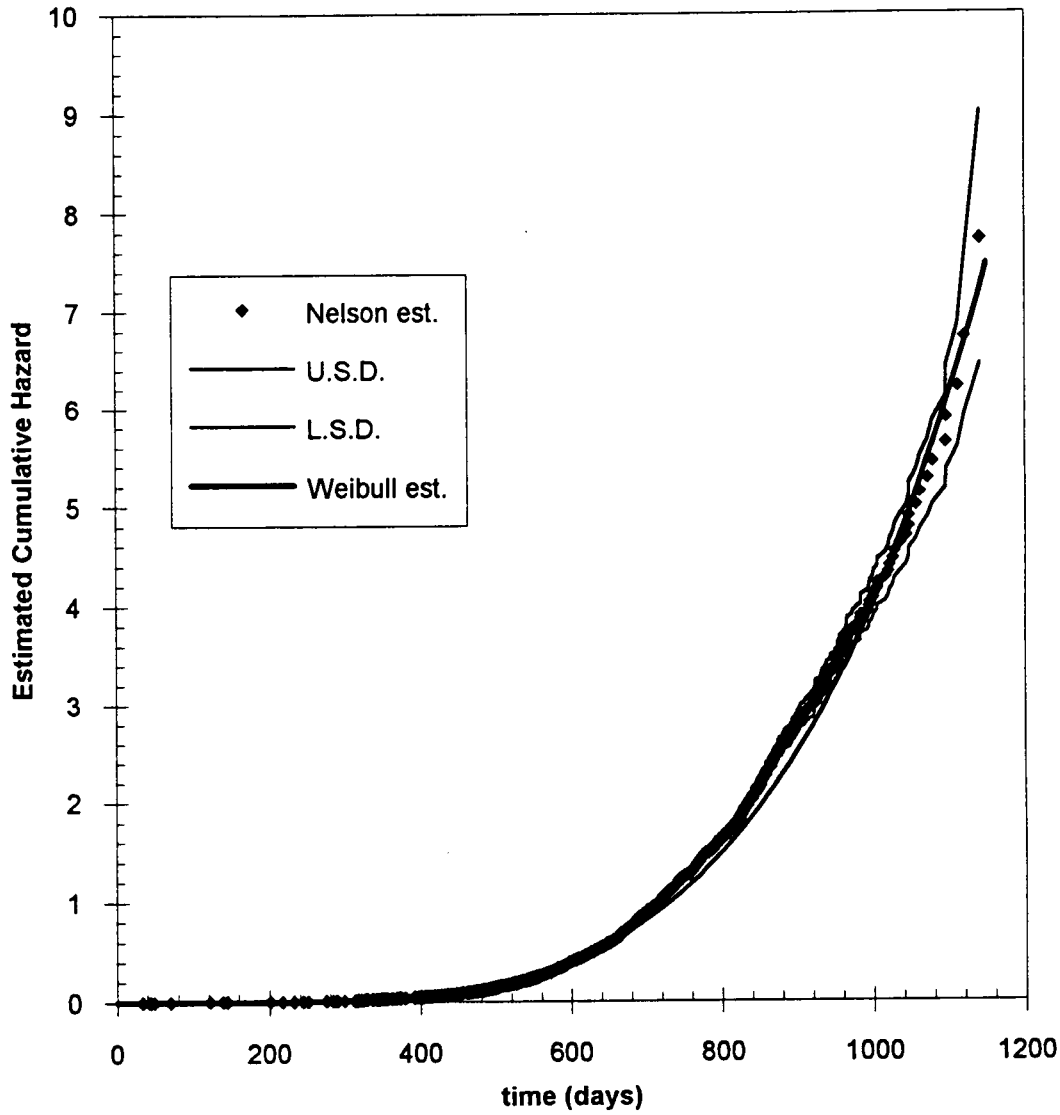

Figure A4.16 Estimated cumulative hazard vs time for BALB/c females using all causes of death: 1.0 Gy @ 0.083 Gy/day

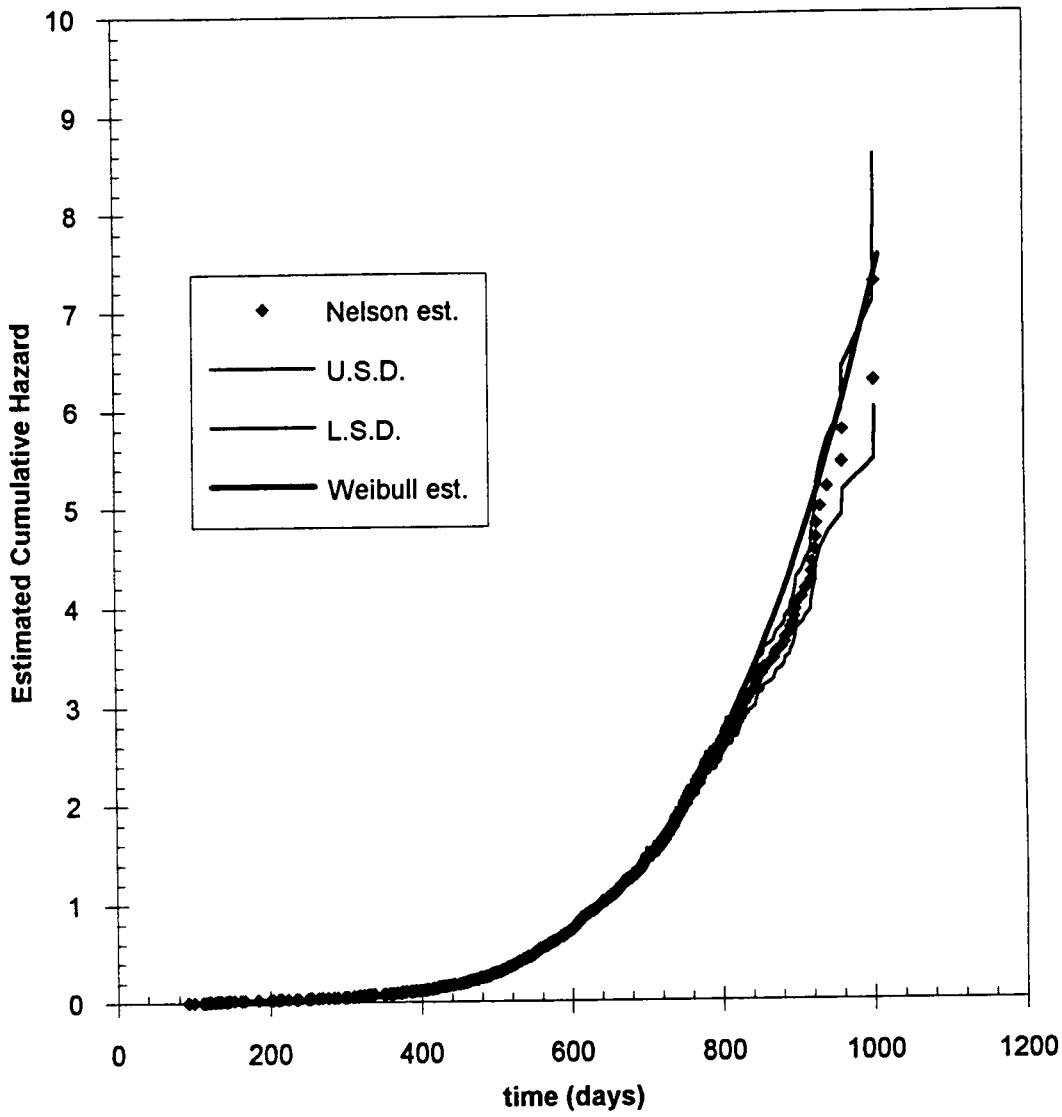

Figure A4.17 Estimated cumulative hazard vs time for BALB/c females using all causes of death: 2.0 Gy @ 0.4 Gy/min

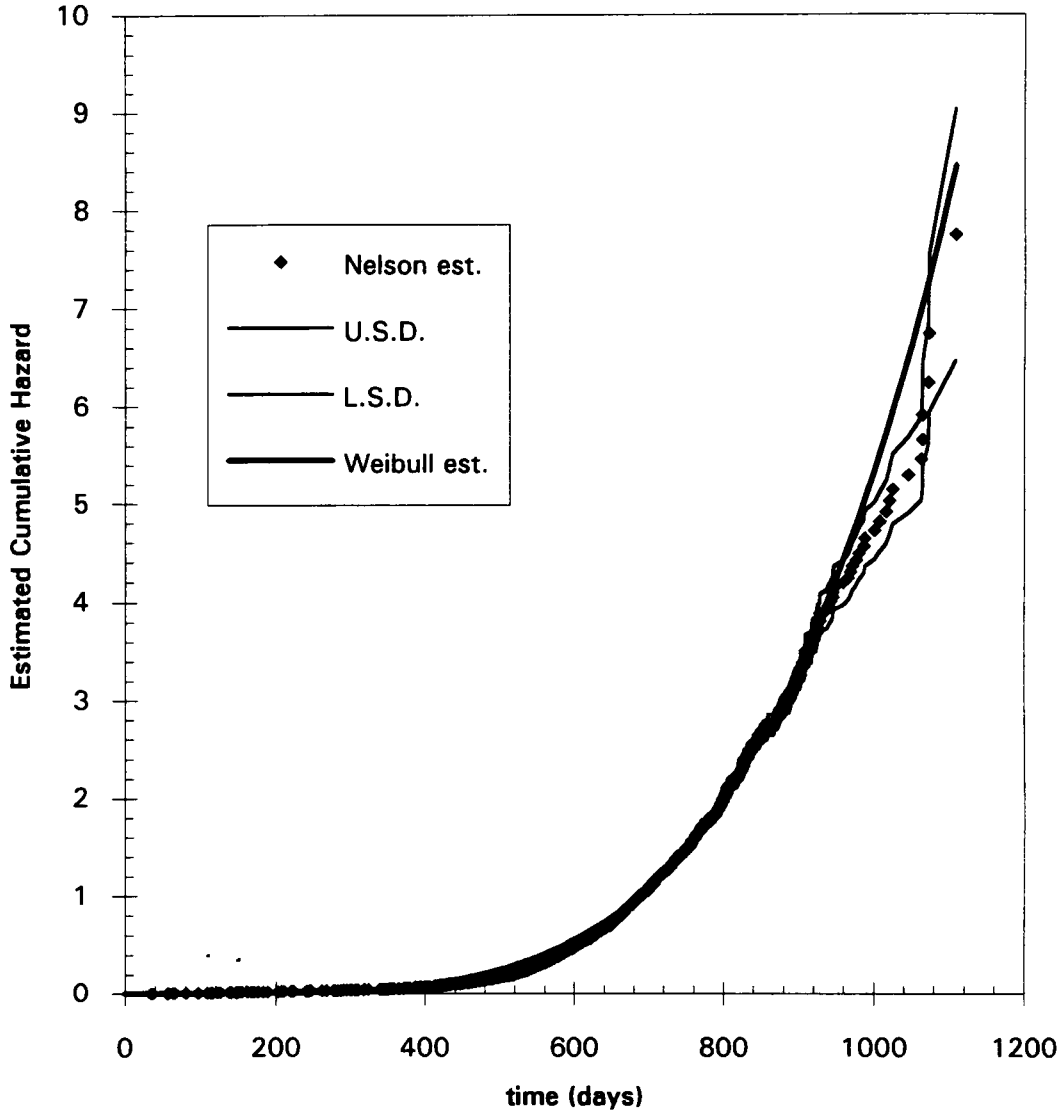

Figure A4.18 Estimated Cumulative hazard vs Time for BALB/c females using all causes of death: 2.0 Gy @ 0.083 Gy/day

VITA

John Joseph Arnish was born in Springfield, Illinois on July 9,1969. He attended both elementary and high school in Springfield where he graduated from Lanphier high school in June, 1987. The following August he began work on his Associate of Arts degree at Springfield College in Illinois. After receiving his Associate degree, he continued his education at Southern Illinois University at Carbondale studying physics. In May of 1992 he received his Bachelor of Science degree from Southern Illinois University at Carbondale. The following August he entered The University of Tennessee, Knoxville to pursue his Master of Science in nuclear engineering. August of 1994 he received his Master of Science degree.